博士論文

Study on Spatio-Temporal Variabilities of Indonesian Rainfall Using TRMM Multi-Satellite Precipitation Analysis Data

(TRMM 複数衛星降水解析データを用いた

インドネシアの降水時空間変動に関する研究)

2020 年 3 月

Abd. Rahman As-Syakur

山口大学大学院創成科学研究科

A dissertation submitted in partial fulfilment of the requirements
for the degree of Doctor of Philosophy

DEDICATION

To

my dear parents, *Aji Fi* and *Umi Ija*

my wonderful wife, *Eka*

my lovely son and daughter, *Adla* and *Adila*

and my beautiful sister, *Iien*

in recognition of their prayers and understanding

SUMMARY

The Indonesia is uniquely located in the most active convection area of the world, and influenced by global, regional, and local conditions; e.g. Asian-Australian monsoon, tropical convective zones, intra-seasonal oscillation, and complex land-sea-topography. Because that rain gauges are only located over land and not in the Indonesian sea area, comprehensive study of the rainfall variability over Indonesia is difficult. Using the remotely sensed meteorological satellite data is one of the solutions to record the rainfall data in the land and ocean areas simultaneously. This study aims to determine the quality of satellite rainfall data called the Tropical Rainfall Measuring Mission (TRMM) Multi-Satellite Precipitation Analysis (TMPA) products (TRMM 3B42 for 3-hourly data and TRMM 3B43 for monthly) and their applications for Indonesian region to understand spatio-temporal patterns of climatic rainfall characteristics that are impacted by two main factors including the monsoon and atmosphere-ocean interactions near Indonesia. Hence, this study is motivated by the lack of studies on rainfall variability over Indonesia using long-term satellite meteorological data. This study attempts to analyse and introduce the quality of daily-monthly satellite TMPA products, especially over the Bali area, and use them to explain Indonesian rainfall characteristics from the aspects of diurnal rainfall cycles, the impact of monsoon activity, land-sea distribution, topography diversity and the interaction with the El Niño–Southern Oscillation (ENSO; hereafter conventional El Niño) and the El Niño Modoki.

Chapter 2 describes the first result of this research. This chapter shows the comparison results of daily-monthly rainfall from TMPA 3B42 daily and 3B43 monthly products with rain gauge measurements over Bali. The main objective of chapter 2 is to advance our quantitative understanding of the capability of TMPA products for the analyses of climatic-scale rainfall. The results indicate that TMPA products tend to underestimate the rainfall with large errors on daily timescales but show better agreement on monthly timescales. In general, the TMPA products are usable and valuable in analysing climatic-scale rainfall, particularly over the areas without rain gauge measurements.

Chapter 3 illustrates the second result of this research. This chapter presents the TMPA product analysis for 3B43 monthly data to understand the variabilities of Indonesian rainfall on

annual, seasonal and monthly time scales, as well as their connection with monsoon activity, land-sea scattering, and topography distribution. The results show that the oceans, islands, monsoons, and topographical diversity clearly affect the spatial patterns of Indonesian rainfall. The high-rainfall events in Indonesia peak during the December-January-February seasons and the low-rainfall events occur during the June-July-August seasons. Most of the highest annual and monthly rainfall typically occurs over island areas.

Chapter 4 presents the third result of this research. This chapter explains the role of monsoon, topography, and El Niño Modoki on the rainfall variability in the Maritime Continent (MC) by analysing the long-term monthly TRMM 3B43 data. The results indicate that the north-south MC precipitation is associated with and generated by the monsoon patterns. In addition, the large-scale circulations are linked with heavy rainfall over this land-ocean region. The conventional El Niño (El Niño Modoki) has a higher impact on rainfall variability than El Niño Modoki (conventional El Niño) especially during northern winter and spring (northern fall), while two phenomena similarly affect during northern summer.

Chapter 5 displays the fourth result of this research. The main objective of chapter 5 is to describe spatial and seasonal differences in the diurnal rainfall cycles using long-term (17-year) 3-hourly TRMM 3B42 data over the Sumatera Island. The results point out for the first time that early-afternoon initiation of daily rainfall not only in the Barisan Mountains in the west of island but also in the east-coastal small islands. Westward and eastward migrations of rainfall areas from the Barisan Mountains vary with seasons and regions, with the most remarkable westward migration during September-October-November season in the central region and the least remarkable one during June-July-August season in the southern region.

CONTENTS

LIST OF FIGURES

LIST OF TABLES

CHAPTER 1

Introduction

1.1 Rainfall and Meteorological Satellite

Rainfall is a key variable for the Earth's water cycle and energy balance and also plays a major role in monitoring water-related natural hazards and water resource management. The Indonesian Maritime Continent (IMC) is uniquely located in the most active convection area of the world, and influenced by global, regional, and local conditions; e.g. Asian-Australian monsoon, tropical convective zones, intra-seasonal oscillation, and complex land-sea-topography (Chang *et al*., 2005; Qian, 2008; Hidayat and Kizu, 2010; Rauniyar and Walsh, 2011). The Asian-Australian monsoon creates an annual rainy and dry season cycle (Robertson et al., 2011). The intra-seasonal (30–90 days) Madden–Julian oscillation (MJO) phase is associated with extreme high and low precipitation events (Wu and Hsu, 2009; Oh et al., 2012; Kanamori et al., 2013; Wu et al., 2013), whereas complex land-sea-topography affects diurnal rainfall quantities (Qian et al., 2010; Peatman et al., 2014). The rainfall diversity affects the all associated events and creates high annual and inter-annual space-time climate variability in this region.

The Indonesia is a region with a large population and has extensive agricultural areas (Ito et al., 2011). Rainfall variability, indeed, influences the way of life for several hundred million peoples in the region. Therefore, knowledge about Indonesian fresh water sources is important for the living population depending on the water supply for drinking, industrial purposes and agricultural irrigation (de Angelis et al., 2004). Accountable information on precipitation is needed for improving climate and meteorological forecasts at several spatial and temporal scales. However, the reliable information of Indonesian rainfall characteristic is missing due to the absence of a dense rain-gauge network (Aldrian et al., 2003; Prasetia et al., 2013), because rain gauge data are often not available over the most unpopulated land areas, and gauge observations are not performed for ocean areas.

Rainfall is a critical weather element for determining the habitability of different parts of the Earth, yet it is difficult to obtain adequate measurements with surface-based instruments due to

its small-scale variability in space and time (Huffman et al., 2010). One key in improving the reliability of rainfall analysis is to simply increase the number of surface-based observing stations with good data quality and well-balanced spatial interval. However, establishing such an observing system is still expensive. Continuous and long-term time series data of rainfall are particularly important with respect to highly-variable nature of rainfall on spatial and temporal domains. One of the importance of long-term data is to increase the statistical reliability and delineate the climatological characteristics of rainfall by minimizing the effect of extreme events. Space-borne sensors play a key role in estimating rainfall and accumulating long-term data record. Satellite systems provide unique opportunity to monitor Earth-atmosphere system processes and parameters continuously (Thies and Bendix, 2011; Kidd et al., 2009). As satellite images started to become available to meteorologists around the world in early sixties, the skills of satellite image interpretation developed rapidly. The Television InfraRed Observation Satellite (TIROS-1), that was launched on 1 April 1960 was the first meteorological satellite. TIROS-1 was operational for only 78 days, but it demonstrated beyond doubt the tremendous potential use of satellites for surveying global weather conditions from space and paved the way for future advanced weather satellites (Kelkar, 2007). After TIROS-1, a lot of meteorological satellites were launched, including the National Oceanic and Atmospheric Administration (NOAA) satellite series, the Geostationary Operational Environmental Satellite (GOES) from Meteosat Second Generation (MSG), the Defense Meteorological Satellite Program (DMSP) satellites with Special Sensor Microwave Imager (SSM/I), the Multi-functional Transport Satellite-1R (MTSAT-1R), and the Tropical Rainfall Measuring Mission (TRMM) with TRMM Microwave Imager (TMI) and Precipitation Radar (PR) sensors as main sensors (Kidd, 2001).

A better understanding of the spatial and temporal variability of precipitation is indispensable for advancing climate change research, as well as for assessing the potential impacts of climate change on water resources (Nickl et al., 2010). Satellite observations of rainfall may be the best solution for adequate temporal and spatial coverage of rainfall where the rain gauge measurements are sparse. Meteorological satellite observations are making important contributions to gain a better understanding of the global water cycle. Large-scale, time-area-averaged precipitation estimates from satellite platforms provide essential information about the mean climatological distribution and variability of precipitation on a global scale (Petty, 1995).

Therefore, the use of satellite data such as by TRMM is important for observing spatial-temporal Indonesia rainfall patterns.

1.2 Rainfall Measurement by Satellite Remote Sensing

Precipitation shows high spatial and temporal variabilities. Rain gauges, disdrometers, and ground radars are the ground-based measurement tools usually being used for measuring rainfall, especially over the land (Kidd et al., 2017). Using only ground-based measurements results in a lack of coverage over the ocean or unpopulated regions. Satellites provide valuable measurements, covering large regions of the earth (Stephens and Kummerow, 2007). Rainfall measurements from space are based on the interpretation of the electromagnetic radiation that is scattered and emitted from clouds, precipitation and the underlying surface, and is monitored by the satellite instruments at the various wavebands (Rosenfeld, 2007). There are three groups of satellite instruments which are capable of precipitation retrieval. The first group is the visible (VIS) and infrared (IR) wavelength instrument; the second is the passive microwave radiometer (PMW); and the third is the active microwave instrument (AMW) or radar (Alemohammad, 2014). VIS/IR images from low-Earth-orbiting (LEO) or geostationary (GEO) satellites provide regular observations of clouds from which precipitation is estimated (Kidd et al., 2016), but with less accuracy (Serrat-Capdevila et al., 2014). PMW instruments allow more direct measurement of precipitation since the frequencies are more sensitive to precipitation-sized particles (Kidd and Levizzani, 2011), but has a difference in accuracy between land and sea. AMW/radar provides the most direct measurement of surface precipitation and also the vertical distribution of precipitation in the atmosphere (Kidd and Levizzani, 2011), but with long revisit times and limited global coverage (Behrangi et al., 2014). Since each of them has both advantages and disadvantages, all instruments are jointly used to produce satellite precipitation products to complement each other.

1.2.1. VIS and IR instrument

VIS/IR data have been most commonly used to make estimates of rainfall. These estimates are made by relating the reflectivity of clouds in the visible wavelengths and the thermal infrared radiation emitted by cloud-top temperatures with surface precipitation to retrieve precipitation (Collier, 2016). Present in many satellites, VIS/IR sensors provide very frequent precipitation

estimates with a large spatial coverage but with less accuracy (Serrat-Capdevila et al., 2014). VIS/IR data are generally obtained from instruments on board GEO satellite platforms, providing IR precipitation estimates imagery 24 h a day with a high resolution (~ 4 × 4 km) (Hong et al., 2018). IR sensors measure cloud upwelling radiances depicting the cloud properties at the upper levels (cloud-top temperatures) (Kirstetter et al., 2018), as illustrated in Figure 1.1. The simple principle of IR in estimating rainfall is based on inversely proportional relationship between the cloud-top temperatures to the rainfall rate, where colder clouds are associated with the heavier rainfall (So and Shin, 2018). IR sensors provide indirect information on the occurrence and magnitude of precipitation at the surface. Indirect measurements are defined as such that inferring the precipitation by observing other cloud properties (Rosenfeld, 2007). Potential rain clouds are sufficiently optically thick to be opaque in the visible and IR wavebands and precipitation is inferred from cloud top structure (Levizzani et al. 2001). Therefore, the radiation that reaches the satellite sensors typically comes from the cloud droplets and ice particles near the cloud tops, with little or no contribution from the actual precipitation particles (Rosenfeld, 2007). Depending on the cloud type and life cycle, a given IR brightness temperature can be associated with various rain rates, since not all clouds produce precipitation or produce it at the same rate, lead to low accuracy on precipitation estimates. However, the accuracy of these precipitation estimates tends to increase when the estimates are integrated over larger time- and space-scales (Kirstetter et al., 2018).

1.2.2. PMW instrument

The use of the microwave region of the electromagnetic spectrum to make measurements of precipitation has the advantage over visible and infrared techniques of detecting the precipitation itself, with clouds being wholly or partially transparent (Collier, 2016). The PMW band is used for direct measurements of precipitation because precipitation particle size lies within this waveband (roughly 10 to 0.1 cm wavelength) (Rosenfeld, 2007). In microwave region, the electromagnetic wave radiation penetrates through the cloud and hence it can be used to estimate rainfall more accurately compared to VIS/IR based rainfall estimates (Lensky and Levizzani, 2008). PMW instruments exhibit different accuracy in estimating precipitation over ocean and land. Over the ocean the signal comes essentially from the increased amount of emitted radiation from raindrops that makes the rain areas somewhat “warmer” that the surrounding “colder”

ocean background (Alhammoud et al., 2014). On the other hands, over the land surface the emission from rain drops cannot be reliably measured because the emissivities of soils and vegetation are much higher than those of water and very variable from place to place. In this case, there is little contrast to observe the "warm" raindrops (Rosenfeld, 2007).

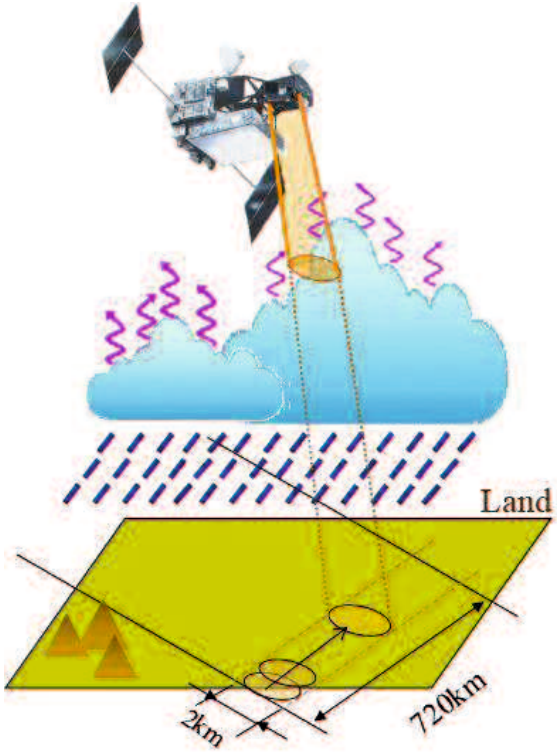

Figure 1.1. Sketch of rainfall measurement by IR instrument, illustrated for the Visible and Infrared Scanner (VIRS) instrument aboard the TRMM satellite (Shimizu, 2009).

The intensity of microwave radiation received by PMW instrument is expressed by brightness temperature, which is the product of physical temperature and emissivity of the target. Since the emissivity usually varies with wavelength and the condition of the target, measuring brightness temperatures at multiple wavelengths is necessary to either determine the physical temperature or estimate more than one physical property from the radiometric measurements (Collier, 2016). Over the ocean, increases in the brightness temperatures of the low frequency channels are strongly linked to increased rainfall, while over land decreases in the brightness temperatures in high frequency channels are linked to the precipitation-size ice in clouds, and thus surface precipitation (Kidd and Levizzani, 2019). For example, microwave radiations at the high frequency channels (85.5 GHz) measured by TRMM Microwave Imager (TMI) are strongly

scattered by ice present in many raining clouds over the land. This reduces the brightness temperatures measured by the satellite and offers a contrast against the warm land background (Kishtawal, 2016). Although PMW-based estimates generally provide higher accuracy compared to those by VIS/IR, they still have some limitations. One of the limitations is that the spatial and temporal resolution provided by the current PMW instruments. PMW has the spatial resolution much poorer than IR sensors. High-frequency channels typically have resolutions about 5 km at best, while low frequency channels have about 30 km (Figure 1.2) (Kidd and Levizzani, 2019). In addition, at present all PMW instruments are on LEO satellites that provide a maximum of only two observations per day per satellite, and thus we need a constellation of sensors to adequately resolve the variability of precipitating systems (Kidd and Huffman, 2011).

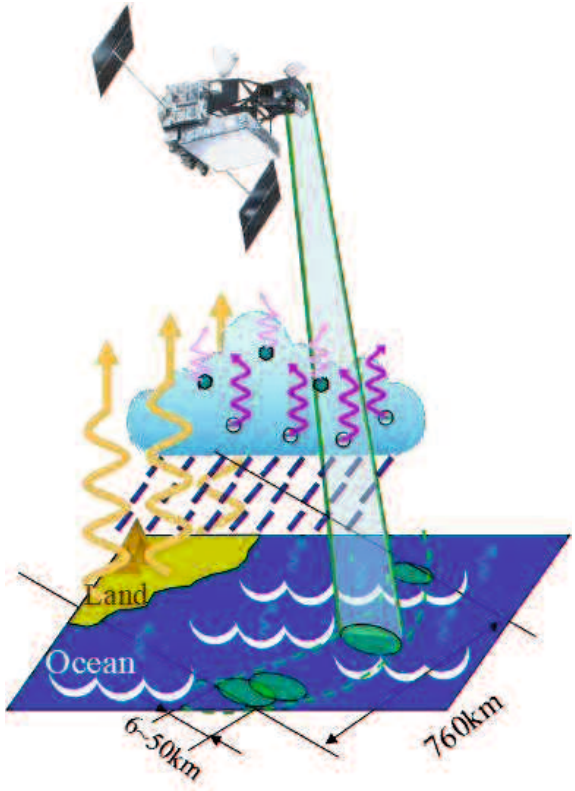

Figure 1.2. Sketch of rainfall measurement by PMW instrument, illustrated for the TRMM Microwave Imager (TMI) instrument aboard the TRMM satellite (Shimizu, 2009).

1.2.3. AMW or radar instrument

AMW techniques offer the most direct and quantitative estimation methods (Kidd and Huffman, 2011). Direct measurements of precipitation use the microwave frequencies that

interact directly with the precipitation size particles (diameter > 0.1 mm) (Rosenfeld, 2007). Despite this, radar technology for spaceborne precipitation estimation has been limited because it is expensive (Levizzani and Cattani, 2019). The first AMW spaceborne instrument was the Precipitation Radar (PR) aboard the TRMM satellite with frequency at 13.8 GHz (Kawanishi et al., 2000). PR provides not only the measurement of surface precipitation, but also the vertical distribution of precipitation in the atmosphere, which is necessary to improve our ability to measure precipitation at the local and global levels (Tapiador et al., 2017). After PR, several AMW spaceborne instruments were launched, including W-band Cloud Profiling Radar (CPR) on board the CloudSat and the Ku-/Ka-band Dual-frequency Precipitation Radar (DPR) onboard the Global Precipitation Measurement (GPM) Core Observatory. The AMW measurements introduced more direct information on the precipitation formation in clouds, providing a 3D description of the precipitation field (Levizzani and Cattani, 2019). The AMW sensors enabled many studies of precipitation systems in great detail over tropics and subtropics, as well as specific precipitation systems, such as monsoon convective systems, shallow precipitation, and intense storms (Liu and Zipse, 2015).

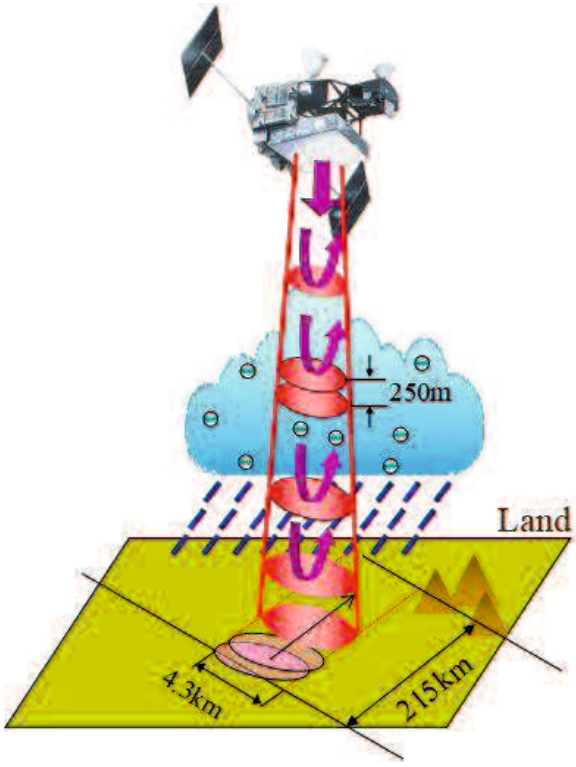

Figure 1.3. Sketch of rainfall measurement by AMW instrument, illustrated for the Precipitation Radar (PR) instrument aboard the TRMM satellite (Shimizu, 2009).

AMW measurements transmit pulses of radiation and receive the backscattered echoes. Simply stated, the echo intensity is converted into precipitation intensity according to the radar equation (Rosenfeld, 2007). AMW instrument relies upon the interpretation of the backscatter of radiation from the precipitation, the amount being broadly proportional to the number of precipitation-sized particles (Kidd and Levizzani, 2011). This relationship is not constant and in heavy precipitation attenuation effects can be significant, for example at the 13.8 GHz frequency of PR (Iguchi et al., 2000). The amount of backscattered energy is also related to the surface roughness, orientation, slope and dielectric constant of the material of which the surface is composed. It also depends upon any rainfall intercepted by the radar beam, as short wavelengths are attenuated by heavy rainfall (Collier, 2016). A drawback of AMW instruments is the small footprint size, i.e. they have narrow swath compared with passive instruments. For example, the swath width of the TMI and VIRS are about 760 km and 720 km, respectively, whereas that of the PR is only 215 km (Iguchi, 2007).

1.2.4. The TRMM Multi-satellite Precipitation Analysis (TMPA)

TRMM had collected high quality infrared and microwave radiometer and precipitation radar data since November 1997 until April 2015. TRMM was designed to study rainfall for weather and climate research and provided critical precipitation measurements in the tropical and subtropical regions (Simpson et al., 1996). TRMM was in a LEO at an altitude of 402.5 km above the Earth's surface (350 km before boost) and has limited spatial and temporal sampling which only covers the tropics and lower mid latitudes (35 degrees north to 35 degrees south). To mitigate these limitations and in tune with other efforts, the multi-satellite precipitation products based on TRMM data was developed.

As previously mentioned and summarized in Table 1.1, all different sensors have advantages and disadvantages in observing precipitation, and therefore they need to be jointly used to produce satellite precipitation products to complement each other. At a quasi-global and continuous temporal scale, the most accurate satellite precipitation estimates are from a combination of IR sensors on GEO satellites with high sampling frequency and microwave sensors on LEO satellites with less-frequent temporal sampling (Huffman et al. 2007). One of the merged product is the TRMM Multi-satellite Precipitation Analysis (TMPA), including 3-hourly 3B42 and monthly 3B43 products (Huffman et al. 2007, 2010). TMPA products were designed to integrate estimates from different satellites and ground gauge analyses to produce the ‘‘best’’ estimate with calibration by TMI. All the polar-orbiting microwave data were intercalibrated to

the TRMM Combined Instrument (TCI), that is product 3B31, which also includes the information from PR. The TMPA uses the Global Precipitation Climatology Centre (GPCC) gauge analyses to enhance calibration (Maggioni et al., 2016).

Table 1.1. Summary of advantages and weaknesses for different types of sensors.

Sensor	Measurement method	Advantage	Weakness
VIS-IR	• Inferred from cloud-top structure	• Good space and time resolution (~1-4 km and ~15 minutes) from GEO satellites	• Low accuracy due to indirect information of precipitation • Many assumptions
PMW	• Over land by using scattering-based algorithm (by large ice particles, at higher frequency). • Over ocean by using emission-based algorithm (by water content, at lower frequency)	• High accuracy over ocean • Better accuracy than VIS-IR estimates	• Low spatial resolution (~5 – 50 km) • Poor time resolution from LEO satellites • Low accuracy over land (different accuracy over land and ocean)
AMW	• Measures reflectivity by raindrops at multiple layers and converts to vertical profile of precipitation	• Most direct measure of precipitation • Better accuracy than VIS-IR and PMW • Equal quality over ocean and land • Provides 3D rainfall structure	• Narrow swath and long revisit time • Poor time resolution from LEO satellites

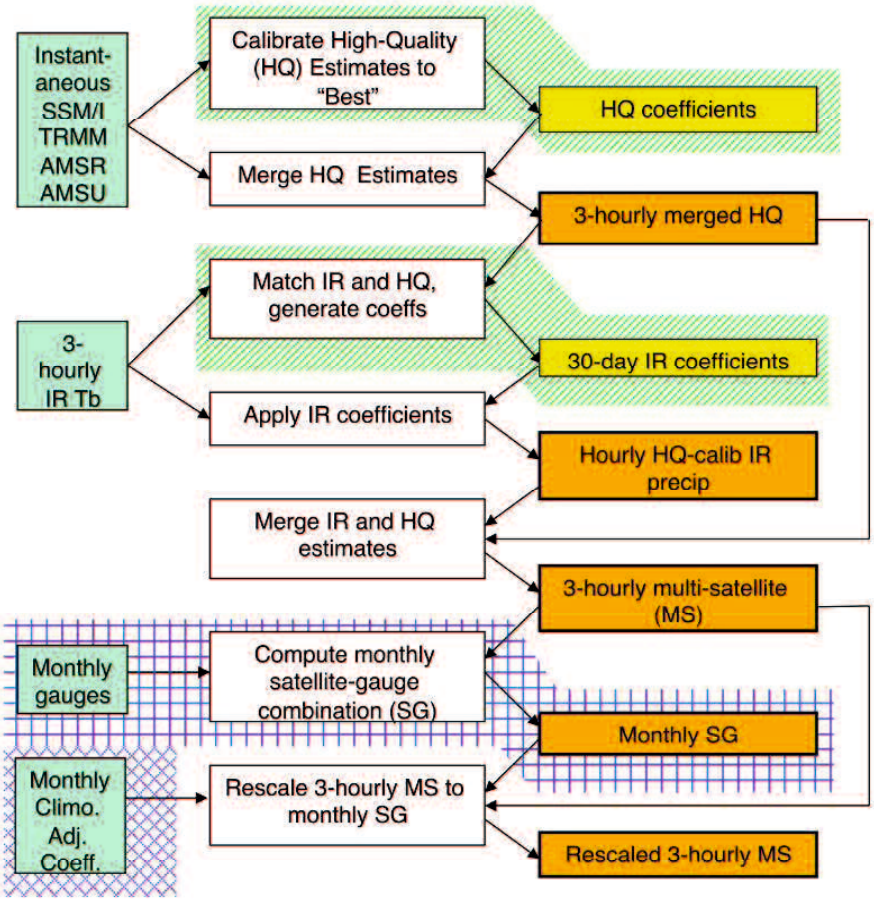

Figure 1.4. Block diagram for the TMPA. Slanted hatched background indicates calibration steps that are different in the RT and research products. Square- and cross-hatched backgrounds indicate final RT and research calibration steps, respectively (Huffman et al., 2010).

The TMPA provides global coverage of precipitation over the 50° S–50 ° N latitude belt at 0.25 °×0.25 ° spatial, three-hour temporal resolutions for 3B42 and monthly temporal resolution for 3B43 (Huffman *et al*. 2007). The TMPA estimates are produced in five stages: (1) the microwave estimates of precipitation are calibrated and combined, (2) infrared precipitation estimates are created using the calibrated microwave precipitation, (3) the IR precipitation estimates are created based on the corrected microwave estimates, 4) the microwave and IR estimates are combined, and 5) an intercalibration is implemented and rescaling to monthly data is applied (Huffman *et al*. 2007; 2010; Maggioni et al., 2016). Detail block diagram to produce 3-hourly and monthly TMPA data is depicted in Figure 1.4. Figure 1.5 shows the snapshot for a particular 3-hourly period of representative of current "full" microwave coverage. The TMPA retrieval algorithm used for this product is based on the technique by Huffman *et al*. (1995,

1997) and Huffman (1997). The TMPA combines the IR-based Precipitation Estimation from Remotely Sensed Information using Artificial Neural Networks-Cloud Classification System (PERSIANN-CCS: Honget al., 2004) algorithm and retrievals from polar-orbiting microwave sensors on board LEO satellites to produce precipitation estimates at high spatial and temporal resolution with quasi-global coverage. The TMPA datasets consist of 45% precipitation from passive microwave radiometers (i.e., TRMM-TMI, AQUA-AMSR, and DMSP-SSMIs), 40% from operational microwave sounding frequencies (i.e., NOAA-AMSUs), and 15% infrared measurements from geostationary satellites (i.e., GOES, METEOSAT/MSG) (Mehta and Yang 2008).

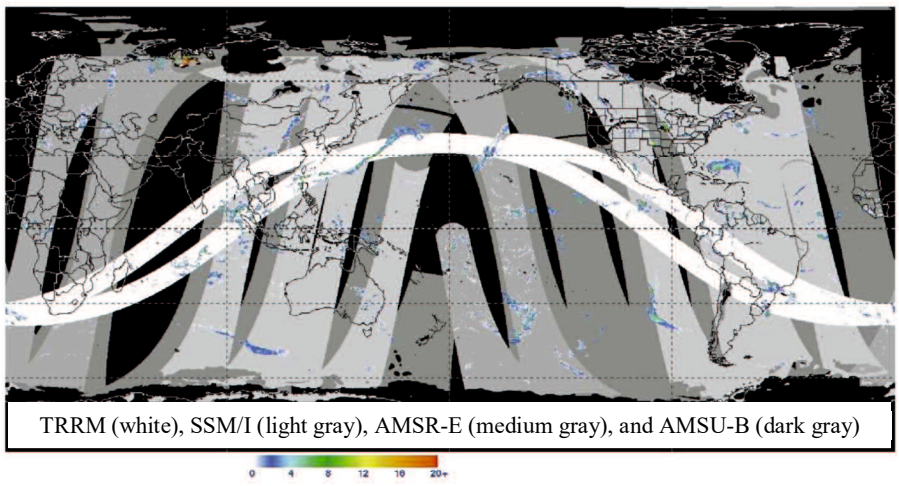

Figure 1.5. Combined microwave precipitation estimate (mm h^{-1}) for the 3-h period centered at 0000 UTC 25 May 2004. Blacked-out areas denote regions that lack reliable estimates, while the zero values in the remaining areas are color-coded to depict the coverage by the various sensors (Huffman et al., 2007).

1.3 Research Motivation

Indonesia as the Maritime Continent (MC) is one of the most high rainfall countries in the world and has a wide ocean that is located between the Pacific and Indian Oceans. Furthermore, the rain gauges are only located over land and not in the Indonesian sea. This is the reason of difficulty to conduct studies in rainfall variability over Indonesia. Using the remotely sensed meteorological satellite data is one of the solutions for that problem to record the rainfall data in the land and ocean simultaneously.

Rainfall is the most important dimension of weather variations in Indonesia and has great impacts on human life, especially for economy and agriculture. Longer dry season results in

extreme drought which contributes to a large forest and peat fires, and air pollution as well as haze from biomass burning (Bell and Halpert, 1998; Gutman *at al.*, 2000; Waple and Lawrimore, 2003; Irawan, 2003; Heil *et al*., 2007; D'Arrigoa and Wilson, 2008; Chrastansky and Rotstayn, 2012). Severe drought also damages agricultural production in Indonesia, causing negative consequences for rural incomes, food prices, and food security (Naylor et al., 2007). In addition, too heavy rainfall in the peak of the wet season may produce devastating floods and landslides (Yamanaka et al., 2008; Liao et al., 2010). In January-February 2007, for example, the Indonesia's capital of Jakarta suffered serious flood damage, affected 80 separate regions in and around the city, leaving behind over 100 dead and over 300,000 affected, and has caused Rp 8 trillion (US$879.12 million) in losses (Wu et al., 2007; Aldrian, 2011). In 2013, 17 landslides in Indonesia killed 402 people, meanwhile 243 people were killed as results of 13 landslides in 2007 (Liao et al., 2010). During prolonged drought in 1997, peat burning and forest fires in Indonesia released carbon to the atmosphere between 0.81 and 2.57 Gigatonnes, which is equivalent to the 13-40% annual mean of global carbon emissions by fossil fuels (Page et al., 2002). On the other hand, in Java, the strong El Niño event in 1997–1998 caused a reduction in rice-cultivated area of 700,000 hectare (ha) and a cumulative production loss of 3.2 million tons of milled rice (Oktaviani et al., 2011).

Spatial and temporal information of rainfall is essential for Indonesia region. The Indonesian region is the largest archipelago with complex topography and mostly surrounded by ocean. The seasonal to inter-annual variabilities of Indonesian rainfall are characterized mainly by the monsoon (Ramage, 1971) and atmosphere-ocean interactions near Indonesia such as the El Niño-Southern Oscillation (ENSO; hereafter conventional El Niño) and the El Niño Modoki, (Ropelewski and Halpert, 1987; Saji et al., 1999; Saji and Yamagata, 2003b; Ashok et al., 2007; Ashok and Yamagata, 2009; Wang and Hendon, 2007; As-Syakur et al., 2016). The meteorology of Indonesian rainfall has been described recently by Oldeman (1977); Haylock and McBride (2001); Hamada et al. (2002); Hendon (2003) Aldrian and Susanto (2003); Moron et al. (2010); and Qian et al. (2010), particularly using rain gauge data or the model outputs. On the other hand, studies on the relationship between rainfall and ENSO or El Niño Modoki in Indonesia also be carried out at many locations (e.g. Weng et al., 2007; Aldrian *et al.*, 2007; Saji and Yamagata, 2003b; Ropelewski and Halpert, 1987). However, the analyses in the Indonesian region, the complex system of islands and shallow seas, still show substantial errors when interpolated rain gauge data or climate model outputs are used to assess rainfall characteristic (Aldrian et al.,

2005; Love et al., 2011). Hence, intensive improvements are expected by using satellite data with better spatial and temporal resolution in investigating Indonesian rainfall characteristics.

Before satellite observation, it was difficult to observe global land-ocean rainfall distribution concurrently (Kubota *et al*., 2010). Although satellite observations are now available, the rainfall data from meteorological satellites have not been fully validated, especially over Indonesia, and need any comparisons with rain gauge data over land, with the assumption that measurements by rain gauges are more reliable than by satellites. Using accurate measurement of rainfall is essential to investigate spatial pattern of rainfall at local, regional and global scale (Cai et al., 2015). In recent years, satellite-based observations have been providing more spatially coherent picture of the rainfall variability over the region (e.g. Hall and Vonder Haar, 1999; Sorooshian et al., 2002; Nesbitt and Zipser, 2003; Mori et al., 2004; Janowiak et al., 2005; Ichikawa and Yasunari, 2006; Yang and Smith, 2006). However, complete studies analyzing the patterns of climatic rainfall characteristics over Indonesia with long-term satellite data have not been conducted.

Motivated by the facts described above, this study will use the TMPA products (Huffman et al., 2007) as rainfall data, to know the spatial and temporal patterns of rainfall over Indonesia. TMPA is a calibration-based sequential scheme for combining precipitation estimates from multiple satellites, gauge analyses where feasible, as well as providing a global coverage of precipitation at fine spatial resolution (0.25° x 0.25°) and 3-hourly temporal resolutions for 3B42 and monthly temporal resolution for 3B43 products (Huffman et al., 2007). In general, this dissertation will be analysing TMPA data to understand the rainfall variability in annual, seasonal and monthly basis.

1.4 Research Problem

The study aims to determine the quality of satellite meteorology of the TMPA products and their application for Indonesian region. For this purpose, different research aspects and approaches are examined. The research questions that will be answered are stated below. Problems were found:

1. Due to the limited rain gauges in Indonesia, satellite precipitation products are indispensable to observe Indonesian rainfall. Since satellite data show a few drawbacks for tropical regions, comparisons between rainfall from TMPA and rain gauges over Indonesia is important to find out the accuracy level of the satellite data;

2. Indonesian region consists of multitudes of large and small islands and seas. Spatial and temporal rainfall information from satellite is essential to understand climate rainfall variability over large complex area of Indonesia;
3. Understanding the MC rainfall variability is important. The use of satellite data is expected to explain rainfall climate system and their associations with monsoons, complex topography, ENSO and El Niño Modoki; and
4. To reveal the seasonal differences on diurnal rainfall change, which is the most significant variations in the Maritime Continent, by utilizing long-term (17 years) 3-hourly TRMM 3B42 over the Sumatera Island.

1.5 Research Scope and Objectives

The objectives of this research are:

1. To validate the TRMM 3B43 and 3B42 rainfall products by using ground-based rain gauge measurements across Bali and Indonesia;
2. To identify the Indonesian rainfall variability by using TRMM 3B43 products from the aspects of the monsoon impact, the existence of land-sea areas, and the diversity of topography, and to show the capability of these products to contribute to analysis of climatic-scale rainfall in Indonesia;
3. To determine MC rainfall characteristics and their associations with monsoons, complex topography, ENSO and El Niño Modoki by using TRMM 3B43 product; and
4. To utilize the long-term 3-hourly TRMM 3B42 products to know the seasonal differences of spatial/temporal patterns on diurnal rainfall variations over the Sumatera Island.

1.6 Research Structure and Outline

The dissertation is divided into five chapters. Figure 1.6 describes the outline of the dissertation. Generally, the dissertation is organized as follows:

Chapter 1 presents the introduction of the research. The chapter discusses the general introduction and basic motivation of this research. The research problem and research scope are listed and the research objectives are given. In addition, overview of the study area is also described.

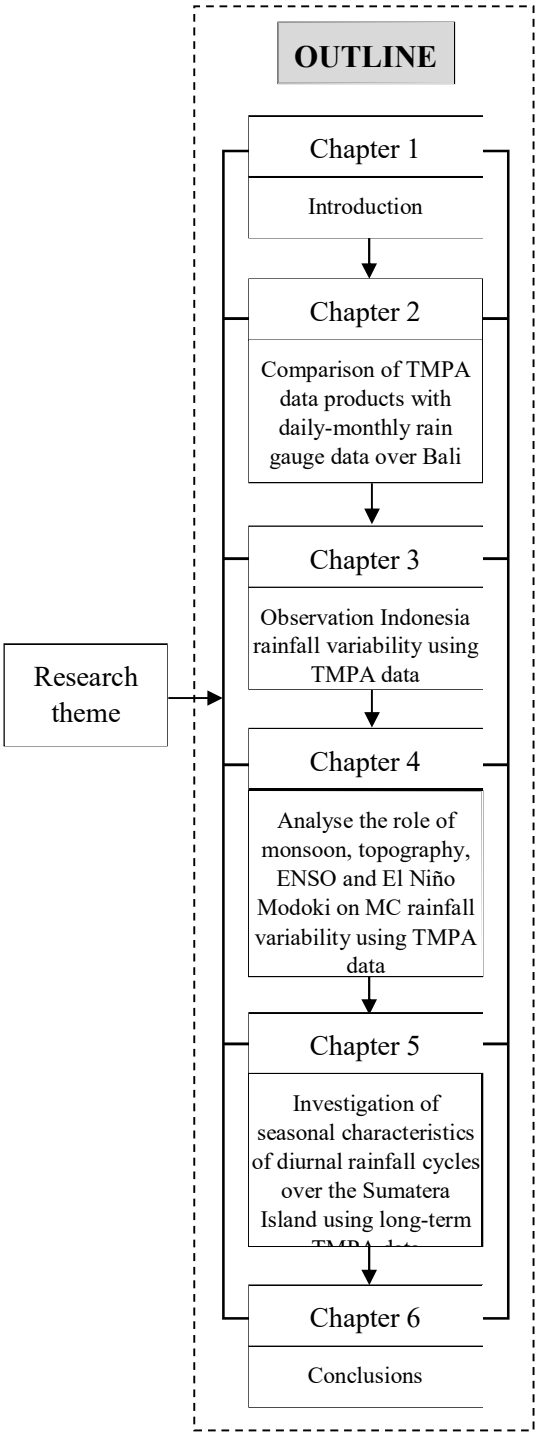

Figure 1.6. Outline of the dissertation

Chapter 2 describes the first result of this research. This chapter shows comparison results of TMPA 3B42 daily product and 3B43 monthly product with rain gauge data over Bali.

Chapter 3 illustrates the second result of this research. This chapter presents the analysis of 3B43 monthly data to understand the variability of Indonesian rainfall on annual, seasonal and monthly scales, as well as their connection with monsoon activity, land-sea scattering, and topography distribution.

Chapter 4 presents the third result of this research. This chapter explains the role of monsoon, topography, ENSO and El Niño Modoki on Indonesian rainfall variability by analyzing monthly TRMM 3B43 data.

Chapter 5 displays the fourth result of this research. This chapter describes the seasonal differences on diurnal rainfall variations by utilizing long-term (17 years) 3-hourly TRMM 3B42 data over the Sumatera Island.

Chapter 6 presents the conclusions of the studies and discusses the possible extension of future works.

1.7 Overview of Study Area

1.7.1 Bali Province

The research described in chapter 2 was conducted over Bali, Indonesia, located at 8°3'40" S – 8°50'48" S and 114°25'53" E – 115°42'40" E with a total area of 5,636.66 km^2 (Figure 1.7). The study area is classified as having a tropical monsoon type of climate, resulting from the monsoon winds, which change direction according to the seasons. Most areas of Bali are mountainous with hills that run from west to the east in the centre of the island. Generally, the land use in this island is dominated by agriculture comprising 65.35% of our study area.

1.7.2 Sumatera Island

The research described in chapter 5 was conducted in the Sumatera Island and the surroundings, which are located at 09°30' N to 12°10' S latitude and 89°10' to 109°35' E longitude. Figure 1.8 illustrates the distribution of Sumatera Island and surrounding area with topographic distribution. Sumatera Island and the surroundings are located in the most active convection area of the world and are influenced by the Asian-Australian monsoon, tropical convective zones, intra-seasonal oscillation, complex land-sea-topography, and regional-local atmosphere-ocean interactions (Chang et al., 2005; Rauniyar and Walsh, 2011; As-Syakur et al., 2013; Peatman et al., 2014).

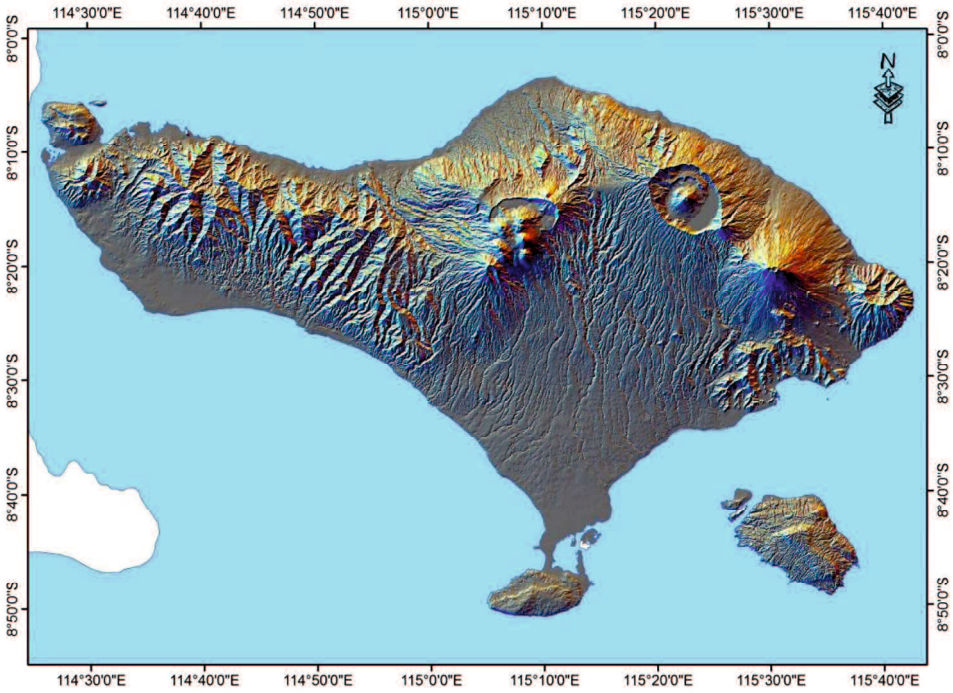

Figure 1.7. The study area of Bali Province, Indonesia with topography.

1.7.3 Indonesia

The research in chapter 3 was conducted in the archipelago of Indonesia which is composed of 17,508 islands with various sizes and located between two continents and oceans (Figure 1.9). The area covers 8°00’ N to 13°45’ S and 92°00’ E to 141°30’ E. The population of Indonesia is reaching 237,641,326 people in 2010. Sumatra, Kalimantan, Jawa, Sulawesi and Papua are five major islands with diverse topographical distributions. Several important mountains in Indonesia are Jayawijaya in Papua, Bukitbarisan in Sumatra, Kendeng in Jawa, Fenema and Gorontalo in Sulawesi, and Muller in Kalimantan. Jawa Island is the most populated island and most important industrial and agricultural region in Indonesia. Meanwhile, Sumatra, Kalimantan, Sulawesi, and Papua are important islands that have tropical rain forests. Small islands in Indonesia are also unique and important, such as Bali, Lombok, and Halmahera.

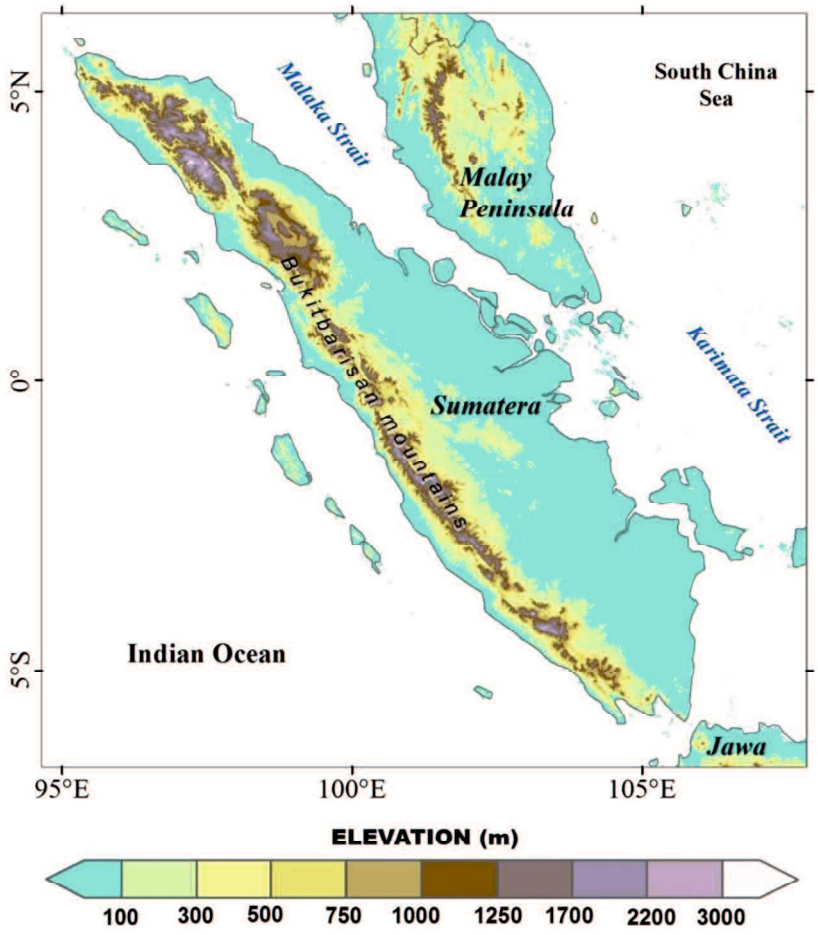

Figure 1.8. Sumatera Island with topography.

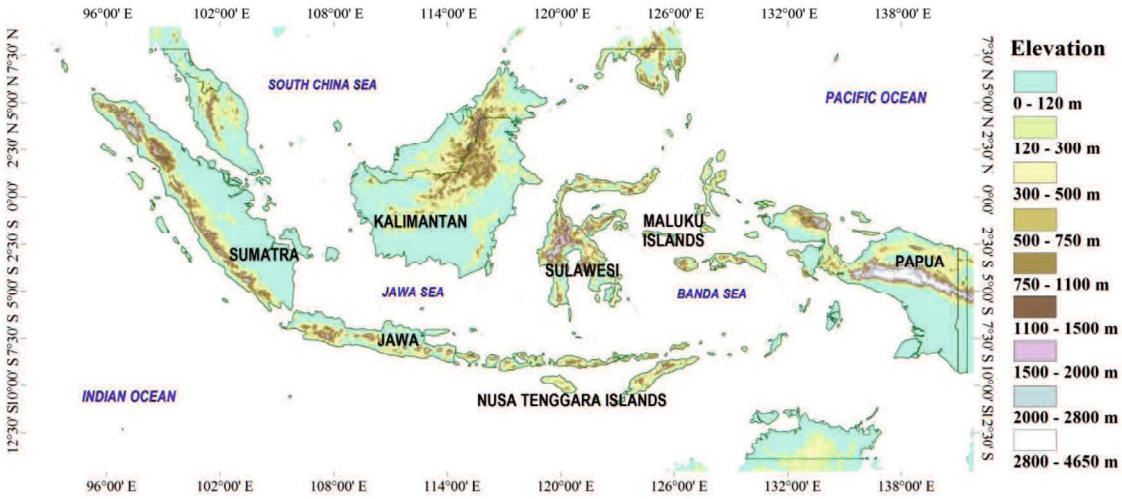

Figure 1.9. The Study area of Indonesia with topography.

CHAPTER 2

Comparison of TRMM Multi-Satellite Precipitation Analysis (TMPA) Products and Daily-Monthly Gauge Data over Bali

2.1 Introduction

Precipitation is probably the most important component in the mixture of hydrologic cycle parameters and is mostly accountable for shaping the climatic state of water in the earth, its variability, and climatic trends (Anagnostou 2007). Accurate and timely knowledge of global precipitation is essential for understanding the multi-scale interactions among weather, climate and ecological systems as well as for improving our ability to manage freshwater resources and predict high-impact weather events including hurricanes, floods, droughts and landslides (Hou *et al.* 2008). However, measuring precipitation is one of the most difficult observational challenges of meteorology because precipitation occurs intermittently and with pronounced geographic and temporal variability (NOAA 2006).

Previous estimates of tropical precipitation have been made on climate prediction models and the occasional inclusion of very sparse surface rain gauges and/or relatively few measurements from satellite sensors (Feidas 2010). Rain gauge observations yield relatively accurate point measurements of precipitation but suffer from sampling errors in representing areal means and are not available over most oceanic and unpopulated land areas (Xie and Arkin 1996, Petty and Krajewski 1996). Remote sensing techniques such as those using radar or satellites are complementary methods for monitoring rainfall over large areas (Chokngamwong and Chiu 2004). A combination of gauge data, radar and satellite measurements is ultimately needed to improve space-time rainfall estimation (Chiu *et al.* 2006a).

Infrared and passive microwave satellite observations, such as the Tropical Rainfall Measuring Mission (TRMM) Multi-Satellite Precipitation Analysis (TMPA) Products, could be used to drive estimates of large-scale precipitation over much of the globe (Xie and Arkin 1996). The TMPA rain products are based on first using the TRMM Precipitation Radar (PR) and the TRMM Microwave Imager (TMI) combined with rain rates to calibrate rain estimates from other microwave and infrared (IR) measurements (Huffman *et al*. 2007). The TMPA product is better

suited for the present study because the available rain gauge measurements are also used in the calibration process (Mehta and Yang 2008).

Extensive details about the TRMM ground validation program, site descriptions, algorithms, and data processing are provided by Wolff *et al*. (2005). For years, other groups studied different locations to validate TRMM data. For example, Feidas (2010) used satellite rainfall over Greece, Mehta and Yang (2008) used TRMM to provide an improved description of the climatological features over the Mediterranean Basin, Su *et al.* (2008) used TMPA to make hydrologic predictions in the La Plata Basin, Islam and Uyeda (2007) determined the climatic characteristics of rainfall over Bangladesh, Ikai and Nakamura (2003) calculated rain rates over the Ocean, Nicholson *et al.* (2003) validated TRMM rainfall for West Africa, Barros *et al.* (2000) studied a monsoon case in Nepal, Chiu *et al.* (2006a) compared TRMM with the rain rate over New Mexico, and Chokngamwong and Chi (2004, 2006) compared the TRMM with rain gauge data in Thailand.

Rainfall information is especially important in the tropics because such a large fraction of the planet's rain falls within low latitudes and because there are large variations therein that are related to climatic events (Adler et al. 2000; Ropelewski and Halpert 1987; Saji and Yamagata 2003b). The tropical Indonesian archipelago is characterized by huge quantities of rainfall throughout the year and plays an important role in Earth's climate system (Ramage 1971). Very warm seawater in and around the Indonesia induces very intense convective activities playing the role of a major heat source driving atmospheric circulation (Hamada et al., 2003). Annual and interannual climate variability in Indonesia is somewhat unusual, as it is not homogenous over the whole region and the coherence of rainfall patterns varies seasonally (Haylock and McBride 2001). Indonesian rainfall information is necessary for the study of climatology, flood predictions, landslide mitigations, irrigation plans, and water resource problems. Overall, rain is the most important climate elements in Indonesia because the diversity and variability depend on the time and space. Therefore, the study about climate in Indonesia focused more on the rain factor.

Generally, rainfall patterns of the Bali area are influenced by monsoons, with the maximum amount of precipitation occurring during the peak of the wet season from December to February and decreasing to a minimum during the peak of the dry season from June to August (As-Syakur 2007, Aldrian and Djamil 2008). In addition to being influenced by monsoons, the rainfall of the

region is also related to large-scale climatic phenomena such as the El Nino southern oscillation (ENSO) (Aldrian and Susanto 2003). Moreover, complex topography also affects rainfall fluctuations (Aldrian and Djamil 2008). In the region of our study, the wet season begins in November and lasts until April, and the dry season begins in May and lasts until October (Hendon 2003, Aldrian and Djamil 2008). The peak of the wet season in January coincides with the northwest monsoon across the Australian-Indonesian region, known locally as the *west monsoon*. Conversely, the dry season coincides with the southeast monsoon, known locally as the *east monsoon* (Hendon 2003). The west and east monsoon rain rates have distinctive features in Bali as well as in the parts of Indonesia that experience monsoons.

In this work, attempts have been made to compare the rainfall determined by TMPA products, which is a combination of TRMM PR and TMI, with the values taken from ground-based rain gauges in Bali. The main objective of this paper was to advance our quantitative understanding of the capability of these products to contribute to analyses of climatic-scale rainfall.

2.2 Study Area

Our research was conducted in Bali, Indonesia, located at 8°3'40" S – 8°50'48" S and 114°25'53" E – 115°42'40" E with a total area is 5,636.66 km^2 (see Figure 2.1). The study area is classified as having a tropical monsoon type of climate, resulting from the monsoon winds, which change direction according to the seasons. Most areas of Bali are mountainous with hills that run from west to the east in the centre of the island. Generally, the land use in this island is dominated by agriculture comprising 65.35% of our study area.

2.3 Data and Validations

2.3.1 Data

Daily fields of precipitation from three rain gauges over the Bali Island were used as references to validate the satellite estimation. The rain gauge data were obtained from the Indonesian Meteorology, Climatology, and Geophysics Agency (BMKG) Bali region and cover the period from 1998 to 2002. The TRMM climate rainfall products used here for comparison with the reference gauge dataset are the TMPA that includes the TRMM and other satellite precipitation (3B42) analysis as well as the TRMM and other sources precipitation (3B43) analysis.

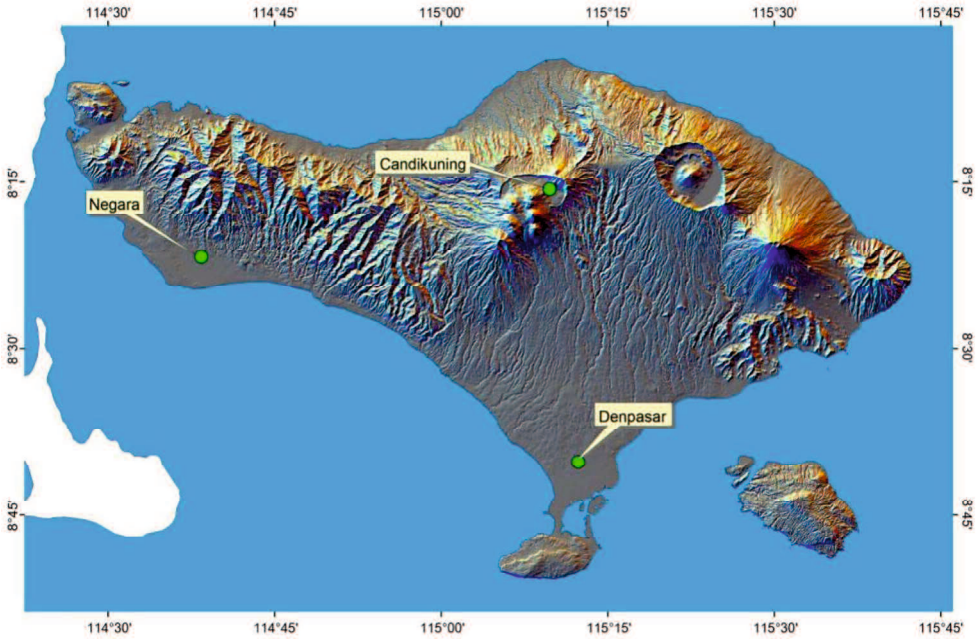

Figure 2.1. The study area.

The TRMM is cosponsored by the National Aeronautics and Space Administration (NASA) of the U.S.A. and the Japan Aerospace Exploration Agency (JAXA, previously known as the National Space Development Agency, or NASDA) and has collected data since November 1997 (Kummerow *et al.* 2000). TRMM is a long-term research program designed to study the Earth's lands, oceans, air, ice, and life as a total system (Islam and Uyeda 2007). The TRMM standard products are classified into three levels. Level 1 products are the calibrated and geolocated raw data. Level 2 products are derived-geophysical parameters at the same resolution and location as those of the level 1 source data. Level 3 products, referred to as climate rainfall products, are the time-averaged parameters mapped onto a uniform space-time grid (Feidas 2010).

According to Chiu *et al*. (2006b), the 3B42 and 3B43 estimates are the optimal combination results of microwave precipitation estimates that are used to adjust IR estimates from geostationary observations. Then, all available three-hour microwave-IR combination estimates are put into their appropriate space-time bins. These high-resolution data are summed over a calendar month to create a monthly multi-satellite (MS) product. Due to the lack of global gauge data on a daily basis, the 3B42 product is scaled so that the short-period estimates sum to a monthly total that includes monthly gauge analyses. The MS and gauge analysis is the result of a combination of monthly rainfall from the Climate Assessment and Monitoring System (CAMS)

and the Global Precipitation Climatology Centre (GPCC) rain gauge analyses and are merged optimally to create a post-real-time monthly satellite-gauge (SG) product, which is the TRMM product 3B43. The 3B42 is then scaled by the ratio of monthly MS to SG to match the monthly rain gauge analyses used in 3B43. The TMPA processing is designed to maximise data quality, so TMPA is strongly recommended for any research work not specifically focused on real-time applications (Huffman and Bolvin 2007).

2.3.2 Validations

The data coverage for this study was five years (1998–2002). The main validation was for the monthly satellite rainfall products, but similar measures were applied to the daily precipitation. Rainfall accumulations for the gauge observations and the satellite estimates were computed by aggregating the daily and monthly values. In this research, the satellite monthly data is obtained from 3B42 and 3B43. Previously, the 3B42 were computed by aggregating three-hour temporal resolutions during 24-hours to obtain daily rainfall data. 3B42 monthly data is obtained by aggregating the daily values. The validation of the monthly satellite products was also conducted separately for the two distinct seasons of the year (wet and dry season), which reflect the influence of the monsoon cycle. The wet season refers to the interval between November and April, and the dry season refers to the interval between May and October (Hendon 2003, Aldrian and Djamil 2008). Two types of analyses were conducted on the daily and monthly data: point-by-point analysis and areal average analysis.

Point-by-point analysis consisted of a comparison between gauge data with satellite data on a daily and monthly basis. All data were then sorted to obtain scatterplot distributions, the mathematical relationships and the error values. Areal average analysis consisted of an areal average comparison for monthly totals as well as for long-term mean of daily and monthly rainfall for the five-year period, where values for the three stations are spatially averaged. That analysis was used to obtain daily, monthly, and monthly time-series spatially averaged patterns.

Several statistical scores could be used to analyse the relationship of the TRMM product to the rain gauge data. The measures of the closeness of the satellite estimates to the observed values consisted of the linear correlation coefficient (r), the mean bias error (MBE), the root mean square error (RMSE), and the mean absolute error (MAE), which were defined as follows (Feidas 2010):

$$r = \frac{\sum_{i=1}^{n} (S_i - \overline{S})(G_i - \overline{G})}{(n-1)\,\sigma S\,\sigma G} \tag{2.1}$$

$$MBE = \frac{1}{n}\sum_{i=1}^{n} (S_i - G_i) \tag{2.2}$$

$$RMSE = \sqrt{\left(\frac{1}{n}\sum_{i=1}^{n} (S_i - MBE - G_i)^2\right)} \tag{2.3}$$

$$MAE = \frac{1}{n}\sum_{i=1}^{n} |S_i - G_i| \tag{2.4}$$

where S_i is the satellite estimated value on i-th day (month) for daily (monthly) analysis, G_i is the reference gauge value, $\overline{S}$ and $\overline{G}$ are the averages of satellite and rain gauge data, σS and σG are their standard deviations, and n is the number of data pairs. MBE represents the systematic component of the error by providing a measure of the overestimation or underestimation of the gauge data by the satellite estimates. In contrast, MAE and RMSE are used to ascertain the random component of the error in the satellite estimates. RSME involves the square of the departures from reality and, therefore, is sensitive to extreme values (Willmott 1982). If the RSME is used, then anomalous values could significantly change the evaluation of a TRMM when comparing it to rain gauge data. MAE uses the absolute difference, thus reducing the sensitivity to extreme differences. In our analysis, the MBE and RMSE were used to ascertain the systematic and the random components of the error, respectively, in our product estimates. The RMSE was calculated after the MBE was removed from the satellite estimates. All errors are expressed in percentage form to account for the daily, monthly and seasonal variations of rainfall in the area and, therefore, to evaluate the reliability of the TRMM product on the daily and monthly scale.

2.4 Results

This study first compared the daily rain gauge data with the 3B42 data. In general, rainfall from 3B42 was lower than the rainfall from the gauge data: the average rainfall from the rain gauge was 6.7 mm d^{-1}, whereas the average rainfall from 3B42 was 4.5 mm d^{-1}. Figure 2.2 shows the scatterplots of the daily gauge data versus 3B42. The amounts of data are also indicated in the plot. The 3B42 had a poor correspondence with the gauge data (r=0.28), and the MBE value

with the daily data was -2.24 mm d^{-1} (-33.50%). In addition, the values of the RMSE and MAE were 11.11 mm d^{-1} (166.04%) and 6.06 mm d^{-1} (90.53%), respectively.

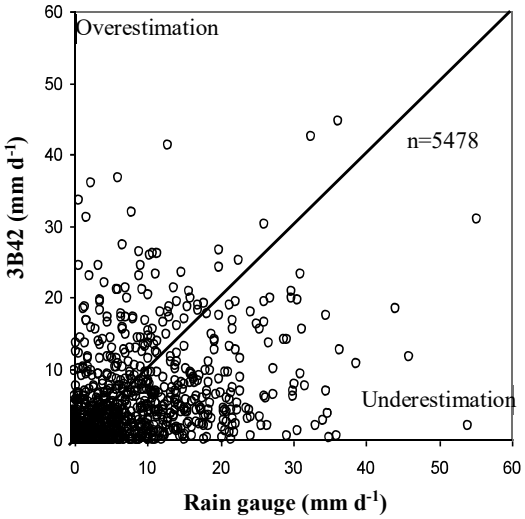

Figure 2.2. Scatterplots of daily TRMM products versus daily gauge data in the period from 1998 to 2002.

The validation result over each station is shown by scatterplot in Figure 2.3. Over Denpasar, the daily 3B42 had the correlation coefficient about 0.46, the MBE value of -1.52 mm d^{-1} (-26.48%), RMSE of 15.03 mm d^{-1} (261.58%) and MAE of 5.77 mm d^{-1} (100.48%). In Negara, the correlation coefficient, MBE, RMSE, and MAE were about 0.17, -2.01 mm d^{-1} (-31.12%), 18.76 mm d^{-1} (289.86%) and 8.06 mm d^{-1} (124.51%), respectively. In Candikuning, which is located on the top of mountain, the correlation coefficient, MBE, RMSE, and MAE were about 0.22, -3.19 mm d^{-1} (-40.60%), 16.52 mm d^{-1} (210.22%) and 8.58 mm d^{-1} (109.22%), respectively. Table 2.1 shows statistical error values of daily comparison between 3B42 and 3 rain gauge data over Bali.

Table 2.1. Daily point-by-point values of correlation coefficient, MBE, RMSE, and MAE for 3B42 compared to the 3 rain gauge data locations in Bali.

Rain Gauges	Elevation (m asl)	r	MBE (%)	RMSE (%)	MAE (%)
Denpasar	15	0.46	-26.48	261.58	100.48
Negara	24	0.17	-31.12	289.86	124.51
Candikuning	1247	0.22	-40.60	210.22	109.22

A comparison of long-term means of daily rainfall measured by 3B42 and gauges for the five-year period is shown in Figure 2.4. Daily rainfall was spatially averaged over the three

stations. Figure 2.4 indicates that the pattern of the long-term mean daily rainfall for the five-year period is similar on both data, whereas the average rainfall measured by TRMM differs substantially from the rain gauge values. The relationship between these data is slightly correlated (r=0.59) with an underestimated bias error. When comparison is made for each season separately, correlations in the wet period were lower than in the dry period. In the wet period, the correlation coefficients were 0.35, and in the dry period, the correlation coefficients were 0.57. In the wet period, the value of MBE was -3.08 mm d^{-1} (-29.08%), and the values of RMSE and MAE were 6.62 mm d^{-1} (62.40%) and 5.67 mm d^{-1} (53.46%), respectively. Furthermore, in the dry period, the value of MBE was -1.42 mm d^{-1} (-49.97%) with values of RMSE and MAE of 3.29 mm d^{-1} (115.55%) and 2.28 mm d^{-1} (80.17%), respectively.

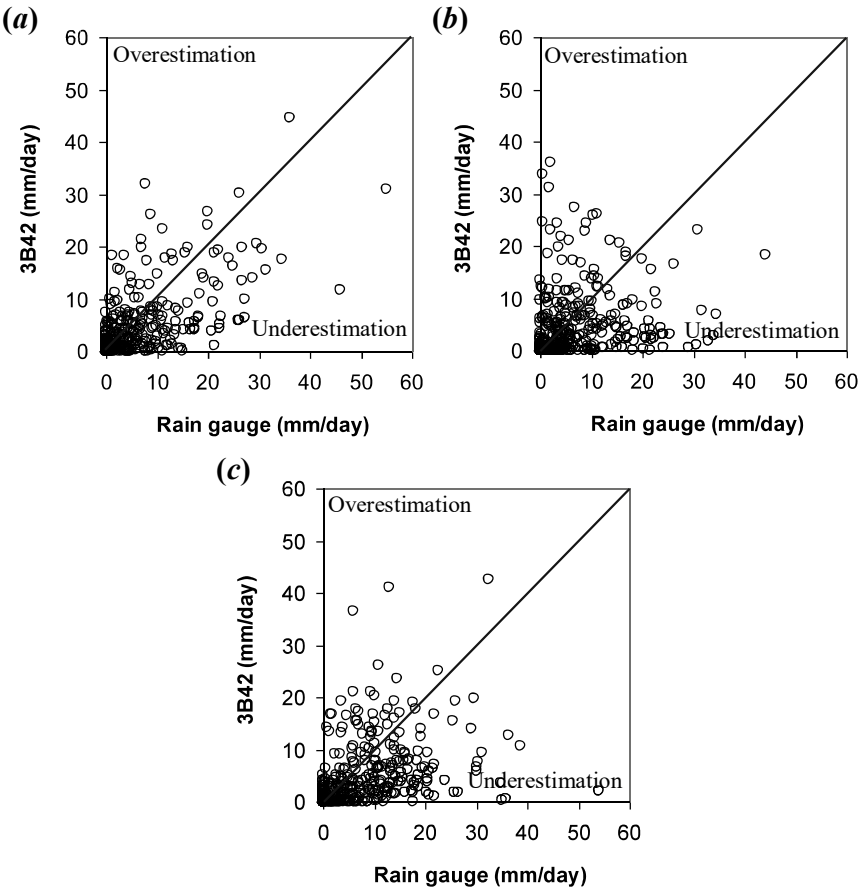

Figure 2.3. Scatterplots of daily 3B42 product versus gauge data over (a) Denpasar, (b) Negara, and (c) Candikuning.

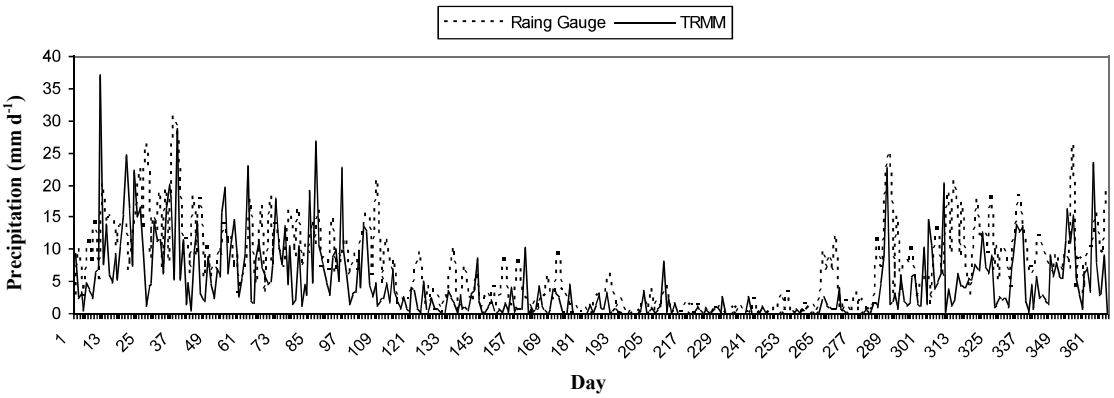

Figure 2.4. Long-term means of daily rainfall measured by 3B42 and gauges for the five-year period. Daily rainfall was spatially averaged over the three stations.

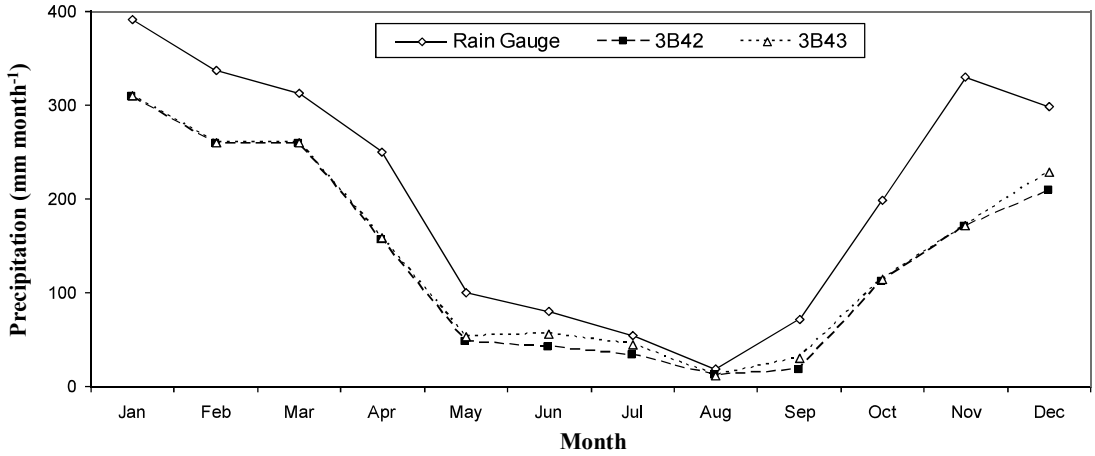

Figure 2.5. Monthly average rainfall pattern measured by TRMM and rain gauges. Spatially averaged over the three stations.

The second result of this research is the comparison between monthly rain gauge data and monthly TMPA 3B42 and 3B43 data, spatially averaged over the three stations. The intra-annual variation of the long-term mean monthly rainfall measured by TRMM and the rain gauge data, spatially averaged over the three stations are shown in Figure 2.5. This figure indicates that the patterns of monthly rainfall are quite similar. The data show very good agreement with the ground reference, yielding high correlations for these products. The correlation of 3B42 is 0.97, and the correlation of 3B43 is 0.96. The patterns of 3B42 and 3B43 are quite similar, which indicates that both types of data can be used as one reference to determine rainfall patterns in the locations that do not have a rain gauge. In Indonesia, the pattern of rainfall is important because Indonesia have a three different rainfall patterns (Aldrian and Susanto, 2003). Time-series of

monthly totals, spatially averaged over the three stations, for 3B42, 3B43, and gauge data, are shown in Figure 2.6. The amounts of data for each product are also shown in the figure. The time-series relationship between the rain gauge with 3B42 and 3B43 is very high (r=0.93).

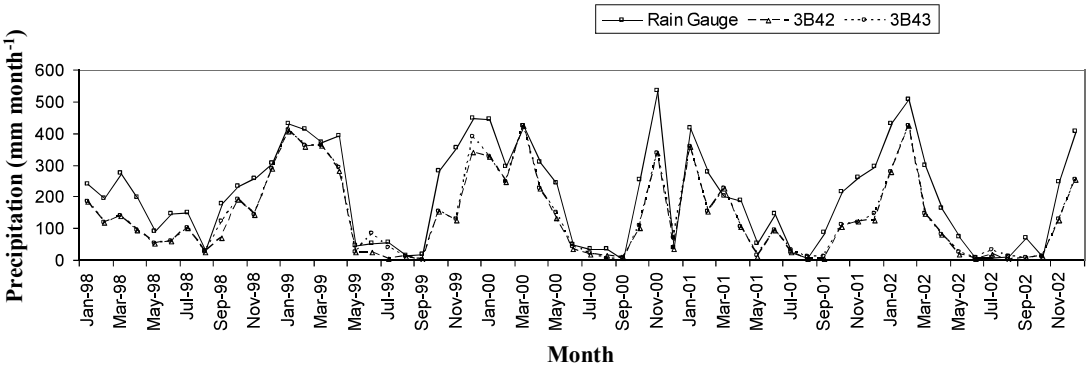

Figure 2.6. Time-series of monthly totals, spatially averaged over the three stations, for 3B42, 3B43, and gauge data from 1998 to 2002.

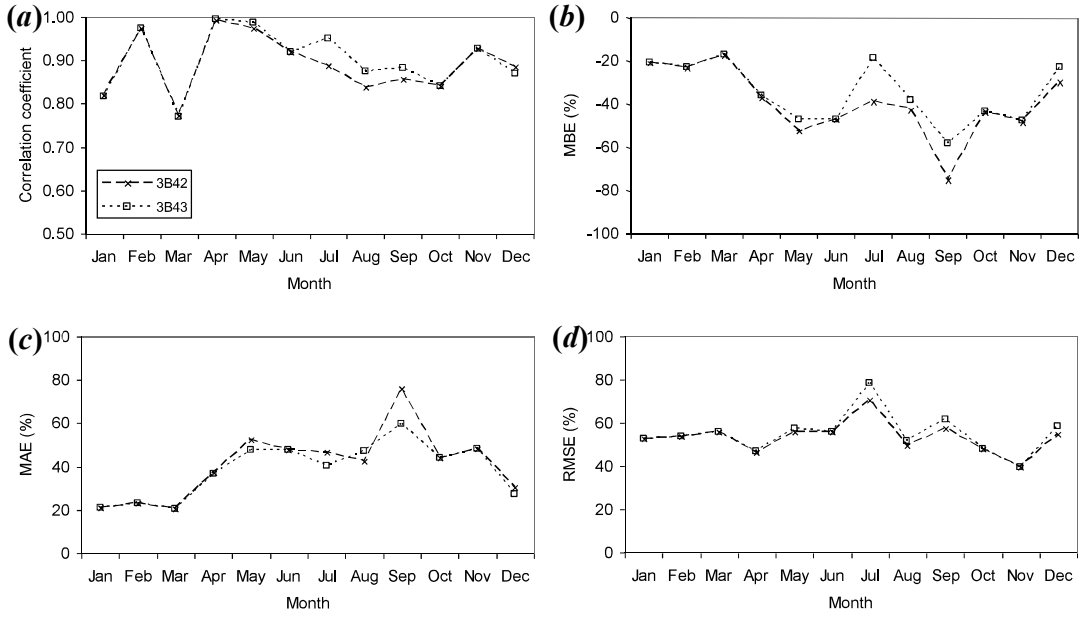

Figure 2.7. Monthly values of the error statistics of (*a*) the correlation coefficient, (*b*) MBA, (*c*) MAE, and (*d*) RMSE over the period from 1998 to 2002.

Figure 2.7 compares monthly values of the error statistics for the TMPA products. The correlation between 3B42 and 3B43 with gauge data is high (r>0.8) except in March (r=0.77). Correlation levels during the wet season are very unstable, whereas, in the dry season, they are quite stable. However, the correlation levels declined from the beginning until the end of the dry season. This trend occurred in both types of products (see Figure 2.7(*a*)). Bias and MAE values

have the same pattern in those products. In the beginning of the wet season, the values were low. Then, the values increased and stabilised in the mid-season before declining again at the end of the season. Unstable bias values seen during the dry season, especially for the 3B43 products, were low in July and high in September. The bias values of the 3B42 product were quite stable in the range of 38% to 47%, except in September (see Figure 2.7(*b*)). The same trend also occurred in MAE values during the dry season. The MAE values were relatively stable in the range of 40% to 52%, except in September (see Figure 2.7(*c*)). The value of the RMSE was relatively large in the range of 46% to 61%. However, the RMSE value was relatively stable, except in July and September (see Figure 2.7(*d*)). In general, if the random errors of a product estimate were more than 50% of the measured rainfall amount, then the estimates were deemed to not be reliable in relative terms.

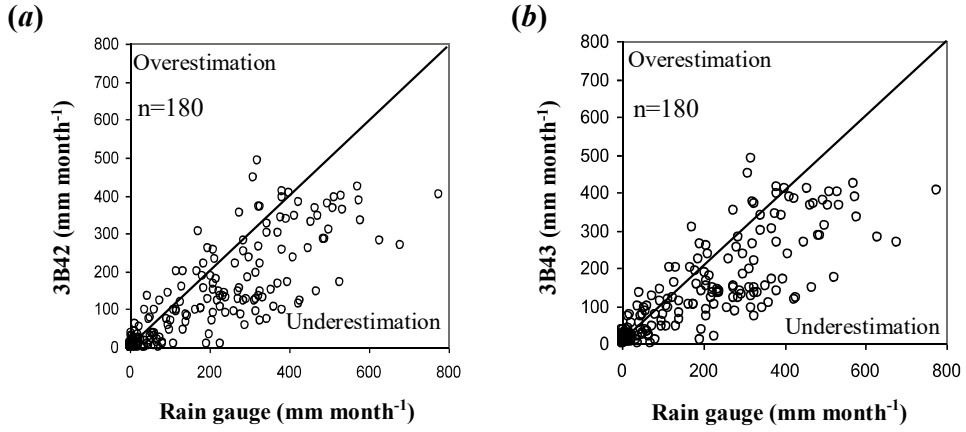

Figure 2.8. Scatterplot of the 3B42 and 3B43 product versus the gauge data for monthly rainfall (period 1998–2002) using (*a*) 3B42 and (*b*) 3B43.

In general, average monthly rainfall derived from TMPA was lower than the rainfall from the gauge data. The average rainfall from the rain gauges was 203.6 mm month^{-1}, whereas the average rainfall from 3B42 was 135.4 mm month^{-1} and from 3B43 was 141.3 mm month^{-1}. Figure 2.8 compares the scatterplots of the monthly TMPA products versus the gauge data. The amounts of data are also indicated in the plot. Monthly data show good agreement with the ground reference, yielding high correlation coefficients. The correlation between the monthly 3B42 and 3B43 with the reference data is generally high (0.81 and 0.82, respectively), but a lot of data have distributions that underestimate. This underestimation is evident from the negative bias error. The bias error of 3B42 is -33.50%, and the bias error from 3B43 is -30.60% (see Figure 2.9(*a*)). The other error statistic values between the two types of TMPA as compared with

the rain gauge data are quite similar; the MAE value is 28% (see Figure 2.9(*b*)), and the RMSE value is 34.12% for 3B42 and 32.61% for 3B43 (see Figure 2.9(*c*)).

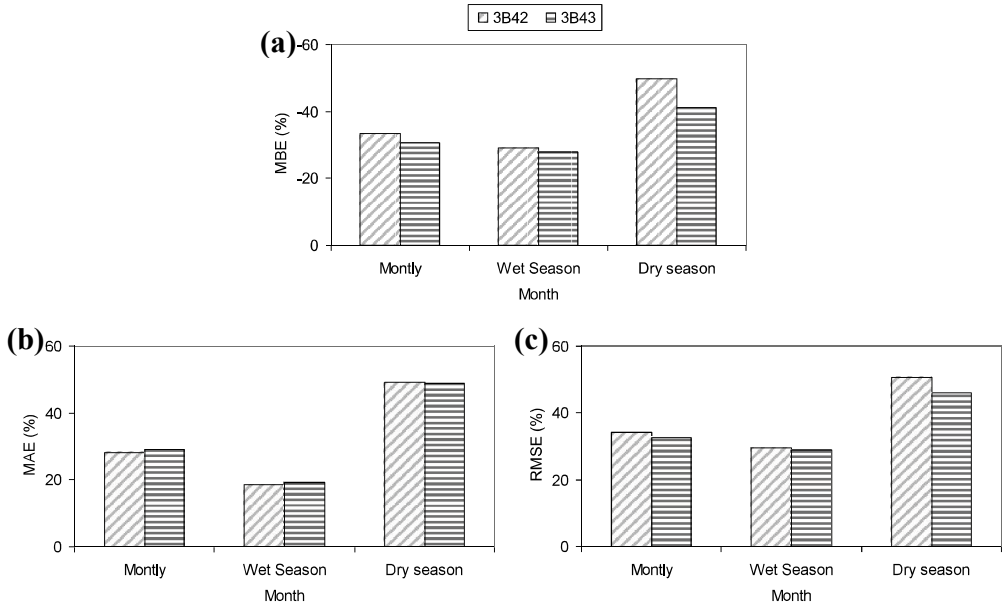

Figure 2.9. Statistical scores between the TMPA products and the rain gauge data for the monthly rainfall values and monthly rainfall for wet and dry season (period 1998–2002). (*a*) MBE, (*b*) MAE, and (*c*) RMSE.

In general, monthly point-by-point analysis results from 3 rain gauges over Bali indicate that the correlation coefficient between both TMPA products with rain gauge is high to very high (0.70 to 0.91), where the highest value occurs over Denpasar and the lowest over Negara. The point-by-point statistical error analysis from both 3B42 and 3B43 indicated that Denpasar has the lowest statistical errors, the highest MBE occurs over Candikuning, and the highest RMSE and MAE occurs over Negara. Point-by-point monthly values of the correlation coefficient, MBE, RMSE, and MAE for 3B42 and 3B43 compared to the 3 rain gauge data locations in Bali are summarized in Table 2.2. Figures 2.10 and 2.11 compare the scatterplots of the monthly 3B42 and 3B43 products versus the gauge data over 3 rain gauge stations, respectively.

Table 2.2. Monthly point-by-point values of correlation coefficient, MBE, RMSE, and MAE for 3B42 and 3B43 compared to the 3 rain gauge data locations in Bali.

Rain Gauges	Elevation (m asl)	r		MBE (%)		RMSE (%)		MAE (%)	
		3B42	3B43	3B42	3B43	3B42	3B43	3B42	3B43
Denpasar	15	0.90	0.91	-26.48	-22.10	46.50	44.56	35.85	32.99
Negara	24	0.71	0.70	-31.12	-27.80	54.39	54.26	46.13	44.80
Candikuning	1247	0.86	0.85	-40.60	-39.12	46.12	46.80	44.19	43.73

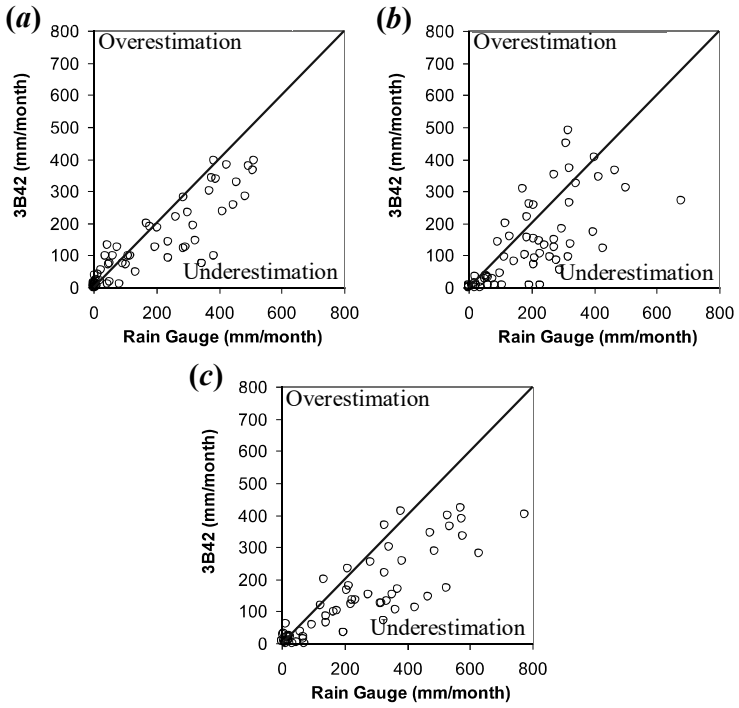

Figure 2.10. Scatterplot of the monthly 3B42 product versus the gauge data over (a) Denpasar, (b) Negara, and (c) Candikuning.

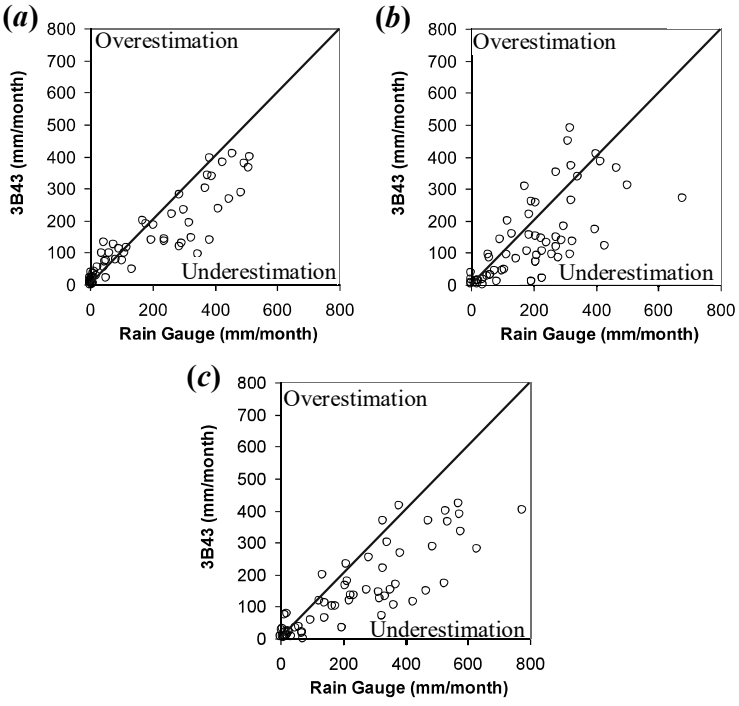

Figure 2.11. Same as Figure 2.10, but for monthly 3B43 product over (a) Denpasar, (b) Negara, and (c) Candikuning.

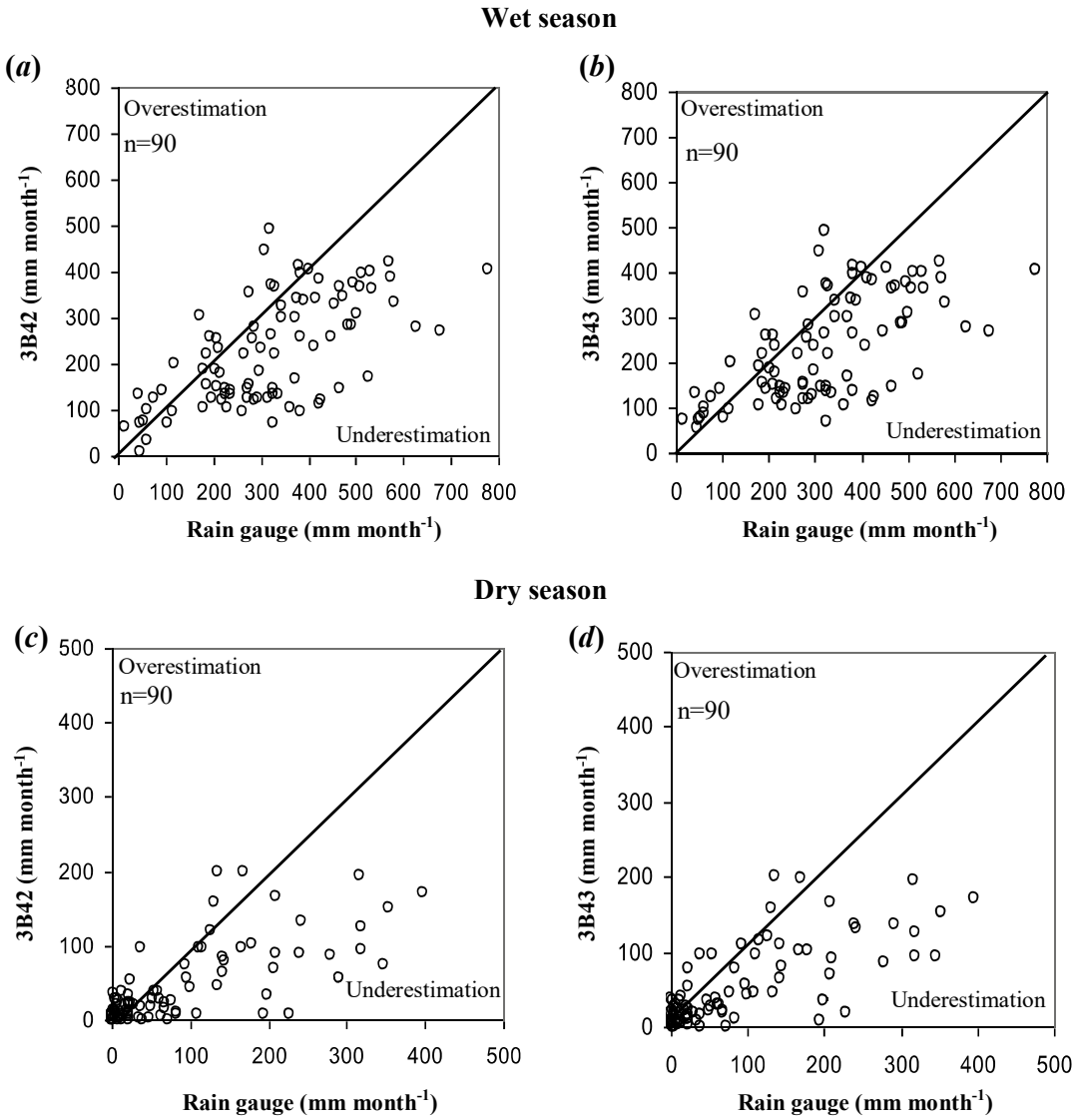

Figure 2.12. Scatterplots of the 3B42 and 3B43 product versus the gauge data for monthly rainfall for wet and dry season; (*a*) 3B42-wet season, (*b*) 3B43-wet season, (*c*) 3B42-dry season, and (*d*) 3B43-dry season.

The scatterplots of the monthly rainfall estimates of the two products against gauge data for the wet and dry period of the year are presented in Figure 2.12. The amounts of data for each product are also indicated in the plot. Coefficient correlations during the wet period were lower than in the dry period. The 3B42 and 3B43 had very similar scatterplots and correlations in wet and dry period, which is the same as the monthly condition. The only difference was in the level of correlation for each period season. The 3B43 was lower than 3B42 in the wet season (0.64 and

0.63, respectively), whereas in the dry season, 3B43 was higher than 3B42 (0.73 and 0.74, respectively). However, the differences were insignificant. Although the correlation during the dry season was better than during the wet season, this condition does not occur above statistical error. The value of the error statistic in the dry season was lower than in the wet season, and the statistical error value of 3B43 was better than the corresponding value for 3B42. Bias values between 3B42 with 3B43 were similar during the wet season, and, during the dry season, error values were relatively large (see Figure 2.9(*a*)). The MAE value was quite similar in these seasons (see Figure 2.9(*b*)), while, at the same time, random error values from 3B42 and 3B43 were similar in the wet season and relatively large in the dry season (see Figure 2.9(*c*)).

2.5 Summary and Conclusions

An overview of the comparison of the TRMM Multi-Satellite Precipitation Analysis (TMPA) products and daily to monthly gauge data from Bali Island is presented. An extensive comparison of the gauge observations and satellite-derived estimates of daily to monthly rainfall were performed over a five-year period on daily, monthly and seasonal timescales.

The comparison of five years of daily, monthly and seasonal variations of rainfall in the study site from TMPA combined with gauge data shows that the satellite gave lower values than the gauge estimates. The validation analysis demonstrated that both of the TRMM-merged rainfall products (3B42 and 3B43) showed very good agreement with gauge data in Bali on monthly-to-seasonal timescales. On the other hand, a very poor relationship was shown between the daily data analysis from 3B42 in comparison with the gauge data.

Because the daily data could only be obtained from 3B42, the daily analysis was only performed by this product. Very poor correlation was shown in the results of the point-by-point analysis. In contrast, a better daily correlation was obtained by averaging all points. This result indicates that point-by-point analysis would be very poor as a stand-alone daily climate product. Furthermore, if the 3B42 daily data were used to cover large areas by averaging, then this product would be capable of adequately estimating the variability in daily precipitation (see Su *et al.*, 2008).

The 3B42 and 3B43 products showed the same levels of relationships during the wet season and dry season. The error levels in the wet season were better than in the dry season. Monthly values of the error statistics showed instability during the rainy season. However, the instability did not affect the bias error, the absolute error or the random error. The 3B43 showed slight

improvements when compared with the 3B42 in terms of its abilities to reduce both the random error and the scatter of the estimates.

The intra-annual variation of the comparison statistics showed relatively high correlations between the satellite estimates and the gauge data during the dry season and lower correlations during the wet season. There were, however, higher error values when the correlation was higher, a behaviour that is opposite to what we would expect. This pattern has been also found by Feidas (2010). The lower rain amounts recorded during the dry season affect the situation. During the dry season, the amount of rainfall from the rain gauge data and the satellite data are small, and the level of correlation becomes lower while the error values become larger. However, because the error values in percentage, the error values become large even though the actual value of the rainfall (mm $month^{-1}$) error is small. The opposite trend occurs during the rainy season. This explains why the logarithms of 3B42 and 3B43 are not very accurate when the amounts of rainfall are low.

The accuracy levels of the rainfall data obtained from 3B42 and 3B43 are generally similar, as indicated by the correlation values between both data with the gauge data. However, error analysis shows that 3B43 is better than 3B42. In general, the data from TMPA are potentially usable to replace rain gauge data, especially with the monthly data if the inconsistencies and errors are taken into account.

CHAPTER 3

Indonesian Rainfall Variability Observation Using TRMM Multi-Satellite Data

3.1 Introduction

The Indonesian archipelago is a central atmospheric heat source characterized by huge quantities of rainfall, which are important contributions to understanding the world's climate system. Due to Indonesia's geographical location, rainfall is strongly influenced by the Asian-Australian monsoon system. Wyrtki (1961) described the peaks of the southeast monsoon as June–July–August (JJA), while the northwest monsoon peaks in December–January–February (DJF). The transition between monsoons occurs during the months of March–April–May (MAM) and September–October–November (SON). However, Susanto *et al*. (2006) described April and October as transition months between the northwest monsoon from November to March and the southeast monsoon from May through September.

Moreover, Indonesian rainfall is also influenced by year-to-year fluctuations in El Niño/Southern Oscillation (ENSO), El Niño Modoki, Indian Ocean Dipole (IOD) phenomenon (Vimont *et al*. 2010; Nicholls 1988; Saji *et al*. 1999), local air-sea interactions (Hendon 2003) and local topography (Chang *et al*. 2005; Qian 2008). The ENSO and El Niño Modoki events create extreme high and low rainfall values in some parts of Indonesia, resulting in the incidence of floods and droughts (Hendon 2003; Hamada *et al*. 2002; Saji and Yamagata 2003b). On the other hand, complex distribution of land, sea, and terrain, results in significant local variations of the annual rainfall cycle (Chang *et al*. 2005). The complex topography of the Indonesia islands affects the rainfall quantities (Sobel *et al*. 2011). The different solar heating between surface types such as land versus sea, or highland versus lowland, causes strong local pressure gradients (Qian 2008). The different solar heating produces in sea-breeze convergence over islands and orographic precipitation (Qian *et al*. 2010), causes diurnal cycle of rainfall over islands. Furthermore, heavy precipitation also could be found along coastal plains in some part of Indonesia, possibly due to ascent over near-coast hills or seaward propagating orogenic convective systems. Qian (2008) explained in convective process in the case of land–sea breezes.

The land heats up rather quickly during the day under the influence of solar radiation, while sea surfaces remain cooler because the thermal inertia of water is relatively large and because waves, turbulence, and penetration into deep water mix heat downward from surface water. As a result, convectional cells rise over land and sea breezes develop. At night, land cools off more rapidly than the ocean surface through longwave radiation loss, reversing the pressure gradients and forming land breezes.

Indonesia, covered mostly by ocean, is the world's largest archipelago. Therefore, there are several problems in studying and simulating rainfall of the region for an appropriate land–sea representation (Aldrian *et al*. 2007) and a complex topographical distribution (Qian 2008). In Indonesia, rain gauge data represents precipitation throughout the country. However, rain gauge measurement networks in the Indonesian archipelago are not as dense or regular as in other major continents. Thus, satellite observations of rainfall may be the best solution for adequate temporal and spatial coverage of rainfall. Remote sensing data provides spatial-temporal resolution covering large rainfall study areas (As-Syakur 2011) and has become a viable tool to capture the variability of the precipitation systems (Villarini *et al*. 2008). The availability and global coverage of satellite data offer effective and economical means for calculating areal rainfall estimates in sparsely gauged regions (Artan *et al*. 2007). Rainfall data with better spatial and temporal resolution allows a more quantitative understanding of causal links between Indonesian rainfall and larger scale climate features (Aldrian and Susanto 2003).

The Tropical Rainfall Measuring Mission (TRMM), jointly cosponsored by NASA and JAXA, has collected data since November 1997 (Kummerow *et al*. 2000). The main objective of TRMM data collection is to provide a better understanding of precipitation structure and heating in the tropical regions of the earth (Simpson *et al*. 1996). The TRMM standard products are classified into three levels. Level 3 products, referred to as climate rainfall products, are time-averaged parameters mapped onto a uniform space-time grid (Feidas 2010). Product level 3 TRMM 3B43 data are often called TRMM Multi-Satellite Precipitation Analysis (TMPA) products. The data products of 3B43 are the first rain products, combining TRMM Precipitation Radar (PR) and TRMM Microwave Imager (TMI) rain rates to calibrate rain estimates from other microwave and Infrared (IR) measurements (Huffman *et al*. 2007).

Over the years, several groups have studied Southeast Asia and its surrounding areas to validate TRMM data. TRMM derived product research included: Chokngamwong and Chiu

(2008) used rain gauge data from Thailand, As-Syakur *et al*. (2011) compared the TRMM 3B43-3B42 with rain gauge data in Bali-Indonesia, Fleming *et al*. (2011) evaluated the TRMM 3B43 using gridded rain-gauge data over Australia, and Semire *et al*. (2012) validated TRMM 3B43 rainfall for Malaysia. On the other case, Vernimmen *et al*. (2011) and Prasetia *et al*. (2013) validate for other types of TRMM in Indonesia. Vernimmen *et al*. (2011) compared and used real time TRMM 3B42 to monitor drought in Indonesia and Prasetia *et al*. (2013) validated TRMM Precipitation radar over Indonesia and was showed the accuracy is low to high (0.07 to 0.73). The results underscore the superiority of the TRMM products, especially for TRMM 3B43 and suggest that the goal of the algorithm was largely achieved.

Rainfall distribution information and the structure of precipitation systems from large areas of Indonesia are important for TRMM data validation. This study observes the Indonesian rainfall variability determined by TRMM 3B43 products, showing the capability of these products to contribute to analysis of climatic-scale rainfall in Indonesia. To validate the results, the rainfall estimated from satellite data were compared with gauge observations over Indonesia sought to determine how well the 3B43 product an adequate representation of monthly rainfall in Indonesia.

3.2 Study area

Research was conducted in the archipelago of Indonesia composed of 17,508 islands of various sizes. Spatial data covered 8°00’ N to 13°45’ S and 92°00’ E to 141°30’ E. Figure 3.1 indicates the distribution of Indonesian topography and six north-south cross section lines used to compare between values of rainfall and elevation. Indonesia is located between two continents and oceans with a population reaching 237,641,326 people in 2010. Sumatra, Kalimantan, Jawa, Sulawesi and Papua are five major islands with diverse topographical distributions. Several important mountains in Indonesia are Jayawijaya in Papua, Bukitbarisan in Sumatra, Kendeng in Jawa, Fenema and Gorontalo in Sulawesi, and Muller in Kalimantan. Jawa Island is the most populated island and most important industrial and agricultural region in Indonesia. Meanwhile, Sumatra, Kalimantan, Sulawesi, and Papua are important islands that have tropical rain forests. Small islands in Indonesia are also unique and important, such as Bali, Lombok, and Halmahera.

The Indonesian monthly rainfall pattern is dividing into 3 climate regions (Figure 3.2): Monsoonal Type (A), Semi-Monsoonal Type (B) and Anti-Monsoonal Type (C; Aldrian and

Susanto 2003). Region A has one peak and one valley rainfall which is influence by two monsoon systems, the Northwest Monsoon (wet seasons) from November to March, and the Southeast Monsoon (dry seasons) from May to September. Region B has two peaks of rainfall in October-November and March-May. Those two peaks are associated with the southward and northward movement of the inter-tropical convergence zone (ITCZ). Region C has one peak and one valley rainfall, namely June-July for the wet season and November-February for the dry season. There is strong evidence of Arlindo (Indonesia Trough Flow) ocean influence and due to the onshore windward movement of the austral winter monsoon from the southwest Pacific and Arafura Sea.

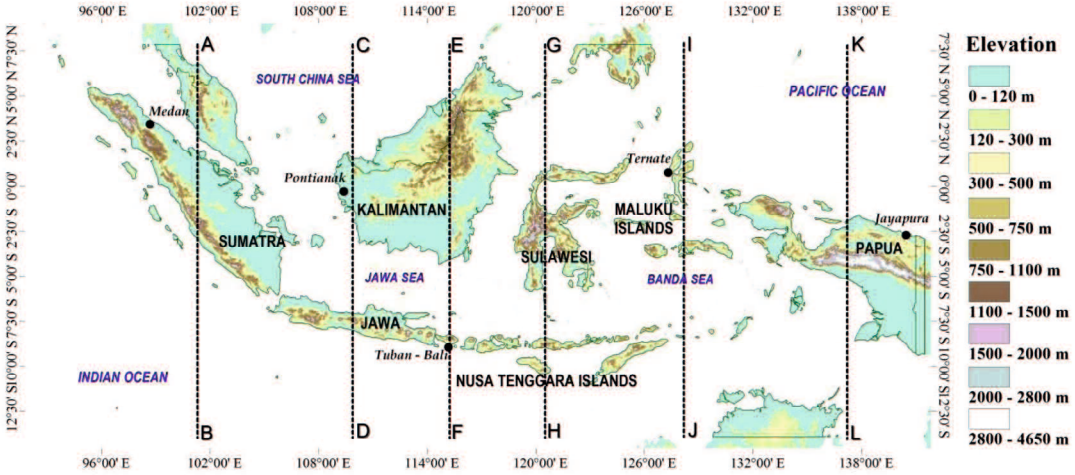

Figure 3.1. The Study area includes the Indonesian topography. Lines A-B to K-L indicating the south-north cross sections used to compare values of rainfall and elevation. Black dots indicating the rain gauges location

In addition, Hamada et al. (2002) classified Indonesian area into four climatological regions, based on analysis of the amplitude and phase of annual oscillation from the pentad-mean rainfall amounts average. The divisions of climatological regions are (Figure 3.3): A-I: Annual cycle is dominant, and the maximum rainfall occurs during September–February (during pentads 14–49); B-I: Annual cycle is dominant, and the maximum rainfall occurs during July–August or March–June (during pentads 1–13 or 50–73); A-II: Semi-annual cycle is dominant, and the maximum rainfall occurs during September–February (during pentads 14–49); and B-II: Semi-annual cycle is dominant, and the maximum rainfall occurs during July–August or March–June (during pentads 1–13 or 50–73). However, they also classify region with rainy and dry seasons do not clearly exist that called type-C.

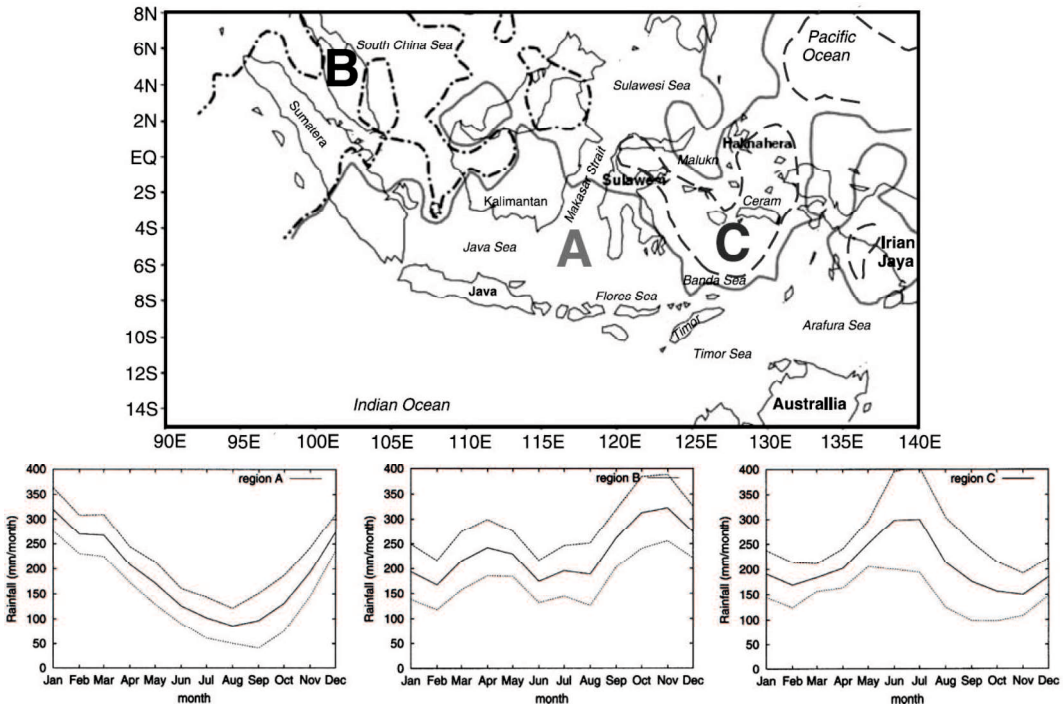

Figure 3.2. Three climate regions and their rainfall patterns from Aldrian and Susanto (2003). The map shows three climate regions divided into region A (solid curve); the southern monsoonal region, region B (dashed–dotted curve); the semi-monsoonal region and region C (long dashed curve); the anti monsoonal region. Graphics show the annual cycles of the three climate regions (solid lines). Dashed lines indicate one standard deviation above and below the mean average.

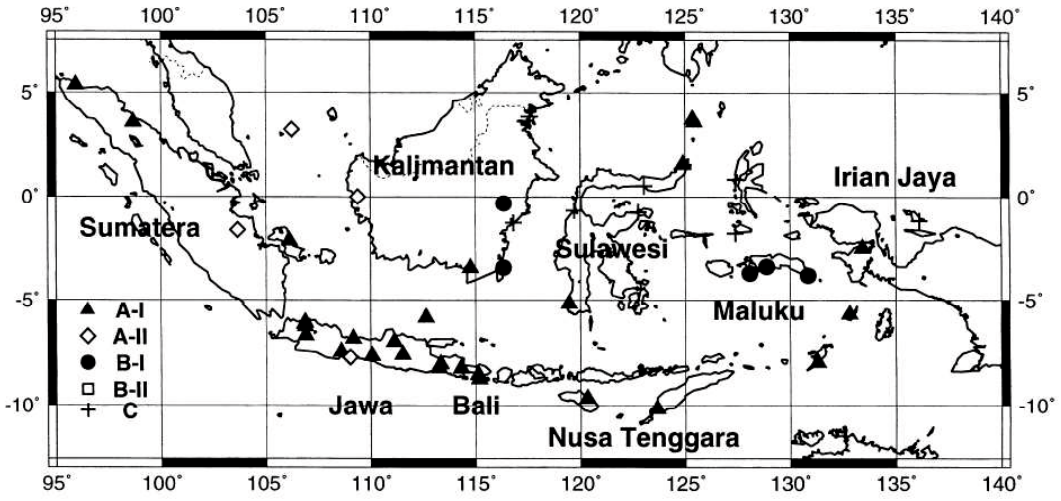

Figure 3.3. Climatological classification map base on Hamada et al. (2002) analysis. Type-A (type-B) means that maximum rainfall occurs during September–February (March–August). Type-I (type-II) means that annual (semi-annual) component is dominant. Plus symbols denote stations at which seasonal variations are not clear (type-C).

3.3 Data and Methods

Monthly Rainfall data from 1998 to 2010, measured and collected by TRMM 3B43 satellite data, were employed to observe Indonesian rainfall variability. The TMPA is a calibration-based sequential scheme for combining precipitation estimates from multiple satellites and gauge analyses (where feasible), providing global coverage of precipitation spatially over the 50° S–50° N latitude belt at 0.25° ×0.25° at 3-hourly temporal resolutions for 3B42, and monthly temporal resolution for 3B43 (Huffman *et al*. 2007). The TMPA estimates are produced in four stages: (1) microwave estimates of precipitation are calibrated and combined, (2) infrared precipitation estimates are created using the calibrated microwave precipitation, (3) microwave and infrared estimates are combined, and (4) monthly data is rescaled and applied (Huffman *et al*. 2007, 2010). The TMPA retrieval algorithm used for this product is based on the technique by Huffman *et al*. (1995, 1997) and Huffman (1997). The TMPA data sets consist of 45% precipitation from passive microwave radiometers (TRMM-TMI, Aqua-Advanced Microwave Scanning Radiometer (Aqua-AMSR) and Defense Meteorological Satellite Program – Special Sensor Microwave Imagers (DMSP-SSMIs)), 40% from operational microwave sounding frequencies (NOAA-AMSUs) and 15% infrared measurements from geostationary satellites [Geostationary Operational Environmental Satellite (GOES)] Meteosat/Meteosat Second Generation (Meteosat/MSG) (Mehta and Yang 2008). According to Huffman and Bolvin (2007), the TMPA is designed to maximize data quality, so TMPA is strongly recommended for any research work not specifically focused on real-time applications.

Several statistical scores were used to determine Indonesian rainfall variability. The types of analysis were monthly means, total means, maximum and minimum variability, standard deviation and trends. To investigate the effect of the Asian-Australian monsoon on Indonesia rainfall, peak-to-peak amplitude phase analysis extracted the annual signal in each grid point of rainfall. After calculating the mean of the annual signal the mean was removed to reveal the monthly peak amplitude phase. Furthermore, the analyses were also carried out for the effect of land area and topography on rainfall quantities. The distribution of island, sea and topography obtained from the Shuttle Radar Topography Mission (SRTM) mission were used to compare values of rainfall with regards to island distribution and elevation.

Monthly, seasonal and long-term time series analyses were conducted. Monthly analysis compared data from the same months of annual observation. Seasonal analysis is conducted

based on the monsoon activity, described by Wyrtki (1961), over the entire observation period. Likewise, long-term analysis observed all time series data over the entire observation period.

Monthly accumulated rainfall data from 5 rain gauges (derived from daily measurements) over Indonesia (see Figure 3.1), observed by the Indonesian Meteorology, Climatology, and Geophysics Agency (BMKG) standard manual (Observatory) and automatic (Hellmann) rain gauges, were used as references to compared satellite estimations. The rain gauge data cover the period from 1998 to 2010. These data were checked for consistency where unreasonable values from a climatological viewpoint, for instance zero-rainfall months during the wet season, were deleted. The locations of rain gauges are Medan, Pontianak, Tuban-Bali, Ternate, and Jayapura. The monthly average rainfall estimated from satellite data is compared with the rain gauges data, particularly to determine the accuracy level between the rainfall estimated from satellite and the rain gauges data. Point-by-point analysis was conducted on the monthly data. Point-by-point analysis consisted of a comparison between gauge data with satellite data.

3.4 Results and Discussion

3.4.1 The Indonesian rainfall variability

The distributions of annual averaged rainfall over Indonesia during 1998–2010 are shown in Figure 3.4. In general, the highest total annual rainfall extends across the equatorial belt. The lowest rainfall occurs in the southeastern Indonesia around the Nusa Tenggara Islands. The four main islands of Indonesia, except Jawa Island, show high annual rainfall. Complex topography affects rainfall quantities in this area (Sobel *et al*. 2011), such as in the Jayawijaya and Bukitbarisan Mountains of Papua and Sumatra islands, respectively. This figure also shows that rainfall was distributed more heavily over land than sea, except the west coast of Sumatra. These patterns were different than those modelled by Aldrian (2003) and Gunawan (2006) which showed higher rainfall over sea than land. Higher rainfall over land seems to be caused by the magnitude of convergence determined by the different heating qualities of land and sea. The differential heating controls the direction of land–sea breezes which distributes the precipitation centrally over islands where sea-breeze fronts converge between coasts, lifting moist air and triggering convection (Qian 2008). Figure 3.4 also shows the closer to the coast, the heavier rainfall distributed over sea especially at the western coast of Sumatra. Heavy rainfall found along the coastal plain possibly due to ascent over near-coast hills or seaward propagating

orogenic convective systems. Nocturnal rainfall activity along the coast in the western of Sumatra Islands is created by land breezes (from Bukitbarisan Mountains) converge with western Walker cell (from Indian Ocean) to generate offshore convection and produces heavy rainfall. As noted by Wu *et al*. (2009), the heavy rainfall offshore west of Sumatra Island is controlled by the mountainous topography of the island and by the thermally and convectively induced local circulations and diurnal changes in thermodynamic stability in the atmosphere offshore.

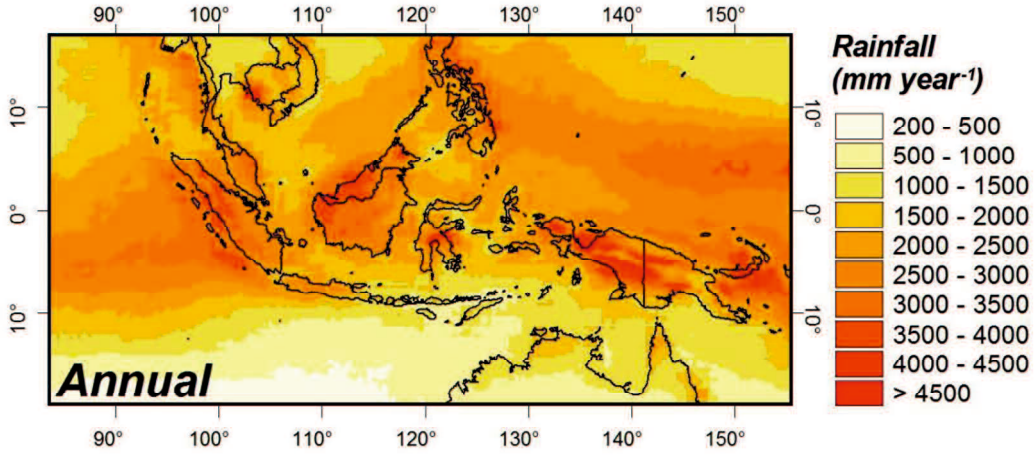

Figure 3.4. The distributions of annual averaged rainfall over Indonesia during 1998–2010

Figure 3.5 shows mean annual rainfall over land and sea in Indonesia during 1998–2010. The figure shows annual rainfall over land higher than sea. Over land the total mean rainfall was 2779.82 mm year^{-1} while over sea mean rainfall was 1998.21 mm year^{-1}. This condition makes it increasingly clear that Indonesian rainfall is greater over land than sea.

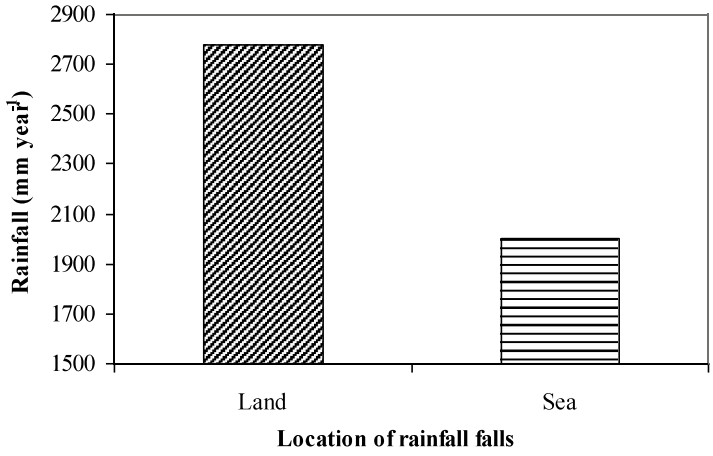

Figure 3.5. Total mean of annual rainfall values over land and sea in Indonesia during 1998–2010.

The monthly climatological mean of rainfall from January 1998 to December 2010 is shown in Figure 3.6. Throughout the year the highest rainfall concentrations are observed centered over the major Indonesian islands such as in Sumatra, Kalimantan, Papua and Sulawesi. During the northwest monsoon (November through February), high rainfall patterns are observed in all parts of Indonesia except the Nusa Tenggara region of islands. Around Nusa Tenggara high rainfall only occurs from December through March in southeastern Indonesia. The high rainfall in these months is consistent with the phase of the southwest monsoon.

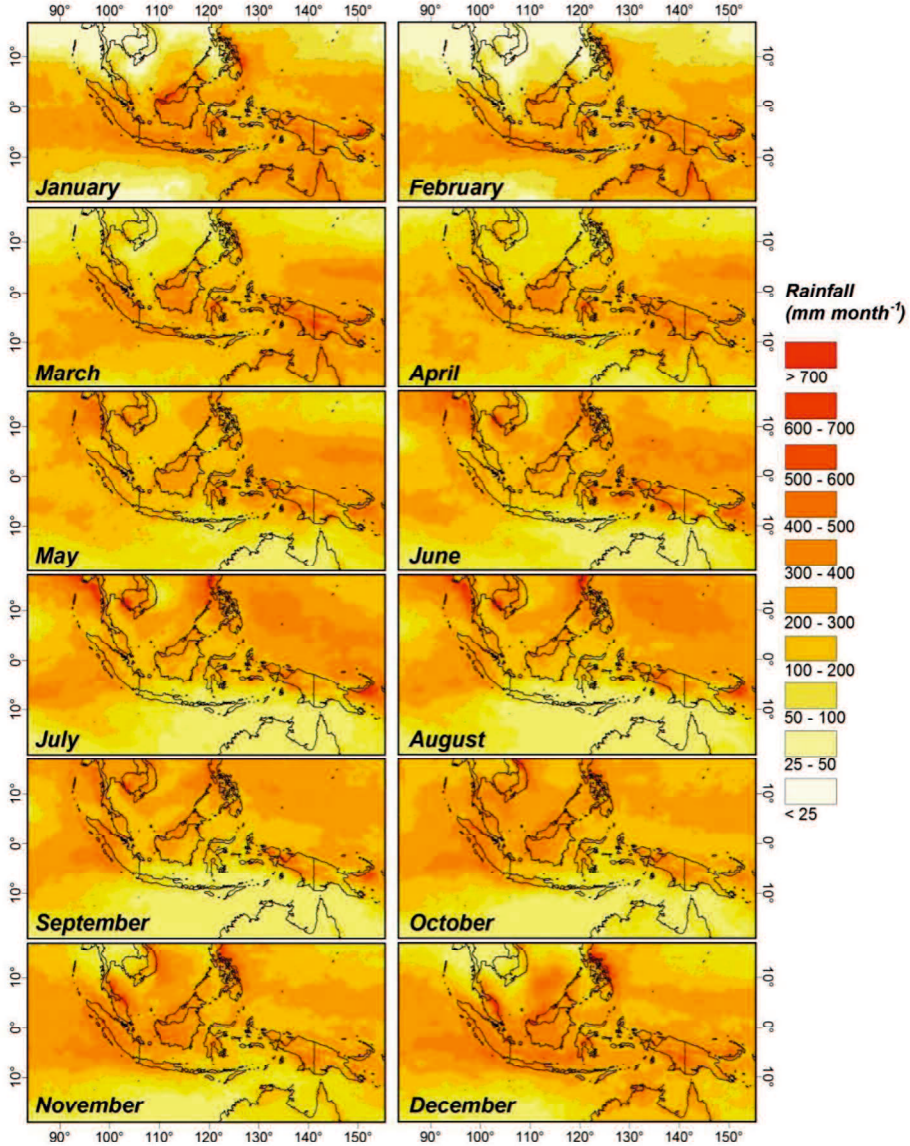

Figure 3.6. Monthly climatological mean of rainfall derived from the TRMM 3B43 based on monthly composites from January 1998 to December 2010.

Low rainfall in Indonesia started around the island of Timor in April and continued extending towards the southeast coast of Sumatra, the south coast of Kalimantan, southern Sulawesi, and reached the southern area of the Maluku Islands in August. This phenomenon is consistent with northwestward movement of the Asian-Australian monsoon system, of which the peak of the southeast monsoon occurs in August. During September through to November the high rainfall moves northwest to southeast. In these months, the southeast monsoon weakened while the southwest monsoon strengthened (Susanto *et al*. 2006). The seasonal shift of heavy rainfall in January and poor rainfall in July is associated with the seasonal migration of the intertropical convergence zone (ITCZ). In January, the central mass of heavy rainfall is south of the equator while in July in is north of 10°N (Chang *et al*. 2005).

The monthly climatological mean of rainfall also shown throughout the year, the highest rainfall concentrations fall over land as compared with over sea (see Figure 3.7). The largest and smallest differences occurred in November (95.54 mm month^{-1}) and June (21.73 mm month^{-1}), respectively. The annual cycles of rainfall differences between land and sea are similar to the annual cycles of the monsoonal climate regions which have one peak and one trough and experience strong influences of two monsoons (see Aldrian and Susanto 2003).

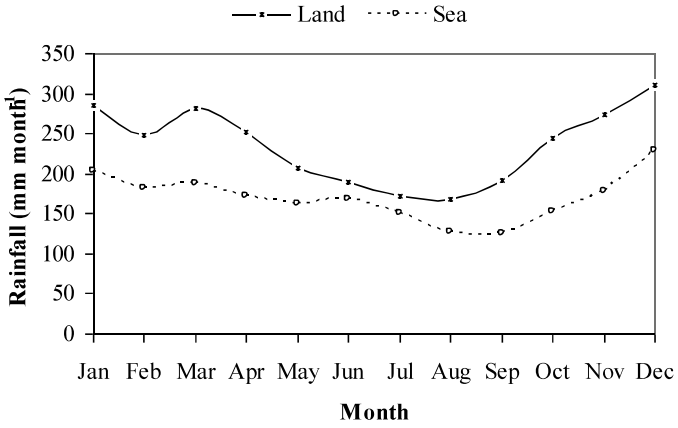

Figure 3.7. Average mean of monthly rainfall values over the island and the sea in Indonesia derived from the TRMM 3B43 based on 1-Month composites from January 1998 to December 2010.

As described previously, complex topography affects quantities of rainfall over this area (see Figure 3.4 and 3.6). To illustrate the impact of topography on the annual and seasonal climatological average rainfall distribution, Figure 3.8 shows six North-South cross section lines of rainfall and elevation (see Figure 3.1). Clearly seen in this figure areas around the region

which have high elevation also have high rainfall compared with low elevations and sea, which manifests more during wet seasons than during dry and transition seasons. However, in some part, topographical effects do not only lead to increasing rainfall amount in the high elevation region, but also in the vicinity of low elevations. This is partly responsible for a very poor correlation (r=0.01) between total rainfall and elevation in this area (see Figure 3.9). Additionally, the low spatial resolution of the satellite data (0.25° × 0.25°) may also affect the very poor correlation result. The influence of topography on seasonal rainfall is generally similar to its annual pattern except during JJA season in southern Indonesia when high elevation does not enough affect rainfall.

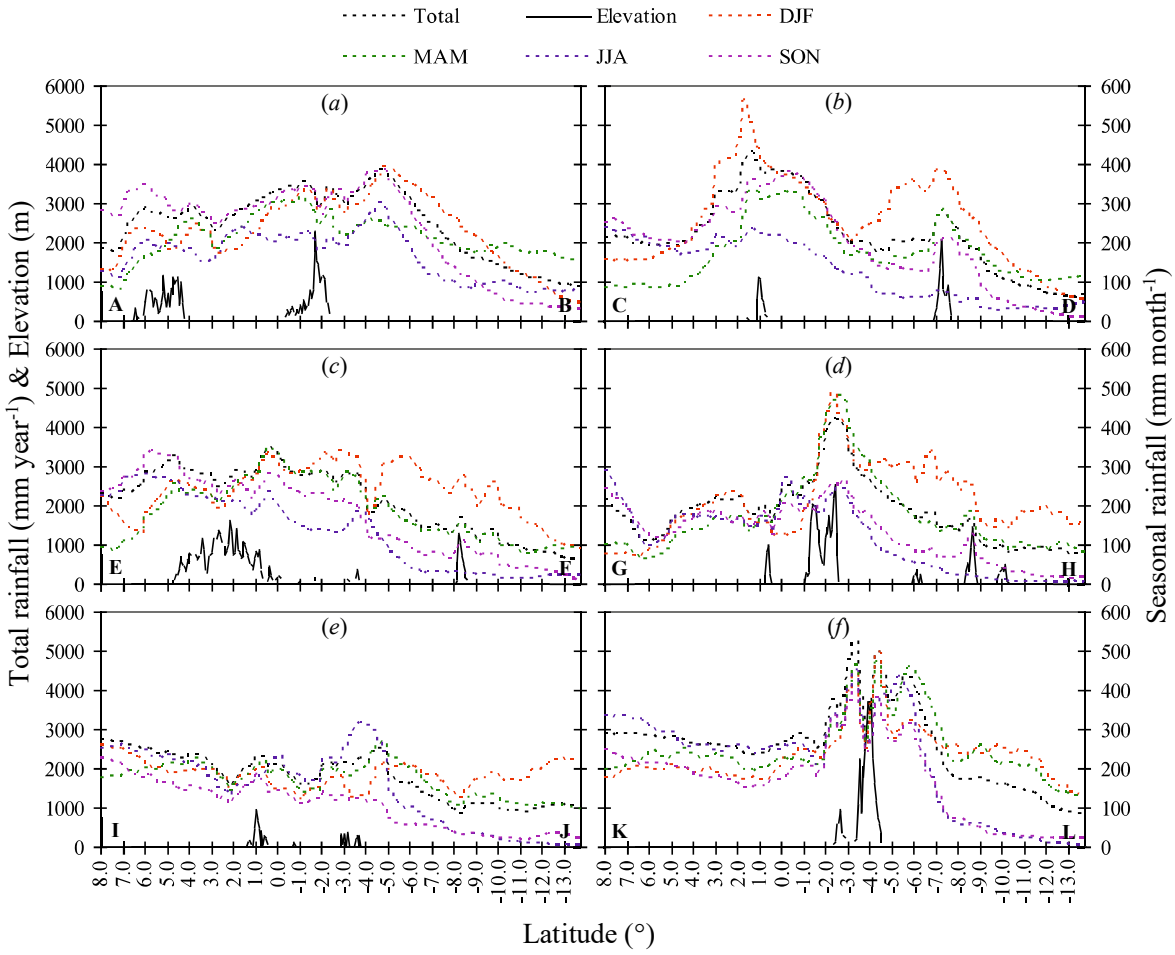

Figure 3.8. North-south cross section between Indonesia rainfall with elevation at six different places (see Figure 3.1). (*a*) A–B cross section, (*b*) C–D cross section, (*c*) E–F cross section, (*d*) G–H cross section, (*e*) I–J cross section, and (*f*) K–L cross section.

In surrounding islands around the sea heavy rainfall also occurred, such as in between the islands of Jawa and Kalimantan, the northwestern coast of Kalimantan, and the southern coast of Sumatra. This condition is caused by several factors, varies at each place, and all of it is clearly seen by remote sensing data. As explain by Qian (2008), heavy rainfall over the Jawa Sea (between the islands of Jawa and Kalimantan) (see Figure 3.8(*b*) on -5° – -7°) is affected by the diurnal cycle of land breezes from both Kalimantan and Jawa. Heavy rainfall on the northwestern coast of Kalimantan (see Figure 3.8(*b*) on 3° – 2°) was also influence by land breezes. In this area, the locally large-scale convergence concentrated over the sea was due to diurnal land breeze interaction with the prevailing winter monsoon flow, producing offshore convection (Houze *et al*. 1981; Geotis and Houze 1985). On the other hand, the influence of the western Walker cell over the Indian Ocean (with an anomalous low-level equatorial zonal wind) affects the rainfall on the sea region southwest of the island of Sumatra (see Figure 3.8(*a*) on -4° – -6°; Chang *et al*. 2004).

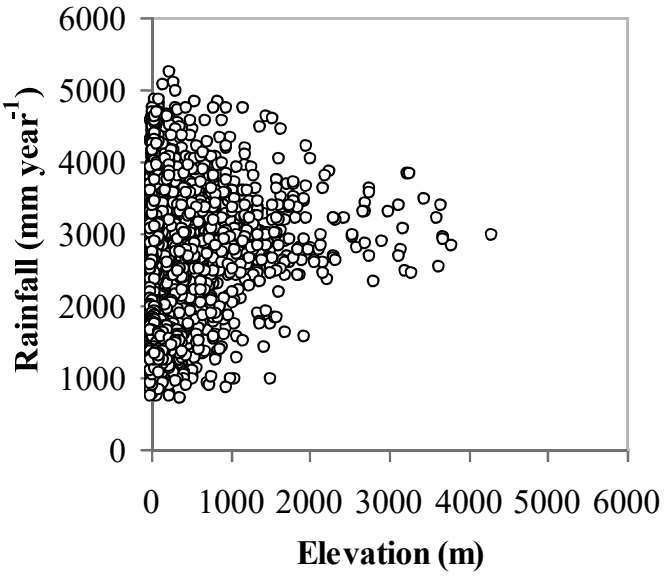

Figure 3.9. Scatter plots of annual rainfall versus elevation in all research regions which are over land.

Figure 3.10 show the spatial rainfall distribution of peak maximum, peak minimum, amplitude variability (difference between peak maximum and minimum), and standard deviation. Indonesian peak maximum rainfall ranged from 103.9 to 632.21 mm/month and mostly occurred in DJF (see Figure 3.11(*a*)). Peak minimum rainfalls of 0.06 to 362.07 mm/month mostly

occurred in JJA (see Figure 3.11(*b*)). Peak maximum rainfalls were unevenly distributed, but in general occurred over the land. Meanwhile, minimum peak rainfalls spread across the equator belt. The amplitude variability shows that high rainfall variability occurred over Jawa Island and Jawa Sea, indicated by high variability (see Figure 3.10(*c*)) and standard deviation values in the region (see Figure 3.10(*d*)). The variability of rainfall is smaller in the north than in the south of Indonesia, indicating southern Indonesia is influenced by movement of the Asian-Australian monsoon system.

The spatial distributions of peak maximum and minimum rainfall phase amplitude (months) derived from TRMM 3B43 are shown in Figure 3.11. As described previously, the maximum and minimum peak phase of rainfall mostly occurs in DJF and JJA, respectively. In the months of DJF, especially in January, the northwest monsoon is fully developed, while during JJA this region is influenced by the southeast monsoon (Wyrtki 1961). In western Sumatra and areas of Kalimantan, the maximum peak phase of rainfall occurs during SON. This phase is associated with the southward and northward movement of the ITCZ. The ITCZ, characterized by active convection, covers the equatorial region during SON. Furthermore, the ITCZ passed the same region during MAM (Sakurai *et al*. 2005), hence, this region usually has two peaks of heavy rainfall (Aldrian and Susanto 2003). These phenomena were not supported in this study.

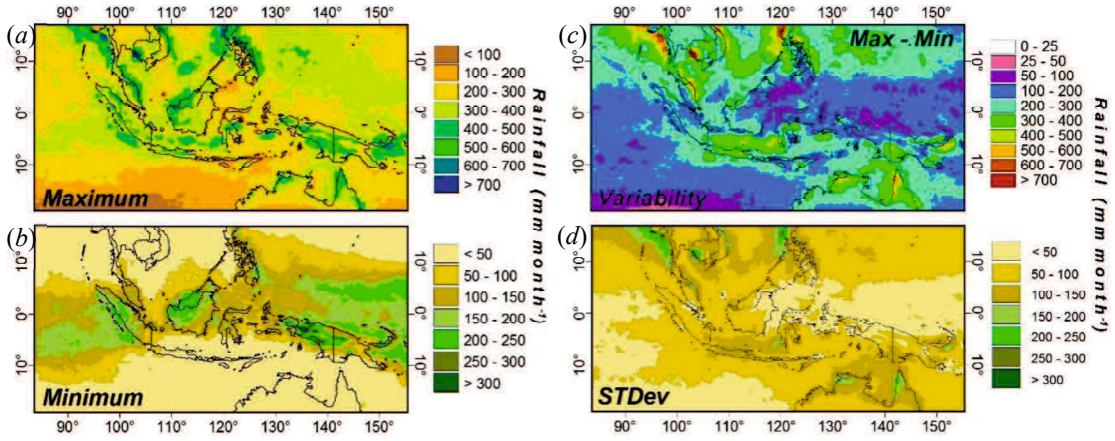

Figure 3.10. The distributions of (*a*) maximum, (*b*) minimum, (*c*) amplitude variability (difference between peak maximum and minimum), and (*d*) standard deviation of monthly averaged rainfall in TRMM 3B43 from January 1998 to December 2010.

In Papua Island the peak phase of maximum rainfall occurred in MAM and minimum peak phase occurred during JJA (see Figure 3.11(*a*)). In addition to the ITCZ, these conditions are also influenced by the effects of the northwest monsoon and a large-scale zonal (east-west)

circulation over the equatorial Pacific (Hall, 1984). In Maluku Islands, the peak rainfall phase maximum differs from other areas during JJA, in phase with the western tropical Pacific region. The climate in this region is affected by the conditions of the western tropical Pacific region (Kubota *et al.* 2011; Aldrian and Susanto 2003). The reason for this influence is unclear, however, Aldrian and Susanto (2003) explain that during JJA the Indonesian Throughflow (ITF) brings warm water from warm pool area of the western tropical Pacific region resulting in heavy rainfall in this season. During dry season in these areas, cooler water moving from the warm pool to the Maluku Sea inhibits the formation of a convective zone and results in a minimum rainfall peak phase (see Figure 3.11(*b*)).

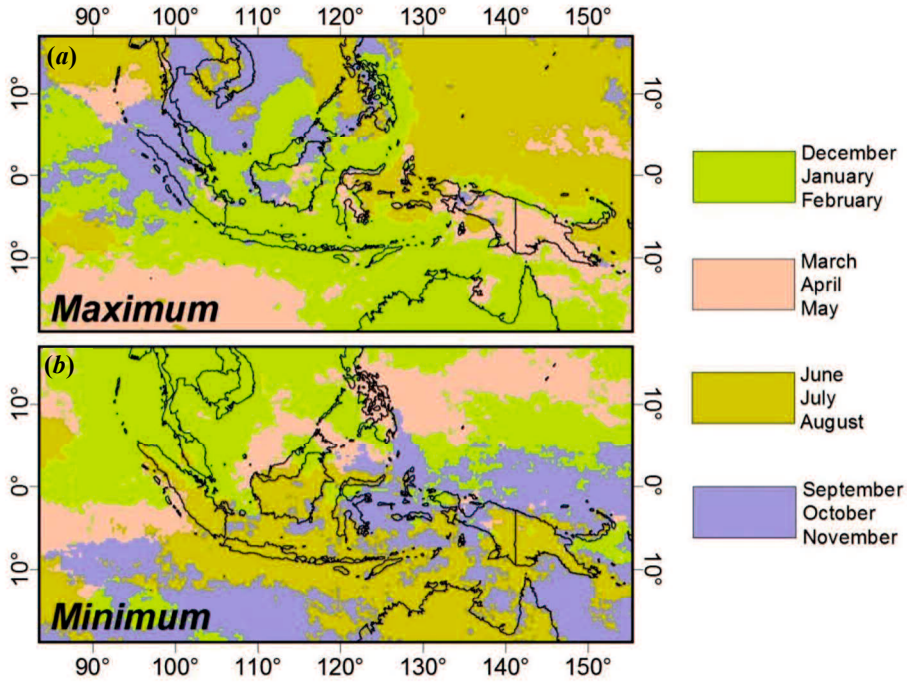

Figure 3.11. The spatial distribution of peak amplitude phases (months) derived from TRMM 3B43; (*a*) maximum phase and (*b*) minimum phase.

Figure 3.12 shows an increasing trend of spatial distribution for monthly rainfall time-series data from January 1998 to December 2010 collected by TRMM 3B43 over Indonesia. In general, rainfall trend was more positive in the north than the south of Indonesia. In addition, rainfall tended to increase over land areas, especially the four major islands, except Sulawesi Island. On the other hand, downward trends in rainfall occur along the western and southern coast of Sumatra, eastern Jawa, southern Sulawesi, Maluku Islands, western Papua, and Bali Island. The

extreme climate of ENSO and IOD were associated with interannual months of Indonesian rainfall variability. During 13 years, several extreme rainfall events were influenced by ENSO and IOD, causing variations in the trends of rainfall.

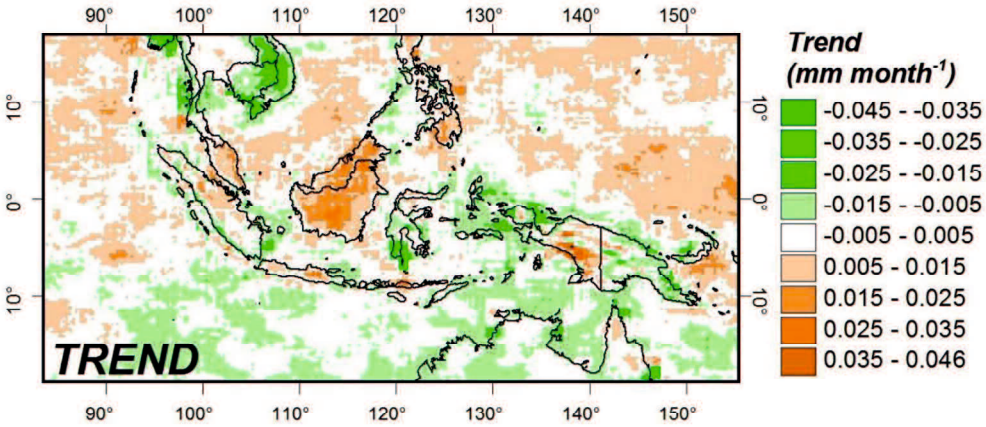

Figure 3.12. The spatial distribution trend of the time-series monthly rainfall from TRMM 3B43 from January 1998 to December 2010.

3.4.2 Comparison with rain gauges

The monthly TRMM 3B43 satellite data products were compared with gauge observations from the 5 stations over Indonesia (see Figure 3.1) sought to determine how well the 3B43 estimated values and the magnitude of rainfall on the ground. The result averages from point-by-point analysis (across all stations) at 5 rain gauges show annual rainfall from 3B43 was lower than the rainfall from the gauge data: the average rainfall from 3B43 was 2414.38 mm year^{-1}, whereas the average rainfall from the rain gauge was 2470.81 mm year^{-1}. However, when viewed from each rain gauge, the amount of rainfall showed varying values. Figure 3.13 shows histograms of annual rainfall from 3B43 and rain gauges estimate in 5 locations during 1998–2010. The histograms of annual rainfall indicate that there are 2 rain gauges (Medan and Pontianak) in the western part of Indonesia that has values lower than satellite estimates (overestimated), whereas 3 rain gauges (Tuban-Bali, Ternate and Jayapura) in the eastern part of Indonesia has rainfall values higher than satellite estimates (underestimated). Overestimated values also found in Malaysia (western part of Indonesia) by Semire *et al*. (2012) and underestimated in Bali (eastern part of Indonesia) by As-Syakur *et al.* (2011).

Figure 3.14 shows the intra-annual variation of the long-term mean monthly rainfall measured by 3B43 and the rain gauge data from 5 stations. This figure indicates that monthly rainfall patterns from 5 locations are quite similar confirmed the close relationship between 3B43

and rain gauges. The satellite data and ground reference data yield high to very high correlations for these products for each rain gauge. The correlations between 3B43 and rain gauges in Medan, Pontianak, Tuban-Bali, Ternate and Jayapura are 0.98, 0.90, 0.98, 0.95 and 0.85, respectively.

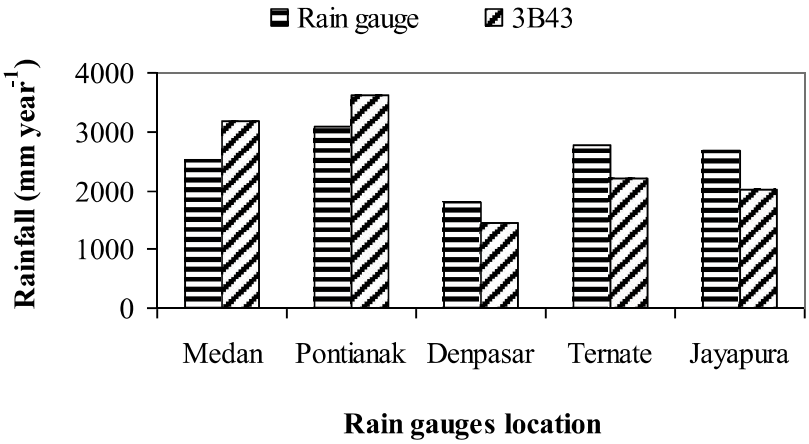

Figure 3.13. Histograms of annual rainfall between 3B43 with rain gauges estimate from 5 locations, over the period from 1998 to 2010.

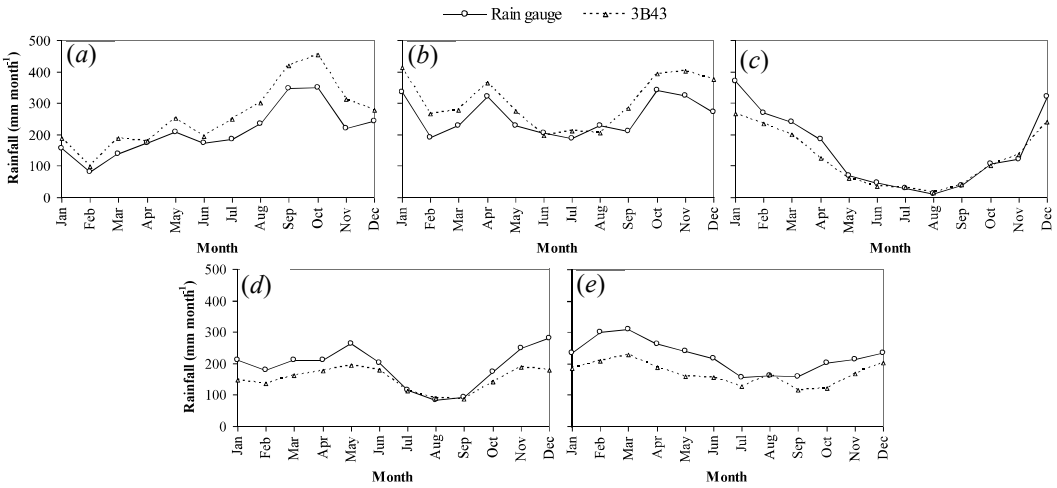

Figure 3.14. Monthly average rainfall pattern measured by 3B43 and rain gauges. (*a*) Medan, (*b*) Pontianak, (*c*) Tuban-Bali, (*d*) Ternate and (*e*) Jayapura, over the period from 1998 to 2010.

The comparison histograms of peak maximum, peak minimum, and amplitude variability derived from TRMM 3B43 and rain gauges from 5 locations are shown in Figure 3.15. The histograms between peak maximum/minimum rainfall phase amplitude and annual rainfall shows similar pattern were 2 rain gauges that has values lower than satellite estimates and 3 rain gauges has rainfall values higher than satellite estimates. Peak maximum and amplitude variability

displays high differences between satellite data and rain gauge compared with peak minimum rainfall phase. Overall, comparison between monthly 3B43 products and gauge observations shows still has instability of differences.

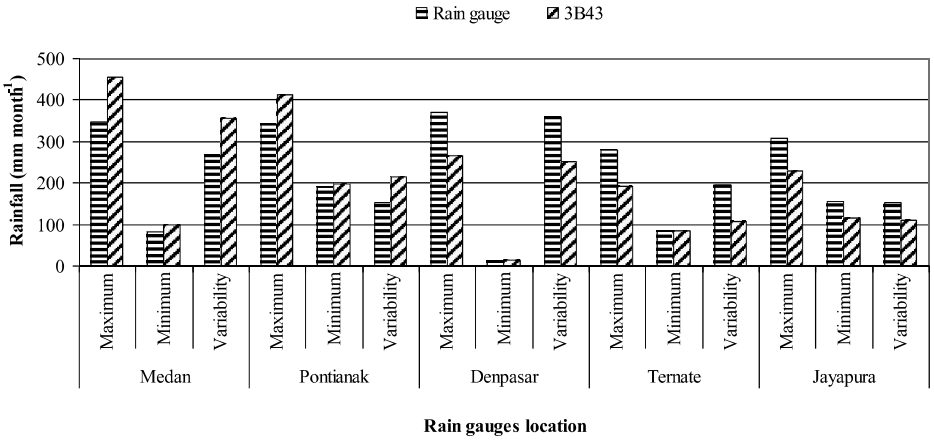

Figure 3.15. The comparison histograms of maximum, minimum, and amplitude variability averaged rainfall measured by 3B43 and rain gauges from January 1998 to December 2010.

We suggest that the causes for these differences between 3B43 and rain gauge data due to temporal and spatial sampling uncertainties. One reason may be that, since TRMM is a major component of the 3B43 product, one would expect it to not record some rainfall owing to unfavorable timing of its overflight of Indonesia. Fleming *et al*. (2011) state these reasons for Australia. Because of non-sun-synchronous satellite orbit, the TRMM records locations once approximately every 3.6 days in the tropical region (As-Syakur 2011). Furthermore, limitations of the TRMM data suffer from both the narrow swath and insufficient sampling time intervals resulted loss information about rainfall values and rainfall types. Indonesian region is characterized by a much higher variability of rainfall and much stronger convective activity. Precipitation events outside of these satellite observation windows directly resulted in monthly and seasonal statistical error. In addition, rainfall data used in this study has limited sampling representation, where 0.25°× 0.25° 3B43 data is only represented by one rain gauge.

Previous studies show convective rainfall predominantly control tropical rainfall peaks in Indonesia (Kubota *et al*. 2004; Mori *et al*. 2004; Tabata *et al*. 2011; Prasetia *et al*. 2013). Liao and Meneghini (2009), from ground-based radar, found (particularly in heavy rain) underestimation of TRMM PR attenuation for convective rain, while stratiform rain was more accurately corrected. In addition, when the convective rain is about 50-70%, is possible due to

the overestimate of rainfall by TMI (Nakazawa and Rajendran 2004). Therefore, instability of differences rainfall in this region is possibly caused by succession of convective and stratiform rain types throughout the year. Both convective and stratiform rain types dominate in the Indonesian archipelago (Schumacher and Houze 2003; Yulihastin and Kodama 2010; Prasetia *et al*. 2013).

3.5 Summary and Conclusions

An investigation of Indonesian rainfalls variability using satellite data from TRMM 3B43 over 13 years (from January 1998 to December 2010) is presented here. Monthly, seasonal and long-term time series analyses were conducted by applying several statistical methods. Rainfall over different elevations was compared to determine the effect of land and topography on rainfall events. Monthly 3B43 rainfall estimates were compared with monthly rain gauge measurements from BMKG to evaluate rainfall variability. Data from 5 rain gauges across Indonesia, covering a 13-year period (1998–2010), were used here.

The results clearly show the effect of oceans, islands, monsoons, and topography on spatial patterns of rainfall. Monthly climatological rainfall means show that rainfall over land area is greater than rainfall over sea throughout the year. The analysis showed that 58.18% (2779.82 mm $year^{-1}$) of the total rainfall in Indonesia falls over land while only 41.82% (1998.21 mm $year^{-1}$) falls over sea. In general, the largest difference between rainfall occurring over land and sea is clearly seen in the monsoon transition months of SON and MAM, with a maximum difference in November and a minimum difference in June.

Looking at a north-south cross section, topography clearly affects rainfall variability in southern Indonesia. In the southern part of Indonesia the highest elevation showed higher levels of rainfall. The effect of topography is also evident in other parts of Indonesia. However, topographical effects not only increase rainfall amounts in the high elevation regions, but also in surrounding low elevations, leading to a very poor correlation between rainfall and elevation.

Most parts of Indonesia have a peak of high rainfall events during DJF and a valley of low rainfall events during JJA. These conditions are associated with the northwest and southeast monsoon. Generally, the maximum peak and trough of rainfall events occurs over land and at higher altitudes. High maximum and minimum monthly rainfall fluctuation occur over Jawa Island and the Jawa Sea. In that area, the fluctuation of rainfall reaches above 400 mm/month.

However, rainfall is relatively stable in the equatorial region. High annual rainfall typically occurs in these island areas, except southeast Indonesia. The trend analysis shows rainfall has a tendency to increase in northern Indonesia, but a tendency to decrease in southern Indonesia.

Comparing the 3B43 with rain gauges show a strong agreement with high to very high correlation coefficient (R = 0.85 to 0.98). However, comparison results still showed instability of differences especially if heavy rain occurs. Temporal and spatial sampling uncertainties possibly cause the instability.

Utilization of TRMM 3B43 remote sensing data helps observe Indonesian rainfall in oceanic and unpopulated land areas that do not have rain gauge data. Rainfall characteristics over Indonesia provide information explaining a regional and global climate system strongly influenced by local conditions. However, to obtain better results remote sensing satellite data needs to improve data quality for better spatial resolution to compare the small islands and complex topography of Indonesia.

CHAPTER 4

Maritime Continent rainfall variability during the TRMM era: the role of monsoon, topography and El Niño Modoki

4.1 Introduction

Rainfall is the most important climatic element of the Maritime Continent (MC; Saha, 2010), a large area of land-sea complex comprising Indonesia, Malaysia, the Philippines and surrounding areas between 15°S and 15°N (Ramage, 1968). The MC is located in the most active convective area of the world and is influenced by global, regional, and local conditions; e.g., the Asian-Australian monsoon, tropical convective zones, intra-seasonal oscillation, and complex land-sea-topography (Chang et al., 2005; Qian, 2008; Hidayat and Kizu, 2010; Rauniyar and Walsh, 2011; As-Syakur et al., 2013). The Asian-Australian monsoon creates an annual rainy and dry season cycle (Robertson et al., 2011). The intra-seasonal (30–90 days) Madden–Julian oscillation (MJO) phase is associated with extreme high and low precipitation events (Wu and Hsu, 2009; Oh et al., 2012; Kanamori et al., 2013; Wu et al., 2013), whereas complex land-sea-topography affects diurnal rainfall quantities (Qian et al., 2010; Peatman et al., 2014). All associated events are affected by the rainfall diversity and create high space-time annual and interannual climate variability in this region.

Moreover, MC rainfall is also influenced by year-to-year regional and local atmosphere-ocean interactions, such as El Niño Modoki and the El Niño–Southern Oscillation (ENSO), hereafter referred to as the conventional El Niño (Wang and Hendon, 2007; Chang et al., 2008; Rauniyar and Walsh, 2013; As-Syakur et al., 2014). Both of these climate modes are important because of their large environmental and societal impacts in this region (Gutman et al., 2000; Glantz, 2001; Juneng and Tangang, 2005; Weng et al., 2007; Liao et al., 2012; Xu et al., 2013; Salimun et al., 2014;). The ENSO is the dominant climate phenomenon affecting extreme weather conditions worldwide (Cai et al., 2015). El Niño Modoki has been identified as a type of pseudo-Niño in the tropical Pacific and differs in obvious ways from the conventional El Niño, particularly in terms of its spatial and temporal characteristics and teleconnection patterns (Ashok et al., 2007; Ashok and Yamagata, 2009; Li et al., 2010). El Niño Modoki is

characterized by warm waters in the central Pacific and cool waters in the eastern and western parts of the basin (Weng et al., 2009; Feng and Li, 2011; Xie et al., 2014). In contrast, conventional El Niño is a recurring pattern of climate variability in the eastern equatorial Pacific that is characterized by anomalies in both sea-surface temperature (referred to as El Niño and La Niña with respect to warming and cooling periods, respectively) and sea level pressure (Southern Oscillation; Philander, 1983; Philander, 1989; Trenberth, 1997; Naylor et al., 2001, Meyers et al., 2007). Many studies have shown that MC rainfall tends to decrease during El Niño and increase during La Niña events (e.g., McBride et al., 2003; Chang et al., 2004; Xu et al., 2004; Lyon et al., 2006; Aldrian et al., 2007; Qian et al., 2013; Slezak, 2014). Changes in rainfall have been attributed to anomalous sea surface temperatures (SSTs) and the associated anomalous Walker circulation over the tropical Pacific (Julian and Chervin, 1978; Kao and Yu, 2009; Tokinaga et al., 2012; DiNezio et al., 2013).

The MC is a region with a large population and has extensive agricultural areas (Ito et al., 2011). Therefore, knowledge about MC fresh water sources is important for understanding drinking water supply, industrial purposes and agricultural irrigation (de Angelis et al., 2004). Accountable information regarding precipitation is needed to improve climate and meteorological forecasts at several spatial and temporal scales. However, reliable MC rainfall characteristic information is lacking due to the absence of a dense rain gauge network (Chokngamwong and Chiu, 2008; As-Syakur, 2011, Semire et al., 2012; Prasetia et al., 2013), because rain gauge data are often not available over most unpopulated land areas, and gauge observation is not obtained for ocean areas.

Satellite observation of rainfall is one of the best solutions to obtain adequate temporal and spatial coverage of rainfall in areas for which rain gauge data are unavailable. Global land and ocean rainfall distribution was difficult to measure (Kubota et al., 2010) before satellite observation. The Tropical Rainfall Measuring Mission (TRMM), an American–Japanese Earth satellite observation mission (launched in November 1997 to an altitude of 402.5 km after boost), has improved our understanding of precipitation structure and heating in tropical regions (Simpson et al., 1996). Product level 3 TRMM 3B43 monthly data, which are often referred to as TRMM Multi-Satellite Precipitation Analysis (TMPA) products, represent the best estimates of quasi-global precipitation. These TRMM 3B43 satellite-based high-resolution rainfall data products are the first way to calibrate rain estimates obtained from TRMM Precipitation Radar

(PR), TRMM Microwave Imager (TMI) and other microwave and Infrared (IR) satellite precipitation measurements (Huffman et al., 2007). These 3B43 products were upgraded from version 6 (v6) to version 7 (v7) in 2012 and became available for the periods from December 1997 to date. Version 7 will evolve as the initial version 0 algorithm of the upcoming Global Precipitation Measurement (GPM) mission. In recent years, several groups have validated the 3B43 v6 data using MC ground data (e.g., Chokngamwong and Chiu, 2008; As-Syakur et al., 2011; Fleming et al., 2011; Semire et al., 2012) and confirmed the effectiveness of the products. Prakash et al. (2013), Fleming and Awange (2013) and Nuarsa et al. (2014) found that 3B43 v7 exhibits improved bias and correlation compared to v6.

Previous MC rainfall and climate systems studies at many locations have relied on rain gauge data or on rain gauge data model utilization (e.g., Hendon, 2003; Aldrian and Susanto, 2003; Tangang and Juneng, 2004; Feng et al., 2010; Chen et al., 2012; Mandapaka and Qin, 2013; Jourdain et al., 2013; Misra and DiNapoli, 2014; Villafuerte II et al., 2014). The MC, due to its complex system of islands and shallow seas, continues to exhibit substantial errors when climate models are applied to rainfall characteristic analysis (Love et al., 2011). Neale and Slingo (2003) reported a systematic underestimation of precipitation in this area using the climate version of the Met Office model (HadAM3), which was caused by land–sea generated complex diurnal circulation patterns. Furthermore, Gianotti and Eltahir (2014a; 2014b) also described findings that the diurnal cycle of Regional Climate Model version 3 (RegCM3) is a major source of MC climate simulation error. Strong improvements are expected due to improved spatial and temporal resolution satellite data regarding MC rainfall characteristics. TMPA datasets yield finer-scale temporal precipitation estimates. Monthly TMPA data (3B43 product) are derived from 3-hourly data (3B42 product). All available 3-hourly data over a calendar month are summed to create a monthly product (Huffman et al., 2007). Therefore, diurnal cycle rainfall data conditions can be recorded and factored into monthly, seasonal, and annual mean rainfall products.

In recent years, several studies have analyzed the rainfall climate system using poor spatial-temporal satellite data in some parts of this region. For example, Mori et al. (2004) applied the TRMM 3G68 dataset to investigate coastal heavy rainfall bands and a diurnal land-sea migrating convective cloud system over Sumatra Island in the IMC. Chang et al. (2005) described annual cycles of rainfall over land areas based on rain gauge data and short-period satellite data. Hirose

and Nakamura (2005) observed precipitation variations in systems over Asia, including the MC, based on TRMM PR data. Dayem et al. (2007) quantified precipitation rates over the tropical western Pacific warm pool and the MC using TRMM 2B31. Weng et al. (2007; 2009) inspected impact of El Niño Modoki and the conventional El Niño in the Pacific rim, including region of MC, during boreal summer and winter using low spatial resolution satellite-gauge precipitation of Global Precipitation Climatology Project (GPCP). Biasutti et al. (2012) described rainfall climatology patterns based on TRMM PR 2A25 observations. Furthermore,Rauniyar and Walsh (2013) examined the influence of ENSO on the diurnal rainfall cycle using TRMM and reanalysis data. However, no studies have utilized long-term satellite data to simultaneously analyze patterns describing climatic rainfall characteristics over the MC and the MC rainfall response to El Niño Modoki and the conventional El Niño.

The main objectives of this paper are to report climate patterns and to analyze regional rainfall rate estimates that utilize long-term MC satellite data; the study includes a limited analysis of rainfall dynamics caused by monsoon activity, topography diversity and their response to El Niño Modoki and the conventional El Niño. It is important to clarify the regional hydrological processes to understand the rainfall characteristics. Therefore, the use of improved spatial and temporal resolution satellite data is expected to illustrate the distribution of the MC rainfall climate system more clearly. In this work, annual, seasonal and monthly analyses were conducted. The remainder of this article is arranged as follows: Section 2 presents data and analysis; Section 3 reveals the characteristics of annual rainfall periods and their trends based on long-term (1998-2013) satellite measurements; Section 4 quantifies the effect of monsoons and topography on rainfall values acquired from satellite data; Section 5 identifies differences in the impact of anomalous rainfall distribution based on a linear correlation analysis of El Niño Modoki and the conventional El Niño; and finally, Section 6 summarizes the findings.

4.2 Data and Analysis

Research was conducted using MC spatial data covering 20° N to 20° S and 80° E to 180° E. Figure 4.1 illustrates the MC topographic distribution between nine west-east cross section lines, which were used to compare rainfall and elevation values. Monthly rainfall data from 1998 to 2013, which were measured and collected using TRMM 3B43 v7, were employed to study the general rainfall characteristics of the MC. The TRMM is a long-term research programme

designed to study the landmasses, oceans, air, ice, and life of Earth as a total system (Simpson et al., 1996). Additionally, TMPA is a TRMM product that is designed to combine precipitation estimates from TRMM, various satellite systems, and land surface precipitation gauge analyses (where feasible) and thereby create a single "best" satellite precipitation estimate (Huffman et al., 2007). TMPA estimates are available in the form of two products: a near-real-time version (TMPA-RT) and a post-real-time research version that provide global coverage of precipitation over the 50° S–50° N latitude belt at 0.25°×0.25° spatial resolution. The TRMM 3B43 (3B42) research product was developed as a post-real-time monthly (3-hourly) satellite–gauge precipitation product. TMPA estimates are produced in four stages as follows: (1) TMI and TRMM PR on TRMM are combined (TMI-PR, 2B31) and serve as a baseline to calibrate a combination of passive microwave data from microwave sensors on multiple satellites; (2) the passive microwave data are used to calibrate IR input; (3) the microwave and IR estimates are combined; and (4) monthly rain gauge data are incorporated (including the Global Precipitation Climatology Centre (GPCC) and the Climate Assessment and Monitoring System monthly rain gauge analysis) to create the 3B43 product, and rescaling is applied to create 3-hourly TRMM 3B42 for the month (Huffman et al., 2007; 2010). The TMPA retrieval algorithm used in this product is based on the technique described by Huffman et al. (1995, 1997) and Huffman (1997).

Several statistical scores were used to determine the MC rainfall characteristics. Annual means, annual linear trends, seasonal means, and percentage of rainfall anomaly, as well as linear and partial correlations, were used in the analysis. Linear and partial correlations were used to analyse the relationship between MC rainfall and El Niño Modoki and the conventional El Niño, which were defined according to the El Niño Modoki Index (EMI) and Niño-3 values. Following Ashok et al. (2007), the EMI was defined as follows:

$$\mathrm{EMI} = [SSTA]_C - 0.5 \times [SSTA]_E - 0.5 \times [SSTA]_W \quad (4.1)$$

where square brackets with a subscript represent the areal mean sea surface temperature anomaly (SSTA) over the central Pacific region (C: 165°E–140°W, 10°S–10°N), the eastern Pacific region (E: 110°–70°W, 15°S–5°N), and the western Pacific region (W: 125°–145°E, 10°S–20°N). Furthermore, the Niño-3 index was defined as the spatial mean SST anomaly over the region 5°N–5°S and 90°–150°W in the east Pacific Ocean (Trenberth, 1989).

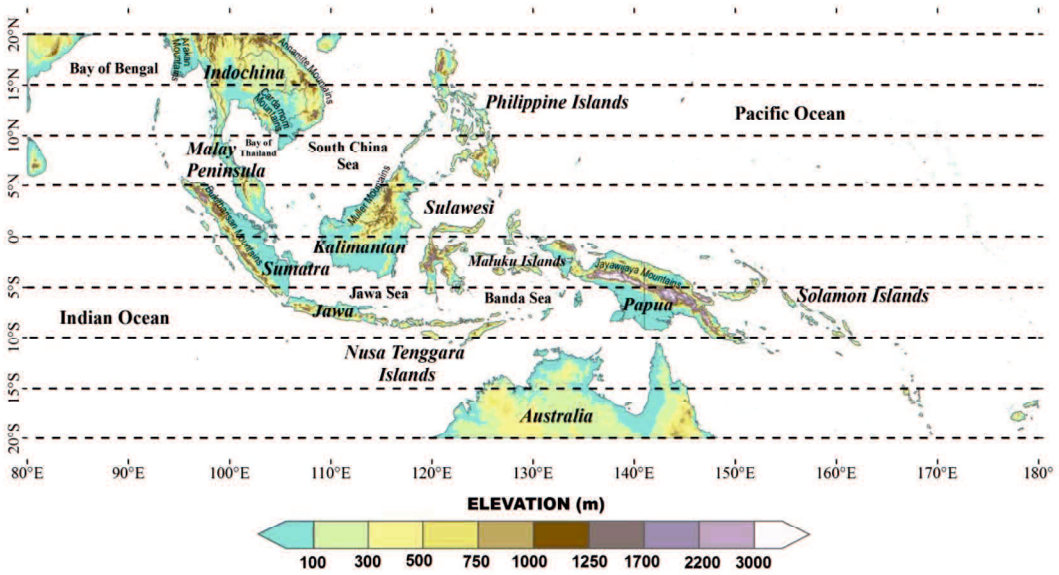

Figure 4.1. The study area of the Maritime Continent with topography shown. Dashed lines indicate west-east cross sections used to compare rainfall and elevation values.

In statistics, correlations are used to describe linear statistical relationships between two random variables; thus, correlated variables are pairs of variables that vary together precisely and that are related to each other by means of a positive or negative scaling factor (von Storch and Zwiers, 1999). Furthermore, partial correlations are used to measure the correlation between two related variables after eliminating the influence of one or more other variables or after assuming that the other variables become constants (Blair, 1918). Two variables may be correlated because both of them correlate with a third variable or set of variables (Cramer, 2003). Partial correlation controls for this possible correlation with a third identified variable or with a set of variables (Delbanco et al. 1998). Conversely, the method may unduly penalize the original driver because the part of the original driver that correlated with the second driver might still reflect the operation of the original driver. The analysis of partial correlations has been applied to determine the impacts of El Niño Modoki and conventional El Niño events on Australian rainfall (Taschetto and England, 2009), on spring rainfall over southern China (Feng and Li, 2011) and on atmospheric circulation in the Southern Hemisphere (Sun et al., 2013). In the case of three quantities, the partial coefficient is calculated using the following equation (Blair, 1918):

$$r_{12,3} = \frac{r_{12} - r_{13}r_{23}}{\sqrt{\left(1 - r_{13}^2\right)\left(1 - r_{23}^2\right)}} \tag{4.2}$$

Where, $r_{12,3}$ is the partial correlation between two random variables (1 and 2) after removing the controlling effect of another random variable (3). When the effect of the conventional El Niño is removed, variables 1, 2, and 3 could represent rainfall, the EMI, and the Niño-3, respectively. Additionally, if the roles of 2 and 3 are reversed, $r_{12,3}$ becomes a measure of the rainfall related to Niño-3, and the effect of El Niño Modoki is removed. If the effect of the conventional El Niño is removed, r_{12} and r_{13} represent simple correlations between rainfall and the EMI and between rainfall and Niño-3, respectively. The opposite occurs when the effect of El Niño Modoki is removed. When the effect of the conventional El Niño is removed, the square of the quantity, $r_{12,3}$, represents the rainfall variance, which is not estimated for the conventional El Niño in the equation, but is estimated for El Niño Modoki. The opposite tends to occur when the effect of El Niño Modoki is removed.

Moreover, El Niño Modoki and conventional El Niño events on 2002/03, 2009/10 and 2006/07 were selected to illustrate spatial patterns of MC anomalous rainfall. Shuanglin and Qin (2012) and Takahashi et al. (2013) classified 2002/03 and 2009/10 as El Niño Modoki events and 2006/07 as a conventional El Niño event (El Niño). June (in the JJA season) was chosen as the initial season in the annual rainfall anomaly analysis because the conventional El Niño usually begins in June (As-Syakur et al., 2014).

Furthermore, the analyses also studied the effects of land area and topography on rainfall amounts. Nine west-east lines (Figure 4.1) were used to compare island distribution and elevation with rainfall values. The distribution of islands, sea areas and topography were obtained from the Shuttle Radar Topography Mission 30 PLUS (SRTM30_PLUS) Version 7 dataset at a spatial resolution of 30 arc seconds (Becker et al., 2009). Annual and seasonal rainfall were compared with elevation values. In addition, monthly rainfall data were used to obtain annual zonal rainfall averages based on the latitudinal divisions from 20° N to 20° S (nine lines). Latitudinal averages across the longitude were employed to create zonal annual rainfall average graphics and to describe monthly rainfall.

The main analysis conducted in this research was based on seasonal data, but similar measures have applied to monthly and annual analyses. The analyses were conducted using coordinates as the reference identity for each pixel. Point-by-point data were generated by extracting data from each TMPA pixel. Each point contained information describing the coordinates, month, year, and rainfall values. Then, the data were sorted in accordance with the

purposes of the analysis. The same sorting process was also carried out using index values (EMI and Niño-3), followed by calculations to determine the linear and partial correlations. After obtaining the desired values (based on the purpose of the analysis), the point data were converted into raster data format having the same spatial resolution as the original data (0.25° ×0.25°).

Annual analyses were used to compare yearly average data over the entire observation period. Seasonal analysis was conducted based on monsoon activity as described by Wyrtki (1961); in this analysis, the seasons were classified as December-January-February (DJF), March-April-May (MAM), June-July-August (JJA), and September-October-November (SON). DJF represents the peak of the northwest Australia–Asia monsoon, and JJA represents the peak of the southeast Australia–Asia monsoon, and MAM and SON represent monsoon transitions (Aldrian and Susanto, 2003). Seasonal linear and partial correlation analyses were conducted by correlating the monthly data for the same season during the annual observation period. Likewise, monthly analyses were conducted by comparing data from the same months of the annual observation period.

4.3 Annual rainfall characteristics

It is important to determine the general characteristics of MC rainfall based on the rainfall annual means and their trend. The distribution of MC average annual rainfall during 1998–2013 from TMPA is depicted in Figure 4.2. The MC received the most rainfall in the central part, especially in the eastern Indian Ocean and in the western Pacific Ocean island chains. Less rainfall occurred over continental landmasses, including the Indochinese Peninsula in the Northern Hemisphere and Australia in the Southern Hemisphere. The relative frequency of land and ocean precipitation is systematic in inland areas, such as within Papua Island, western Sumatra and the Indochinese Peninsula, western Cambodia, northern Kalimantan, and the eastern Philippine Islands.

In general, the highest total annual rainfall extended across the equatorial belt. Maximal rainfall (> 5,000 mm year^{-1}) occurred in Papua Island near the Jayawijaya Mountains. The lowest total annual rainfall occurred at approximately 15° S to 20° S in the southwestern equatorial region. Of the total MC rainfall, 44.66% occurred over the central part of the studied area (7° N to 7° S); only 30.00% and 25.33% of rainfall occurred in the north (7° to 20° N) and south (7° to 20° S), respectively. Regarding the west-east distribution, rainfall was lower in the west (80° to

130° E; 47.82% of the total) than in the east (130° to 180° E; 52.18% of the total). As documented by Waliser and Gautier (1993), Love et al. (2011), and Mori et al. (2005), maximal rainfall values in this region are characterized by rain bands that are associated with the Inter-Tropical Convergence Zone (ITCZ), the South Pacific Convergence Zone (SPCZ), and the topography. As will be discussed below, most rainfall in the western region is influenced by the occurrence of the ITCZ and land topography in western Sumatra. However, ocean rainfall in the eastern region is influenced by the ITCZ and the SPCZ, and land-sea thermal contrasts, such as that which occurs in Papua (Zhou and Wang, 2006), generates heavy rainfall over land.

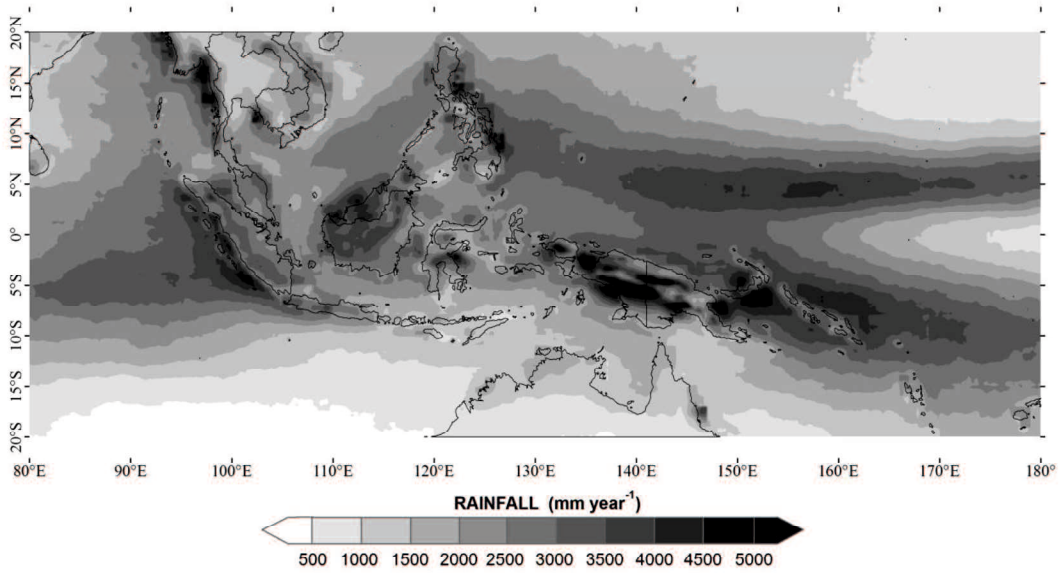

Figure 4.2. The distributions of Maritime Continent averaged TRMM annual rainfall from 1998–2013.

The spatial presentation of the detected rainfall trends can be helpful to improve our understanding of MC rainfall variations. A decline and an increase in the annual rainfall were identified in this region in the period from 1998–2013 (Figure 4.3). Generally, areas showing significant positive trend areas were wider than areas showing negative trends. Positive annual rainfall trends are noticeable in the central MC area, and negative annual rainfall trends occur more peripherally. Positive trends were observed across most of the Pacific ITCZ region, the SPCZ region, the eastern Philippine Islands, and in the North-eastern Indian Ocean. Negative trends were recorded in East Vietnam, Thailand Bay, the southern ITCZ Pacific region, the ITCZ Indian region, a small part of Bengal Bay, Karimata Strait, and the northern ITCZ Pacific region. Furthermore, the strongest positive and negative trends were found in eastern Papua and eastern

Vietnam, respectively. Much of the variability within these trends is associated with MC atmosphere–ocean interactions, such as El Niño Modoki, the conventional El Niño, the Indian Ocean Dipole (IOD), and the Interdecadal Pacific Oscillation (Manton et al., 2001; Juneng and Tangang, 2010; Cai et al., 2011; L'Heureux et al., 2013). Positive rainfall trends were associated with cold events in the central Pacific and with warm events in the East Indian Ocean. During the entire observation period, eight (8) cold events but only 4 warm events occurred in the central Pacific. Cold (warm) conditions in the central Pacific resulted in increased (decreased) rainfall over most parts of the MC area. More frequent cold events lead to an increased possibility of positive rainfall trends in this area.

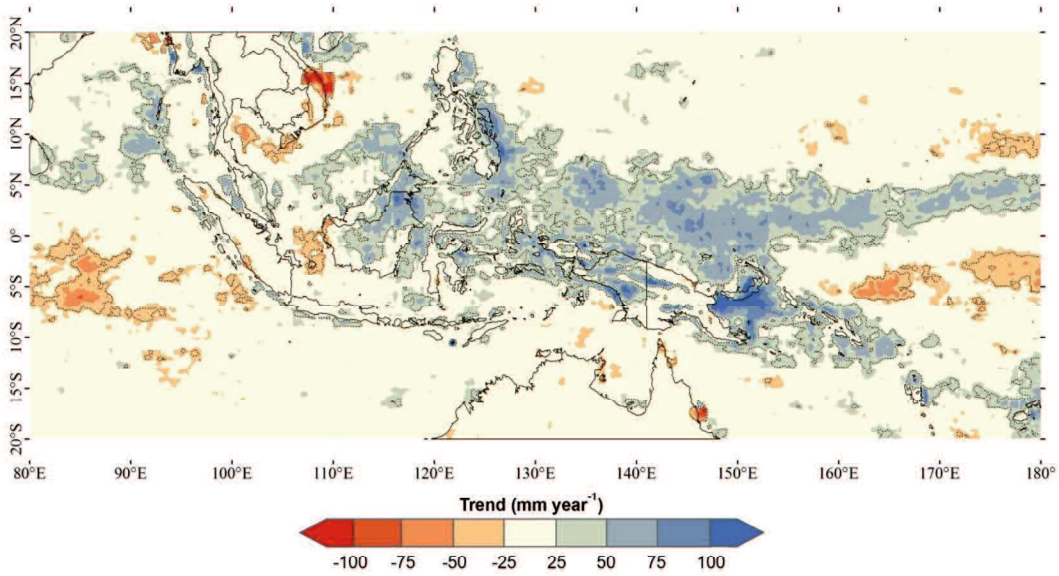

Figure 4.3. The distributions of trend of averaged Maritime Continent annual rainfall derived from TRMM 3B43 from 1998–2013. Dashed line indicated significant level of correlation under 99%.

4.4 The effects of monsoon and topography on rainfall values

A complete understanding of the seasonal rainfall mean for the MC during the satellite era is very important, especially regarding the distribution of land and ocean rainfall. Figure 4.4 presents the spatial and seasonal MC rainfall pattern, indicating the climatological mean from January 1998 to December 2013. Throughout the year, high seasonal rainfall concentration changes were observed over land and ocean areas, and few changes were observed over equatorial areas (see Figure 4.5). As shown in Figures 4.4 and 4.5, the seasonal characteristics of MC rainfall are consistent with north-westward and south-eastward movements of the Asian–

Australian monsoon system. During the DJF season, most heavy rainfall was detected over the central islands in the MC and to the south (over the north of Australia), to the north (over the east coast of the Philippine Islands), and over the ITCZ and SPCZ in the west Pacific.

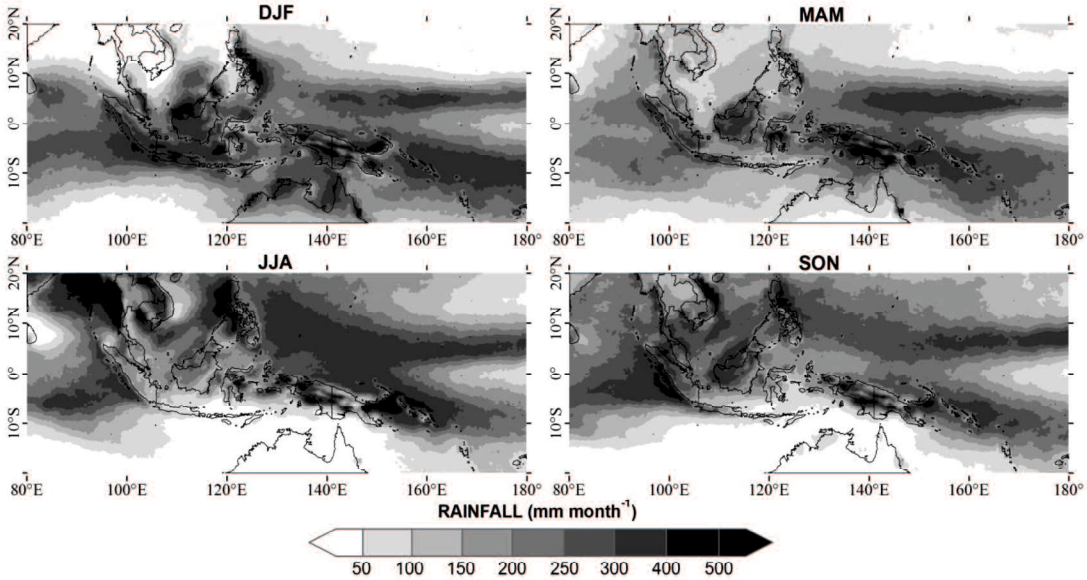

Figure 4.4. Seasonal climatological mean rainfall based on TRMM monthly composites from January 1998 to December 2013.

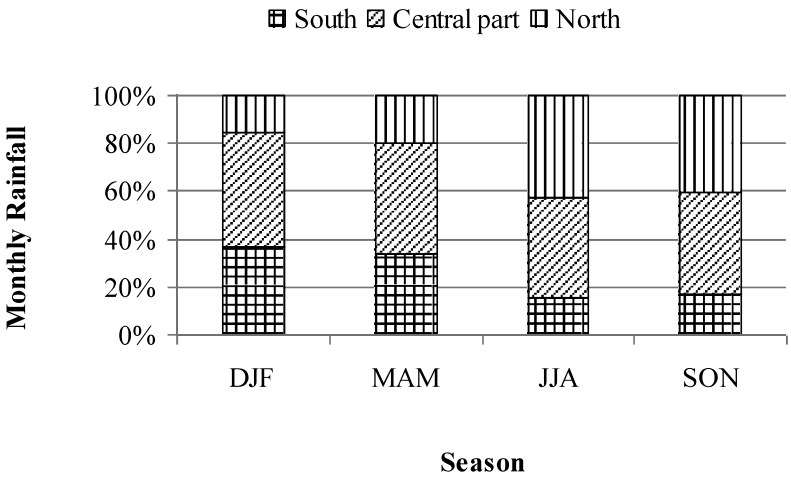

Figure 4.5. Seasonal changes of rainfall values derived from TRMM over three Maritime Continent regions: North (7° to 20° N); Central part (7° N to 7° S); and South (7° to 20° S). Units express as percentages.

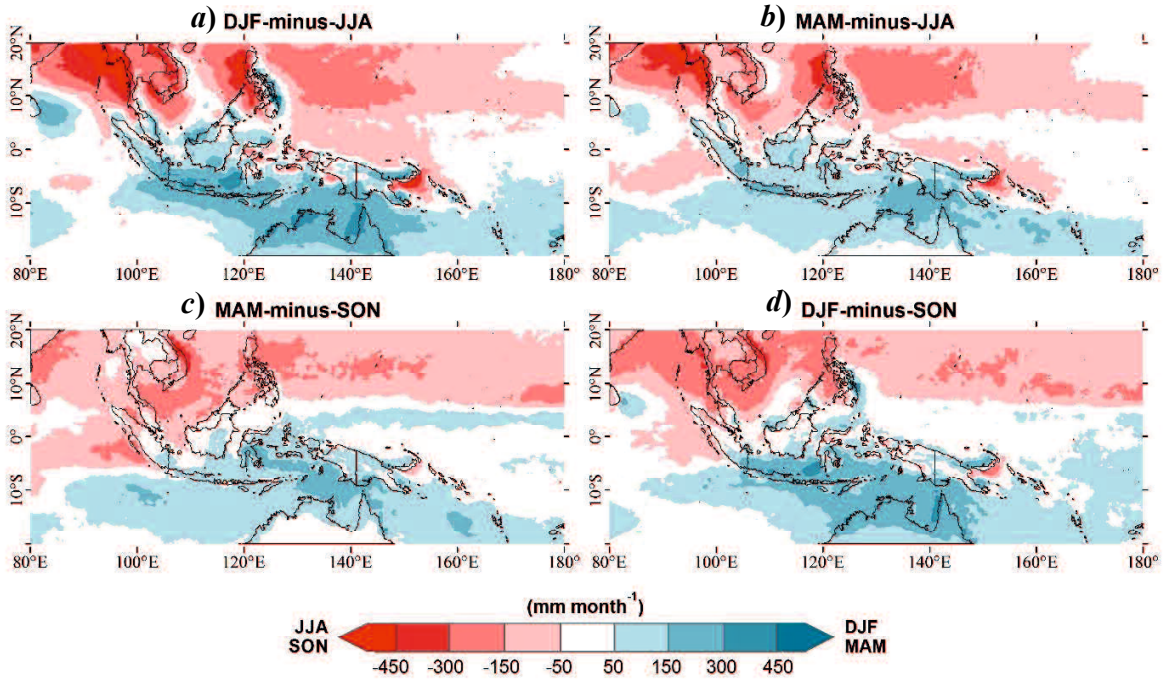

Figure 4.6. Seasonal analysis of rainfall differences between seasons derived from TRMM data: (a) DJF minus JJA, (b) MAM minus SON, (c) DJF minus SON, and (d) MAM minus JJA. Red color indicates high rainfall during JJA and SON seasons, and blue colour indicates DJF and MAM seasons.

The peak of the rainy season over the south, consistent with the phase of the northwest monsoon, continues to decrease during the boreal spring (MAM) transition season. Analysis of rainfall differences between DJF and JJA, as shown in Figure 4.6(a), clearly shows dominant boreal winter rainfall over the south equatorial region, except on the east coast of the Philippine Islands, the Malaysian Peninsula, and the north coast of Kalimantan. However, during the high rainfall in JJA season, rainfall was lower in the southern Indian Ocean than in Indochina and the north Pacific Ocean. Rainfall values were lower over the coastal areas during MAM than during DJF (e.g., over the west coast of Sumatra, the east coast of Philippine Islands, and the north coasts of Australia and Kalimantan). However, the rainfall values remained similar over the north, central, and south parts compared to the DJF season (Figure 4.5); the rainfall values over the south were 36.84% and 33.50% during DJF and MAM, respectively, and the rainfall over central areas during DJF and MAM were 47.44% and 46.80%, respectively. Increased rainfall occurred over Indochina, especially in the western Cambodia, and this was caused by diurnal land breezes resulting from the prevailing north-westward wind movements and their

interactions (Takahashi et al., 2010). The northward effects of the ITCZ caused these conditions, although these effects were still blocked by oceanic regions that were located to the west of the heat sources (Hung et al., 2004).

Northern rainfall was markedly higher during JJA than during MAM (see Figure 4.5), except over the east coast of Vietnam. In this season, heavy rainfall continued to extending to the north, towards the east of Bengal Bay, Thailand Bay, and over Indochina in the west of the Annamite Mountains. The analysis of rainfall differences in the north clearly identified extreme increases in rainfall from MAM to JJA. Figure 4.6b identifies an extreme increase in rainfall over the western Philippines and Cambodia. An interesting phenomenon was found south of the Equator around the Maluku and Solomon Islands, where the peak of the rainy season was detected during the boreal summer (JJA) due to the onshore windward movement of the austral winter monsoon from the southwest Pacific and Arafura Sea (Chang et al., 2005). Large-scale convergence surrounding the Philippine Islands shifted from the east during DJF to the west during JJA season. In the south, large areas with minimum rainfall were identified over southern Indonesia and northern Australia, but high rainfall was observed north of 10°S in the Indian Ocean and in the SPCZ region. During the boreal fall season (SON), heavy rainfall over the Annamite Mountains and the Philippine Islands began shifting from west to east. High rainfall over the Maluku Islands ceased and shifted to areas that are south of the Jayawijaya Mountains. Equatorially, heavy rainfall was observed on the western coast of Sumatra. Heavy rainfall, similar to which occurred during the MAM season (see also Figure 4.6(c)), entered Kalimantan Island from the north. However, the rainfall (Figure 4.5) shows generally higher values in the north, similar to the values observed during JJA. In addition, similar to changes from MAM to JJA, rainfall also markedly increased over the southern Hemisphere (Figure 4.6(d)) from SON to DJF.

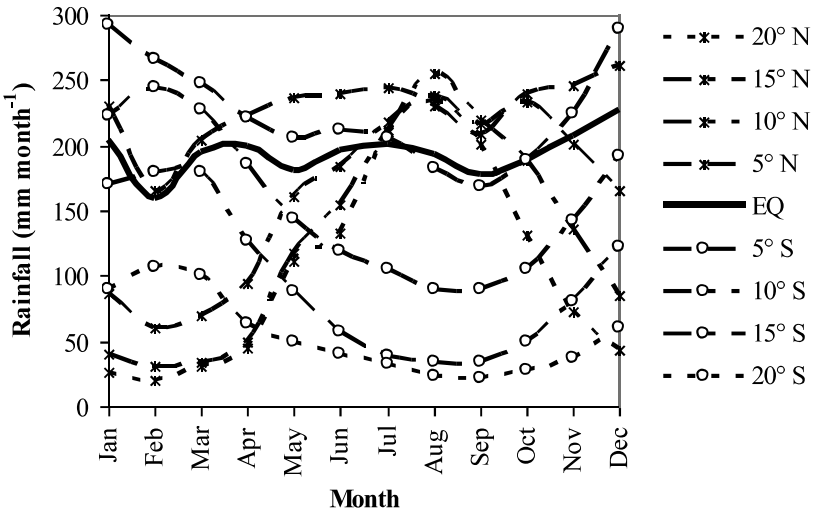

Figure 4.7. 16 years annual zonal averages of rainfall data derived from TRMM. The vertical axis indicates monthly and annual rainfall averages for latitude indices between 20° N to 20° S.

The spatial pattern of seasonal rainfall did not clearly show the times of maximum and minimum rainfall. An analysis of the monthly average rainfall pattern (based on nine cross-sections; see figure 4.1) was also conducted here. Annual rainfall in zonal latitudinal divisions from 20° N to 20° S were averaged (based on 16 years of data). Figure 4.7 illustrates the monthly average rainfall that was measured by TRMM 3B43 v7 in zonal latitudinal divisions. The Equatorial rainfall values were stable, relatively high, and exhibited small seasonal variability. Two monsoons and the presence of a strong ITCZ affected the sub-tropical region, resulting in one peak and one trough. Stable seasonal equatorial region rainfall is associated with the southward and northward movement of the ITCZ when large-scale convection is enhanced. The ITCZ occurs twice in the equatorial region (Hung et al., 2004) and produces high rainfall values in this region. The ITCZ passes through each of the north and south equatorial regions once annually, causing the boreal summer and winter, respectively. This difference contributes to lower rainfall values in non-equatorial regions than equatorial regions. Seasonal rainfall varied and reached a maximum at 20° N in August and at 20° S in February. Average monthly rainfall patterns clearly differed between north and south. High northern rainfall values were found from 5° to 20° N during the August rainy season, and in the south, high rainfall values gradually moved from 5° to 20° S during January and February. During the dry seasons, low rainfall

occurred from 10° to 20° in the north and south during February and August, respectively, and at 5° north and south, the rainfall was similar to that found in the equatorial region (EQ).

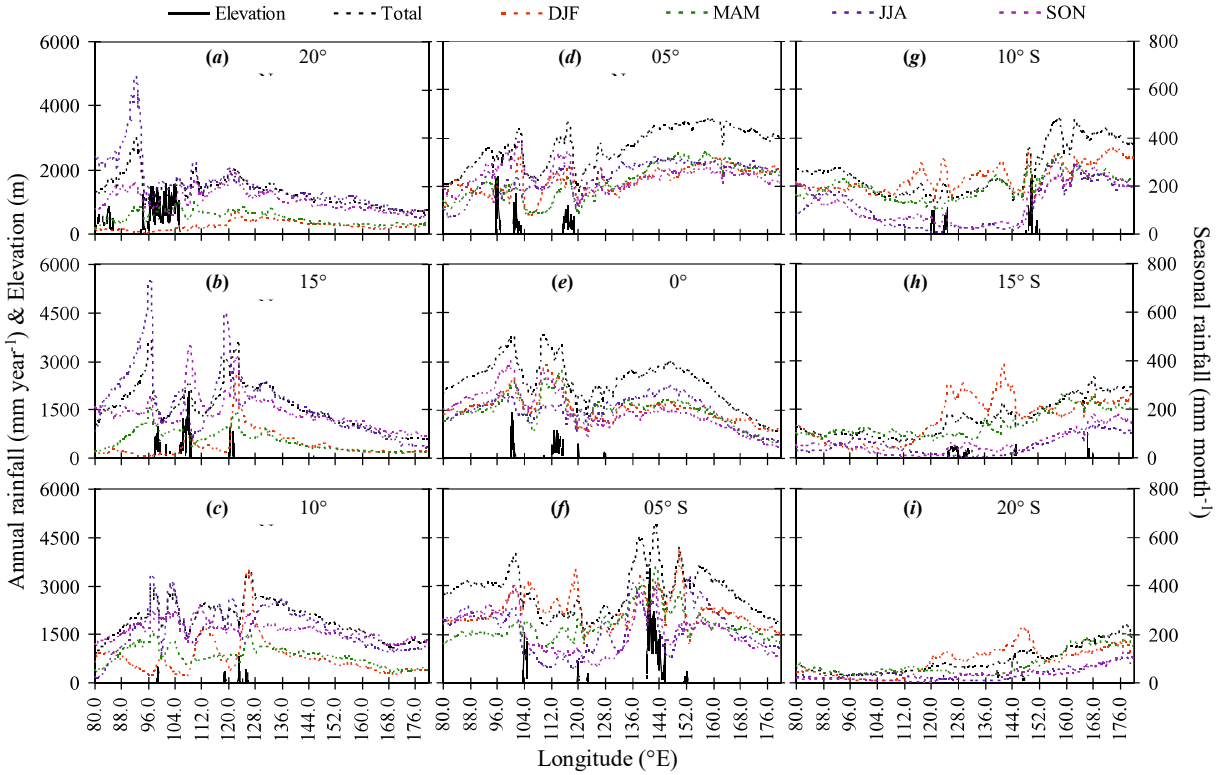

Figure 4.8. Elevation extracted from SRTM and annual and seasonal rainfall derived from TRMM data shown in nine cross-sections as presented in Figure 4.1.

As presented in Figures 4.2 and 4.4, MC rainfall values were greatly affected by topography. Furthermore, monthly average rainfall patterns (based on zonal latitudinal divisions), did not show effect of topography on rainfall variability. West-east rainfall and elevation cross-sectional data clarified the impact of topography on the annual and seasonal climatological average rainfall distribution. Figure 4.8 shows nine west-east cross-sections showing elevation and rainfall extracted from high-resolution TRMM satellite data (based on Figure 4.1). Nine cross-sections clearly show connections between high rainfalls in regions of high elevation compared with low sea elevations. The TRMM data provide clearly capturing in the rainfall characteristics that are affected by topography, especially those caused by heavy rainfall in offshore and steep slopes of the mountainous regions. All figure described the MC rainfall characteristics that were affected by elevations manifested more during wet seasons (both in the south and in the north) than during dry or transitional seasons. However, to some degree, increasing amounts of rainfall

were not only found in regions of high elevation but also in near areas of low elevation, leading to some confusion regarding the connection between rainfall and elevation. Most heavy rainfall at low elevations occurred over areas of convergence between land and sea that were located near high elevations [e.g., in southern Sumatra (see Figure 4.8(e) at 100 °E) and western Myanmar (see Figure 4.8(b) at 97 °E)], thus producing nocturnal rainfall activity along the coast. This rainfall descended seaward from the mountain and interacted with the prevailing northwest monsoon flow (Mori et al., 2004).

4.5 Anomalous rainfall associated with El Niño Modoki and the conventional El Niño

Anomalous MC rainfall could not be separated into MC atmosphere–ocean interactions. Two interaction phenomena that are located very close to the MC are El Niño Modoki, occasionally termed the central Pacific El Niño, and the conventional El Niño, occasionally termed the east Pacific El Niño. Simple linear and partial correlations were measured to determine the relationship between El Niño Modoki and conventional El Niño rainfall. Figures 4.9 described seasonal spatial patterns linear relationship between rainfall with El Niño Modoki and conventional El Niño that were analyzed using TRMM satellite data. Most relationships between MC rainfall and ENSO indexes indicated negative correlations, showing that warm events in the Pacific Basin can lead to decreased rainfall over most MC areas; the opposite situation tends to occur during cold events. Generally, a seasonal dynamic movement of the relationship between El Niño Modoki and conventional El Niño rainfall indicates spatial-temporal patterns like those that are seen over the MC. However, El Niño Modoki and conventional El Niño exhibit similar impacts during boreal summer and fall, and areas impacted by conventional El Nino are wider compared to El Niño Modoki during northern winter and spring. Meanwhile, details of the spatial pattern of El Niño Modoki and conventional El Niño influences the rainfall in areas that has complex system of islands and seas is clearly seen due to the high resolution of TRMM satellite data.

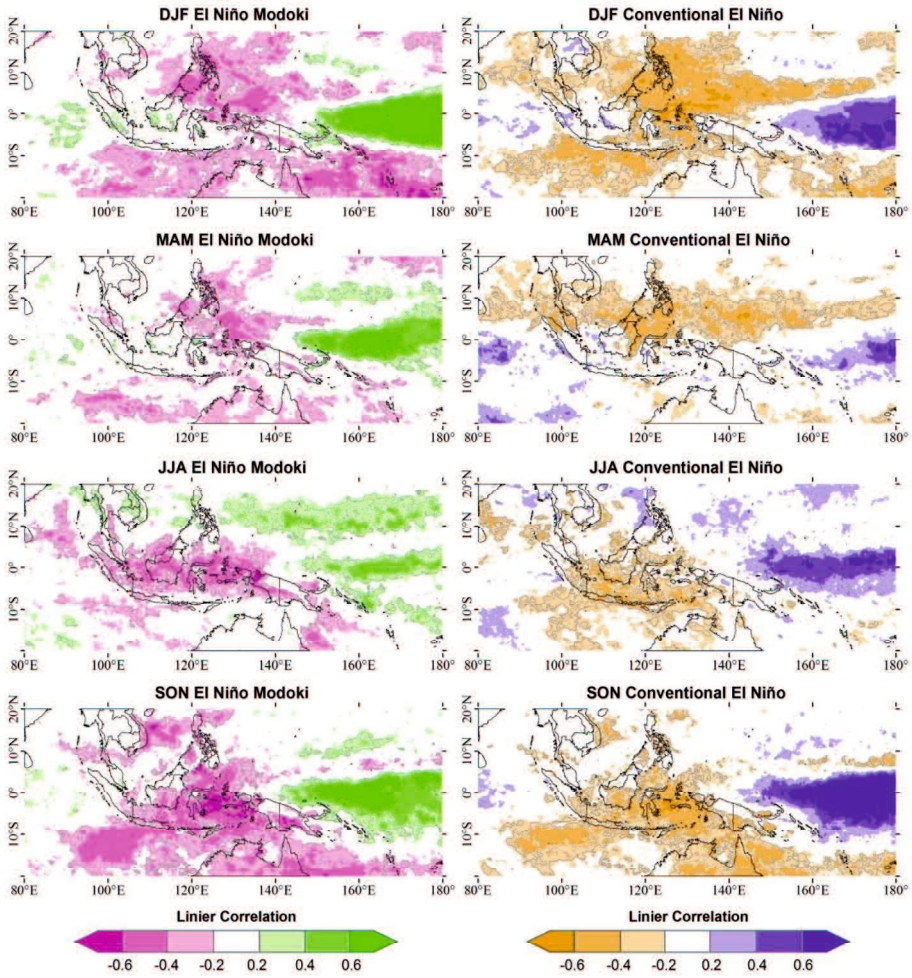

Figure 4.9. Seasonal analysis of the linear rainfall correlation derived from TRMM between El Niño Modoki (left) and conventional El Niño (right). Gray solid line and dashed line indicate significant level of correlation under 95% and 99%, respectively.

During DJF, the negative correlation between rainfall and ENSO indices is wider in the south than in the north when the El Niño Modoki event occurs, vice versa during conventional El Niño phenomenon. Consistent with the result of Chang et al. (2004) who showed negative correlation between rainfall and Niño-3 that present over most of the MC. A positive correlation was observed on the east outside MC region, and an uncertain correlation was observed over west equatorial, including western Indonesia and Indochina areas, which is a region that is heavily influenced by the wet northwest monsoon. Most negative correlations occurred over the sea, excluding areas to the northeast of Kalimantan, the Philippine Islands, the northern coast of Australia, and the eastern Indonesia. However, a relationship was detected for the conventional El Niño but not for El Niño Modoki describing rainfall over the south Malay Peninsula.

Interestingly, detail spatial pattern on rainfall influences by both of ENSO types is clearly seen when applied high resolution of TRMM data. For example during conventional El Nino, the TRMM provide clearly spatial patterns in Java and Sulawesi islands, similar with the result of Chang et al. (2004) who showed most of rain gauges over two islands had no significant correlation with Nino-3. These results demonstrated that a complex system of islands and seas over MC require precise rainfall data to capture the spatial pattern of ENSO influences on the rainfall anomalies.

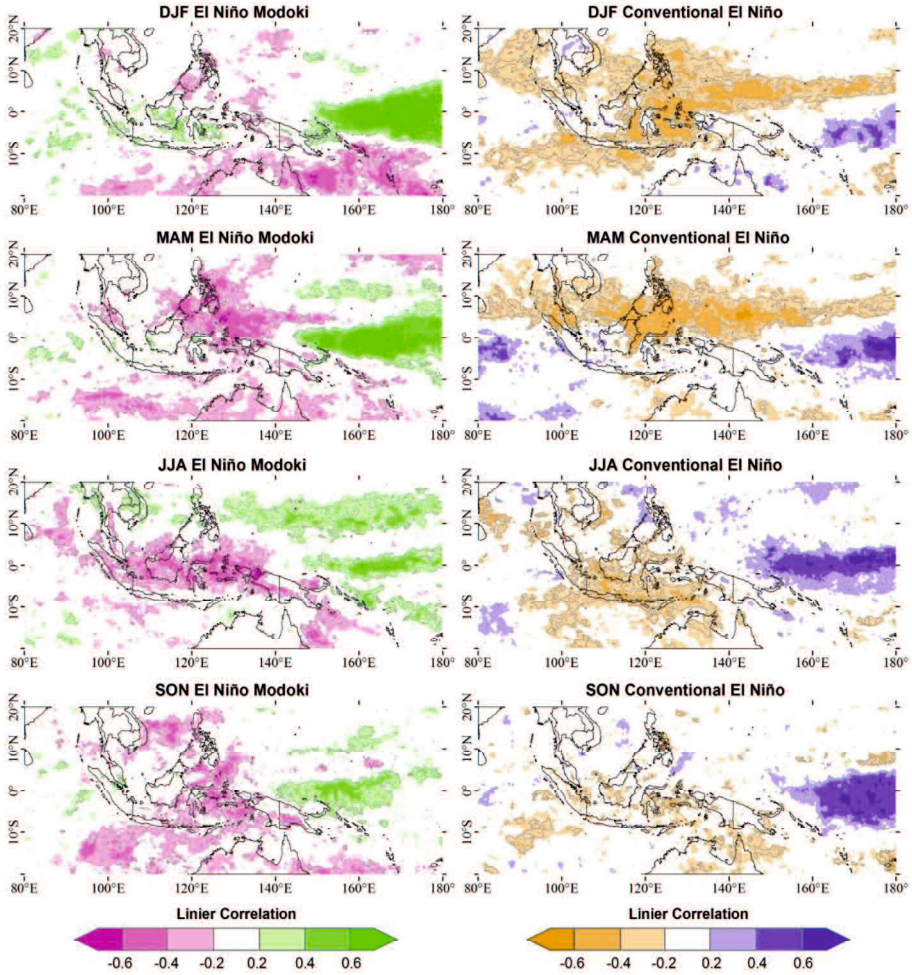

Figure 4.10. Same as Figure 4.9, partial correlation of El Niño Modoki with the effect of conventional El Niño removed (left) and partial correlation of conventional El Niño with the effect of El Niño Modoki removed (right).

During the MAM season, a relationship between the conventional and Modoki El Niño was found for a small area of rainfall in the south, and began to weaken in the north compared with DJF season. Most of negative correlation disappeared over Indonesia and moved to the northen

part of equator to 15° N. The areas showing correlations declined in the south, and positive and unclear correlations remained in the east and west equatorial regions, respectively. The areas affected by the conventional El Niño were wider than the areas affected by El Niño Modoki; in the north lie between 80° to 180°E with the centre of the negative correlation in the northeast of Borneo and southwest of Philippines. In contrast, the centre of the negative correlation which affected by El Niño Modoki occurs in the north part of Maluku Islands. The disappearance of the negative correlation over the sea and the higher impact over mainland Australia indicates that areas in the south that are affected by El Niño Modoki are wider than those that are affected by the conventional El Niño and the opposite tends to occur in the north.

Spatial clustering of negative correlations between rainfall values with both indices in JJA are clearly seen over Indonesia and the Malay Peninsula. Negative correlations over the north side decreased and became positive, with an irregular distribution over the land. Additionally, the relationship between both rainfall indices was unclear to the south. Generally, the areas affected by the El Niño Modoki clustered in the equatorial region from Western Sumatra/Malay Peninsula to Papua, except over southern Java in Indonesia. Meanwhile, the area affected by conventional El Niño clustered more into the south of the equatorial region, including southern Java of Indonesia. The existence of clustering distributions is consistent with the location of the large anomalous outgoing long radiation and strong descending motion of the Walker Circulations (Juneng and Tangang, 2005; Weng et al., 2007). The areas affected by both indices expanded to the south during SON with similar clustering. Most areas below 10°S exhibited negative correlations between both indices. The affected areas in Indonesia shifted eastward, causing unrelated rainfall over the Malay Peninsula, western Sumatra, and northern Kalimantan due to the fact that South China Sea has not been clearly affected by ENSO (Tan et al., 2016). A similar condition appeared in the north, except on the east coast of Vietnam.

Figure 4.10 represent the seasonal patterns of spatial partial correlation between rainfall with El Niño Modoki when the linear effect of conventional El Niño is removed, and with conventional El Niño when the linear effect of El Niño Modoki is removed. Generally, spatial patterns of partial correlations between rainfall due to El Niño Modoki and the conventional El Niño were not completely different from the linear spatial correlation patterns during MAM and JJA, and greatly changed during SON and DJF. During SON, when the effects of the conventional El Niño were removed, areas of negative correlation of El Niño Modoki slightly

evaporated over the south, leaving irregular spatial patterns. Furthermore, spatial distributions of conventional El Niño during SON has been faded compare to the Modoki impact, indicated during SON season the El Niño Modoki phenomenon is more influence to the MC rainfall. The effects are clearly seen over the whole area of MC were reduced significant negative correlation, except significant positive correlation in the central Pacific. In contrast, removing the effect of the conventional El Niño decreased the negative correlation with El Niño Modoki during DJF, especially in the north, and similar situation occurred when the effect of the El Niño Modoki were removed, but with marginal changes. During MAM and JJA, both phenomena affected each other, causing negatively correlated and impoverished spatial distribution values for the MC, especially for Indonesia during MAM and northern MC during JJA. In most cases, partial correlation analysis indicated rainfall anomaly over MC during SON predominantly caused by El Niño Modoki and conventional El Niño during DJF, and influenced by both during MAM and JJA.

Previous analysis showed that both phenomena exerted different impacts on MC rainfall during each season; this result indicates that different spatial rainfall anomaly distributions occur in this area. Further evidence provided an explanation of the rainfall anomaly pattern associated with the conventional and Modoki El Niño events. El Niño Modoki events during 2002/03 and 2009/10 and conventional El Niño events during 2006/07 were chosen to clarify the spatial pattern of rainfall anomalies in this region. The spatial distributions of rainfall anomalies for JJA 2002 to MAM 2003, JJA 2006 to MAM 2007, and JJA 2009 to MAM 2010 (Figure 4.11) were generally related to the spatial distribution of the observed linear and partial correlations but exhibited uncertain seasonal or annual spatial distributions. The dynamic movement of the anomalous rainfall was also seen in a spatial-temporal view. The areas of anomalous rainfall were similar during JJA and SON in 2002, 2006 and 2009. However, when the EMI and Niño-3 values were near zero (see Figure 4.12(b)), the areas of rainfall anomaly were small and weaker (as seen in the 2006/2007 event). The spatial pattern of rainfall anomalies during JJA was different from the linear and partial correlations, except over Indonesia. It is possible that the spatial distribution differences are caused by another phenomenon that develops over the west MC, such as the IOD events that occur in the Indian Ocean (Saji and Yamagata, 2003b) which also causes the SST anomalies in the MC region (Weng et al., 2011; As-Syakur et al., 2014). However, these phenomena are not supported in this study. During SON, below normal rainfall

anomaly clustering distributions were observed over the Indonesian Archipelago and Australia. During this season, the impacts of both these phenomena increased in size, moving westward in the south. Similar spatial distributions were found for the linear correlations, and the greatest effects were observed during SON.

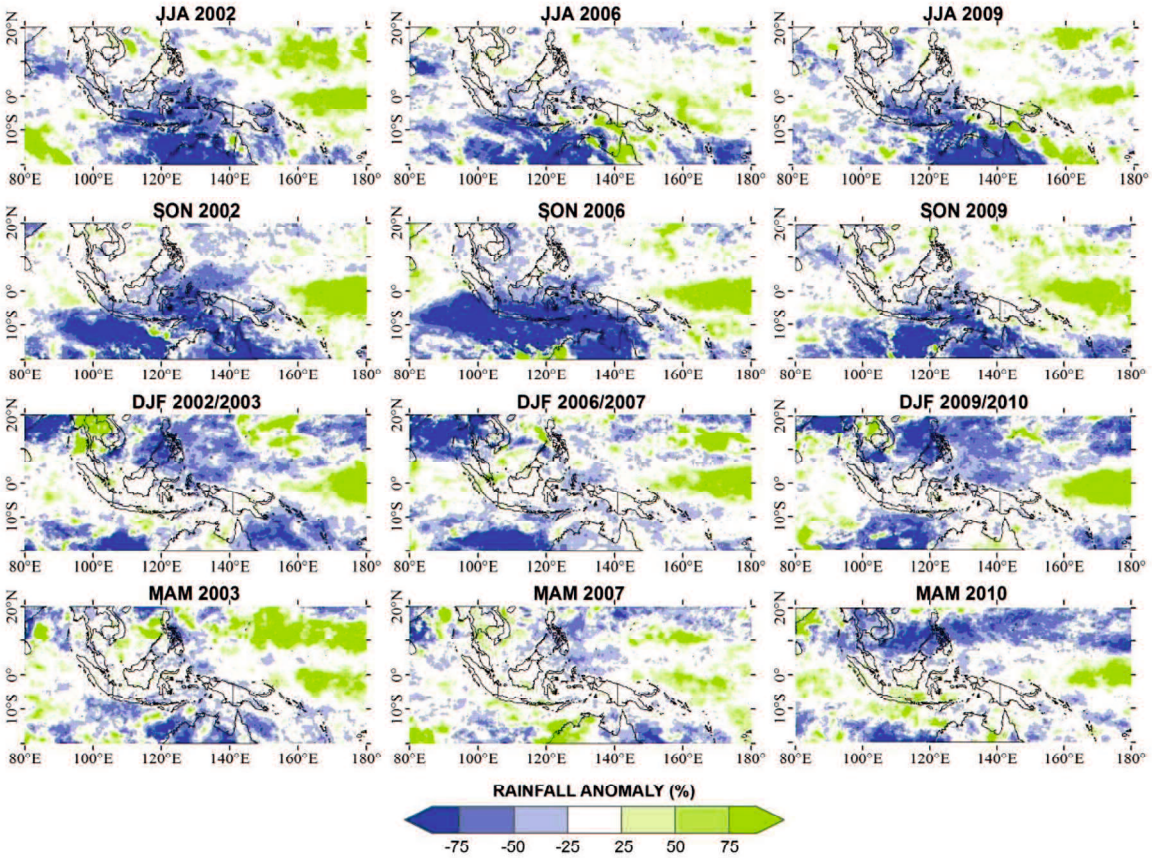

Figure 4.11. Rainfall anomaly (percentage) spatial distribution seasonal analysis for periods from JJA 2002 to MAM 2003 (left), JJA 2006 to MAM 2007 (centre), and JJA 2009 to MAM 2010 (right).

During DJF and MAM, anomalous rainfall was inconsistently distributed in the annual observations, except during DJF of 2002/03 and 2009/10. Slightly less than normal rainfall anomalies were found in the southern area and over the mainland. The spatial distribution of rainfall anomalies exhibited a linear correlation, except in the north where anomalous rainfall was found over Indochina and the Bay of Bengal in 2006/07. The patterns for the indices were not clearly explained during the MAM season, except during 2010, and showed similar linear and partial correlation distributions with conventional El Niño. During DJF 2009/10 and MAM 2010, where there are classified as El Niño Modoki event, the rainfall anomaly has a similar

spatial pattern which was observed for the linear and partial correlations, but for conventional El Niño. In contrast, during DJF 2006/07 and MAM 2007 the spatial distributions of rainfall anomaly are similar with partial correlation of El Niño Modoki, although the year is classified as conventional El Niño. The values for EMI and Niño-3 based on monthly index patterns (Figure 4.12(a) and (b)) during the MAM season, particularly during 2003 and 2007, were smaller than in earlier seasons, creating uneven rainfall anomalies, as seen in the spatial distributions. However, during 2010, the observed rainfall anomalies corresponded reasonably with the spatial patterns of the linear and partial correlations, especially with conventional El Niño event. This condition (consistent with Figure 4.12(c)) exhibited high and positive EMI and Niño-3 values during March-April 2010. These indicated when EMI and Niño-3 values were equally high (Figure 4.12(c)) during the decay phase, conventional El Niño event had a stronger effect than El Niño Modoki to the MC rainfall.

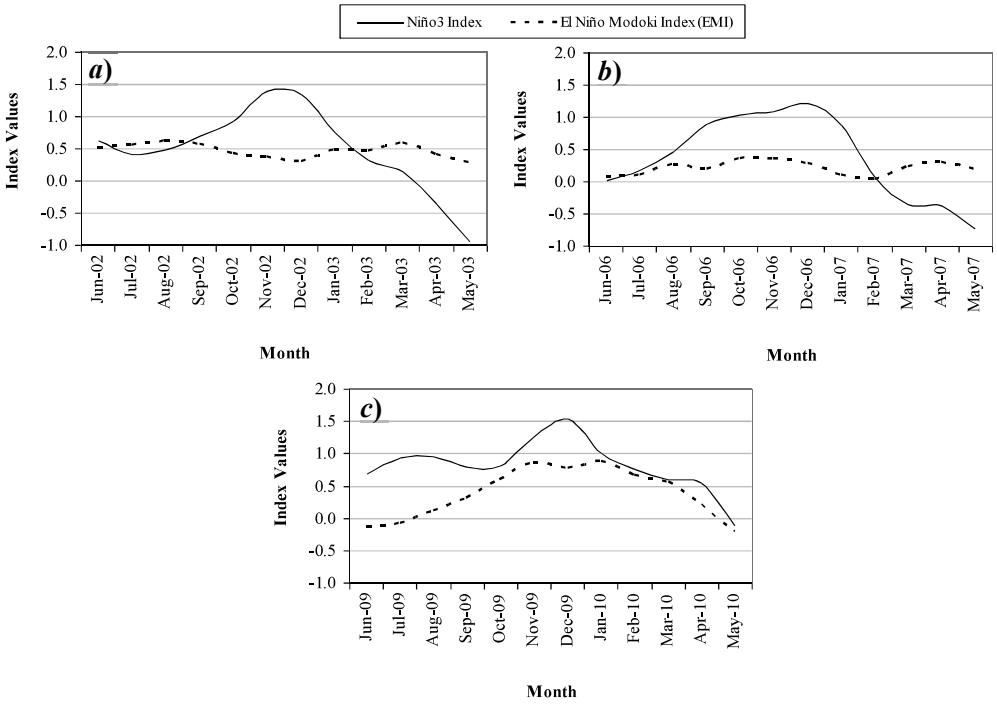

Figure 4.12. Monthly patterns of EMI and Niño-3 indices: (a) June 2002 to May 2003, (b) June 2006 to May 2007, and (c) June 2009 to May 2010.

4.6 Summary

In this study, MC rainfall variability was investigated based on 16 years (January 1998 to December 2013) of monthly satellite data obtained from TRMM 3B43 v7. Annual, seasonal and monthly analyses were conducted. Rainfall over different elevations were compared to determine

the effect of land and topography on rainfall events. In addition, EMI and Niño-3 index values were used to understand how anomalous rainfall was impacted by atmosphere–ocean interactions due to El Niño Modoki (sample cases: 2002/03 and 2009/10) and conventional El Niño (sample case: 2006/07) events. This study demonstrates that MC rainfall characteristics can be determined based on TRMM 3B43 remote sensing data, and this method as the advantage of accommodating different spatial-temporal mainland and sea rainfall information sets.

According to the spatial distribution of annual precipitation over the MC, the mean annual rainfall totals are high in the central tropical area and decrease from the equatorial belts to the south and north. The results are typical of almost all precipitation that accumulates over long periods observed over the land, except in the ITCZ and SPCZ belt, where heavy rainfall was observed over the sea. Complex land-sea thermal contrasts and orographic effects cause heavy rainfall over land areas (Qian, 2008). An increase in the annual average rainfall was evident from the slope of the regression line. A trend analysis indicated mean annual precipitation decreases (negative trends) or increases (positive trends) throughout the region. A marked positive trend was presented over the equatorial area, especially in the eastern part over the ITCZ belt, and a small negative trend was found in a different location. Most of the ITCZ belt over the Pacific exhibited a significantly increasing rainfall trend, which was associated with cold events in central Pacific (Chang et al., 2004). Similar conditions were also found over land, but no effect of topography was observed, except over the eastern part of the Philippines and in the elongated area of high rainfall over the eastern part of Jayawijaya Mountains. Probably not too high resolution of the satellite data (0.25◦ × 0.25◦) might have hidden an effect of topography on rainfall trend. Additionally, the existence of a cyclone track that increased from east to west might influence the significant positive rainfall trend observed over the eastern Philippines (Lyon and Camargo, 2009).

Seasonal rainfall variability (Figure 4.7) was proportional to SST variability, as previously observed by Swardika et al. (2012). In the equatorial region, the stable monthly average SST pattern was similar to the monthly average rainfall pattern, and warm SST condition during JJA in the northern region also created heavy rainfall; the similar events tend to occur in the southern region during DJF. Warm SST enhanced the creation of water vapour by increasing evapotranspiration, thus generating rain in this region. In addition, the distribution of positive rainfall trends over the western tropical Pacific is consistent with the linear trend of SST

described by L'Heureux et al. (2013). As-Syakur et al. (2014) and Hendon (2003) also confirmed the influence of SST in Indonesian seas and surroundings on rainfall patterns in the vicinity of Indonesia.

The MC island-topography-induced convection and large-scale circulation-generated convection were confirmed in this study. Generally, high rainfall was concentrated over the central part of the MC region (see Figure 4.5); this rain was caused by warm SST. However, in land and offshore areas, high and varied topography generated heavy rainfall. Figures 4.8 clearly indicate the impact of complex topography and sea distributions on rainfall values. Heavy precipitation was found along coastal plains, possibly due to ascending air over coastal hills or seaward-propagating orogenic convective systems (Mori et al., 2004). The rising western topography of the Bukitbarisan Mountains of Sumatra, the Arakan Mountains of Myanmar, and the Cardamom Mountains of Cambodia strongly influenced maximum rainfall over the adjacent Indian Ocean, Bay of Bengal, and Bay of Thailand, respectively, and rain fell much less frequently on the eastern side of these mountains. Similar conditions occur over the northwest part of the Muller Mountains of Kalimantan in the South China Sea, as described by Houze et al. (1981). The eastern coast of the Philippine Islands also experienced frequent rain; we suggest that this results from a similar complex land-sea thermal contrast and large-scale circulation as that mentioned above for western regions. Rainfall activity along the eastern coast of the Philippine are probably created by land breezes that converge with easterly Pacific Ocean winds, thereby generating offshore convection that produces heavy rainfall as it develops into an organized precipitation system. As described by Biasutti et al. (2012), rain frequency fields, topographic enhancements and rain shadows capture large-scale seasonal movements of the main precipitation centres throughout the tropics. Thermally and convectively induced local circulation controls this process and diurnal offshore atmosphere thermodynamic stability changes (Wu et al., 2009). We also suggest that wind impinges from the offshore ocean/sea onto the coastal edge of mountains/lands, thereby creating heavy rainfall in the coastal area. These aspects are considered possible due to insufficient parameterization of the convective process (Mori et al., 2004). Additionally, Papua Island is elongated with a windward alignment in the northwest-southeast direction and contains the Jayawijaya Mountains, which exhibit maximum elevations of over 3,000 m above mean sea level and exhibit no distinct rain shadow. Ichikawa

and Yasunari (2008) stated that the heating of regions of high elevation in Papua Island creates bands of frequent precipitation on both slopes throughout the year.

Both the Modoki and conventional El Niño create MC rainfall anomalies and have similar spatial-temporal impacts on rainfall variability during all seasons. Spatial-temporal analysis shows that the dynamic anomalous rainfall movement begins during JJA over the southernmost part of Indonesia and ends during MAM over the northern Philippine Islands. However, in general, the conventional El Niño influences the rainfall fluctuation in MC wider than El Niño Modoki, especially during DJF and MAM, and similar during JJA and SON, indicating that the conventional El Niño has a larger impact than El Niño Modoki. Weng et al (2009) argues that the conventional El Niño produced boomerang-shaped SSTA extending north-eastward and south-eastward in the eastern MC during northeast winter. In contrast, areas of boomerang-shaped are diminish during El Niño Modoki leading to a reduction of the impact (Weng et al., 2009; Liu et al., 2014). Meanwhile, El Niño Modoki and conventional El Niño causes the SST anomalies in the southern MC during JJA and SON resulting in similar impact from both of El Niño (Weng et al., 2007; Juneng and Tangang, 2005; McBride et al., 2003). Seasonally, spatial-temporal patterns of highly anomalous rainfall correspond with spatial-temporal low rainfall means, indicating that areas with poor rainfall are more vulnerable to the ENSO effect. Large-scale clustering patterns indicate that the local complex distribution of the topography was insufficient to influence the spatial-temporal clustering. In addition, the existence of a spatial-temporal clustering zone suggested that the impact of both phenomena on rainfall values over the MC might be associated with the southward and northward sun movements that produce monsoon activity over the ITCZ belt. Moreover, partial correlation analysis showed that El Niño Modoki and the conventional El Niño mutually influence rainfall variability during MAM and JJA at a level that continuously decreases from DJF to MAM. Meanwhile, spatial distributions of rainfall anomalies during SON were greatly affected by the El Niño Modoki phenomenon and conventional El Niño during DJF. Changes in SST anomaly from south to north hemisphere during SON and DJF (McBride et al., 2003) may shift the impact. The MC rainfall anomaly during the mature phase of ENSO was clearly seen during JJA 2006 as a direct consequence of the Southeast Asian monsoon system, which is associated with the ENSO reversal, a similar phenomenon was reported by Chang et al. (2008). As stated previously, El Niño Modoki and the conventional El Niño strongly influence regions that experience low rainfall events. During JJA

and SON, ENSO influences on south equatorial rainfall are at a maximum, at the same time as the dry season. The anomalous south equatorial rainfall tends to correlate well with anomalous SST in the eastern and central Pacific during JJA and SON (McBride et al., 2003; Hamada et al., 2002). Warming SST in the eastern and central Pacific shifts the Walker Circulation towards the equatorial eastern Pacific and suppresses convergence over the MC (Wang et al., 2003). Meanwhile, warming (cooling) events in the eastern and central Pacific cause cold (warm) SST over the southern part of the equatorial region (Susanto et al., 2001), leading to less (enhance) evaporation and less (more) rain in these areas. During DJF and MAM, most anomalous rainfall is found over the north; again, this occurs at the same time as the northern dry season. These findings are in general agreement with those reported by Ropelewski and Halpert (1987; 1996). Juneng and Tangang (2005) argue that in addition to causing anomalous SST in the eastern and central Pacific, the MC rainfall anomaly also causes atmosphere–ocean variations in the Indo-Pacific region. These forces are associated with the strengthening and weakening of two off-equatorial anticyclones over the southern Indian Ocean and over the western North Pacific. The factors that cause this lower than normal (anomalous) rainfall are clearly seen during the MAM 2010. Furthermore, this study also highlighted the negligible relationship between these phenomena and rainfall in the rainy season hemisphere. We suggest that cloudy conditions that occur during the rainy season are affected by convergence and updrafts over the ITCZ area, these conditions reduce the impact of ENSO on rainfall variability over MC during periods of heavy rainfall.

In this study, the general characteristics of MC rainfall variability and their associations with monsoons, complex topography and both types of El Niño were studied based on TRMM 3B43 v7 data. The results show that large-scale circulations, such as ITCZ and SPCZ, create heavy land-ocean rainfall, predominantly over oceans. Equatorial rainfall is more stable than that in northern and southern equatorial regions and occurs predominantly over land areas. Complex topography also contributes to land-sea rainfall variability in this region and causes much rainfall over land and offshore areas. In addition, El Niño Modoki and the conventional El Niño strongly influenced rainfall during all season, except in regions that have spatial-temporal heavy rainfall means. Regionally, monsoons and the ITCZ-SPCZ belt caused seasonal changes in rainfall variability over various locations in the MC, but not at other latitudes Additionally, various characteristics related to wind direction, topography, and the existence of oceans cause different

local rainfall variability characteristics and differences from prevailing conditions for given latitudes. Therefore, MC rainfall characteristics are difficult to generalize due to the complexity of the contributing components. In future work, studies on rainfall variability over the MC should examine specific locations to provide more precise and accurate climate system models. Finally, the utilization of TRMM remote sensing data is very important for studying climatic-scale rainfall to provide information that is useful for water resource management, agricultural practices, infrastructure design, economic development, and policy-making; in this way, the adverse impacts of anomalous ENSO-associated rainfall in the MC can be minimized.

CHAPTER 5

Analysis of spatial and seasonal differences in the diurnal rainfall cycle over Sumatera revealed by 17-year TRMM 3B42 dataset

5.1 Introduction

One of the most dominant variations in the convective activity over the Indonesian Maritime Continent (IMC) is the diurnal rainfall cycle (DRC) (Yamanaka, 2016). It is generated mainly by differences between the heating of the land and sea surfaces, and the rainfall characteristics are closely related to the land–sea distribution, the terrain, and associated local circulation systems. Among many islands in the IMC, Sumatera is a cross-equatorial island located in the westernmost region of the IMC and bordering the Indian Ocean. The island is surrounded by more than 2500 smaller islands, and the Barisan Mountains, with altitudes of 2000–3800 m, run along the west coast and divide the island into its eastern and western portions (Figure 5.1). Because of its unique location and geography, Sumatera is an island that is ideally situated in the IMC with respect to investigating the DRC and its migration. It has been well documented in previous studies (e.g., Mori et al., 2004; Sakurai et al., 2005; Wu et al., 2009) that the DRC begins by generating convections in the mountainous areas in the afternoon and tends to produce the maximum rainfall in early evening over land. The rainfall peak migrates toward the coast around midnight and finally moves offshore in early morning. That pattern is roughly the same over other large islands and adjacent regions such as Kalimantan (Ichikawa and Yasunari, 2006) and Indochina (Takahashi, 2016) with differences being due to different local orography.

Rainfall characteristics over Sumatera are influenced also by intraseasonal, seasonal (monsoon), and interannual variations (Hamada et al., 2002; Chang et al., 2005; As-Syakur et al., 2016). Previous studies have concerned mainly the features of seasonal variability of DRCs over the region. Yanase et al. (2017) observed the diurnal zonal migration and its seasonality from 15 years of Tropical Rainfall Measuring Mission (TRMM) Precipitation Radar (PR) and 3B42 data, but only in the southern part of Sumatera. Furthermore, Sakurai et al. (2005) investigated the seasonal differences in the migration of diurnal cloud systems over Sumatera by using 1-year of blackbody-temperature data from the Geostationary Meteorological Satellite (GMS). Their study

reported that the appearance latitude of eastward cloud migration varied seasonally with the north–south displacement of the Intertropical Convergence Zone (ITCZ), while westward cloud migration appeared over the entire island during virtually all seasons.

It is still worth studying the seasonal and latitudinal changes in the diurnal rainfall migration cycle over Sumatera using data from much-longer periods. Long-term data obtained with spatiotemporally discontinuous TRMM observations can provide averaged features of the DRC for different seasons and latitudes (Mori et al., 2004; Hirose et al. 2008; Yanase et al. 2017). Our primary objective in this study has been to describe spatial and seasonal differences in the DRCs over Sumatera using long-term (17-year) 3-hourly TRMM 3B42 data.

5.2 Data and Method

We used TRMM 3B42v7 data processed by TRMM Multi-Satellite Precipitation Analysis (TMPA), which combines precipitation estimates from multiple satellites and from gauge analyses (where feasible) at fine scales (0.25° x 0.25° and 3-hourly) (Huffman et al., 2007). The observation period spans January 1998 through December 2014.

Our research has focused on Sumatera and the surrounding area (Figure 5.1). Three cross-sectional boxes (I to III), whose long sides are roughly normal to the west coast, were defined to analyze the regional differences in the diurnal variation over the northern, central, and southern regions of Sumatera.

We divide a year into the four seasons: December-January-February (DJF), March-April-May (MAM), June-July-August (JJA), and September-October-November (SON). DJF and JJA seasons represent the peak of the northwest and southeast monsoon, respectively, while the MAM and SON represent monsoon transitions (Aldrian and Susanto, 2003). Rainfall rates were extracted from TRMM 3B42 and unconditionally (including rain-free grids) spatially and temporally averaged over 0.25°×0.25° grids using 3-hourly local time bins, seasons, and regions. Each time-averaged value of 3-hourly rainfall rates is centered in the middle of each 3-hour period. For instance, the 1200 UTC (Coordinated Universal Time) rainfall rate represents the average value between 1030 and 1330 UTC. For all figures presented in this paper, the western Indonesian local time was used as the standard time (UTC +7 h, correct at 105°E) and denoted by LT. For instance, the rainfall rate corresponding to 01 LT on the current day is equivalent to 18 UTC the previous day.

In order to illustrate the tendency of DRC migration over Sumatera in each region and season, we used a Hovmöller diagram to capture the propagation along with the temporal evolution. To measure the distance that the rainfall signals reach over the western sea, we used threshold rainfall rates >0.5 mm h−1, and the distance of migration was calculated from the western coastline (Figure 5.1). We examined the validity of the migration analysis by using the Multifunctional Transport Satellite-1R (MTSAT-1R) data from July 2005 through June 2010, with hourly temporal continuity and 0.04° spatial resolution. The occurrence frequency of tall clouds with the cloud-top temperature less than 230 K was computed, according to the method by Sakurai et al. (2005) who used GMS (the predecessor of MTSAT).

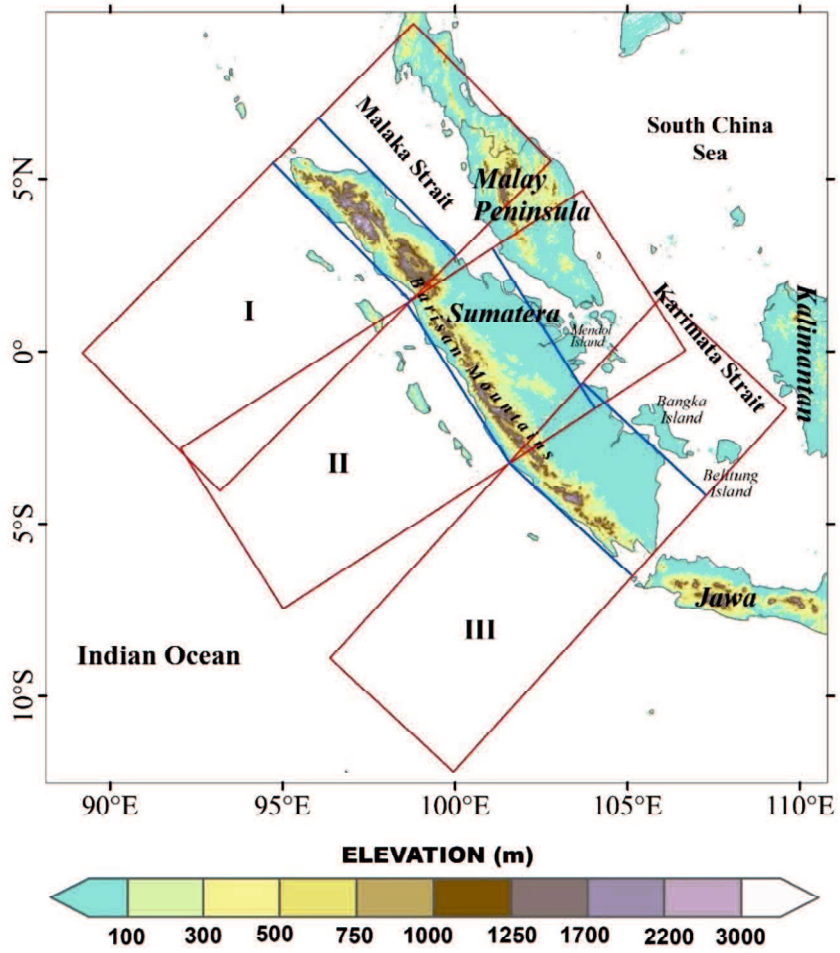

Figure 5.1. Study area and topography. Three red boxes represent north (Box I), central (Box II), and south (Box III) Sumatera regions for analyzing regional differences. Blue lines indicate approximate coastline for land definition in each box.

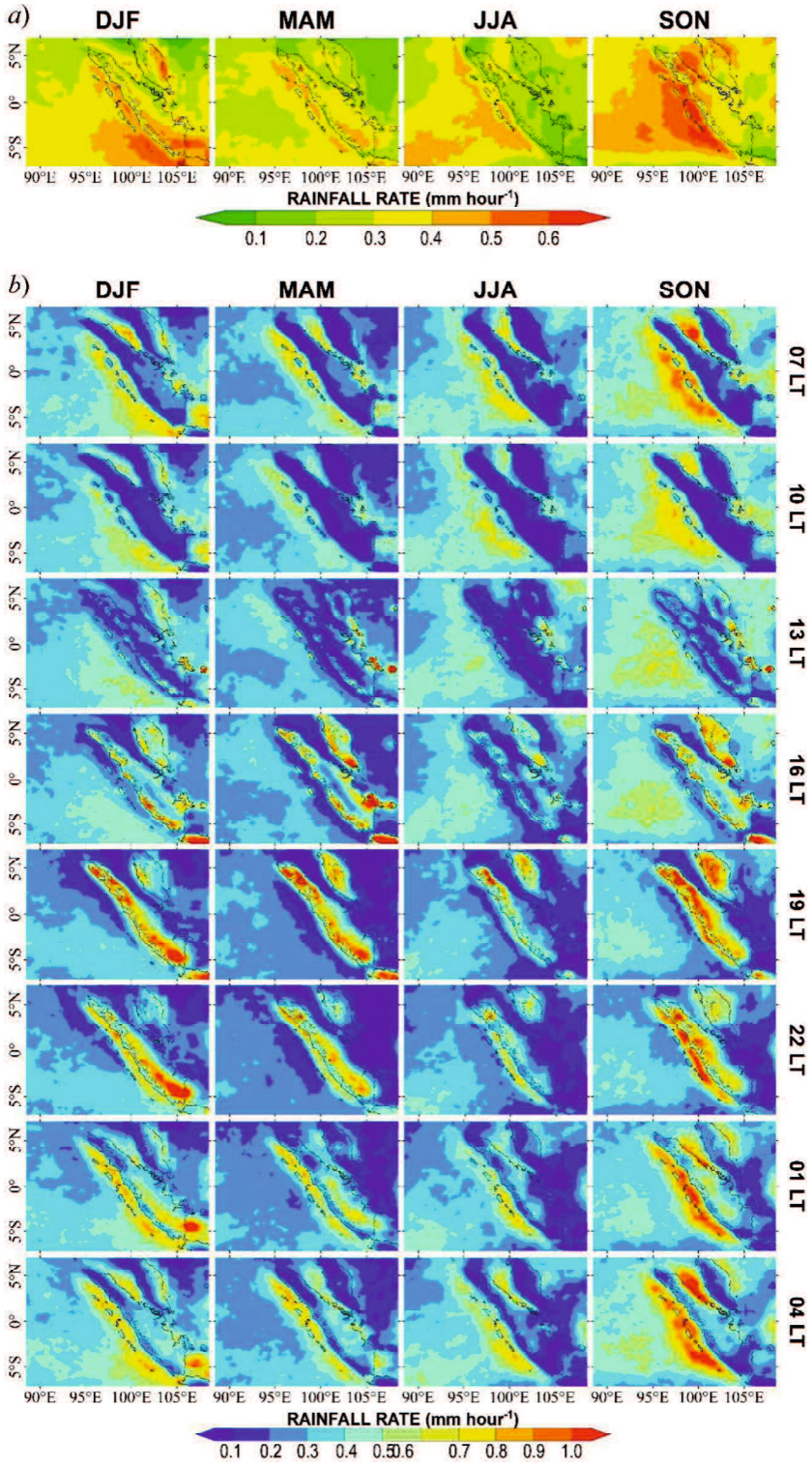

Figure 5.2. Average 17-year 3-monthly rainfall data. All (a) and 3-hourly (b) data of rainfall rate were obtained from 1998–2014 TRMM 3B42 data. Thick lines denote shorelines, and thin lines denote terrain elevation in 1000-m intervals.

5.3 Results

Figure 5.2(a) presents the spatial distribution of the average rainfall rate by season. During DJF, the heaviest rainfall was detected over the southern region, particularly over the sea in this area. In MAM, the rainfall rate begins to decline everywhere. This feature is especially notable over the sea surrounding the southern region, and the rainfall rates tend to be higher over land in the southern region and over the western ocean in the central and northern regions. In JJA, the rainfall rates are the lowest over land and the eastern sea, and they tend to increase over the western sea. During SON, rainfall rates off the central west coast appear to increase more than in other areas.

The DRC averaged over 17 years for each season is presented in Figure 5.2(b). The amplitude of the DRC displayed large north–south and seasonal differences, whereas the phase differences were not distinct. In all seasons, rainfall from sunrise until noon (07 and 10 LT) was distributed almost entirely over the seas surrounding the Sumatera main island and many smaller islands off the west and east coasts of the main island. During early afternoon (13 LT) in all seasons except JJA, the highest rainfall rate was observed on east-coastal small islands (ECSIs), such as Bangka and Belitung in the south region and Mendol in the central region (Figure 5.1), as well as along the Barisan Mountains. In the afternoon (16 LT), rainfall over land continued to increase and began to spread toward the middle of the mainland (eastern part of the mountains), while the rainfall over the ECSIs began to decrease. On the west side of Sumatera, the peak rainfall appeared on land along the coast during the early evening, then migrated westward and eastward, weakening just before midnight (22 LT) as the system moved offshore. In northern Sumatera along the Malaka Strait, rainfall migrating eastward generally began around midnight, which is later than the westward migration observed on the west coast. After midnight (01 LT), the rainfall tended to weaken over the entire island of Sumatera and was then dispersed over the surrounding seas.

It is possible to confirm those rainfall migration patterns using Hovmöller diagrams (Figure 5.3) for time–coastal distance cross-sections averaged along the coastal direction for boxes I–III shown in Figure 5.1. Both eastward and westward rainfall migrations from the Barisan Mountains were observed except during JJA. Those migrations were particularly noticeable during SON in the northern and central regions (I and II) and during DJF in the southern region (III). During JJA, the eastward migration pattern was not clearly observable in the central region

and appeared to be virtually nonexistent over the southern region. During SON over the open ocean off the west coast in the central region, the westward migration of rainfall (higher than threshold rainfall rates of 0.5 mm h−1) generated on the previous day was at about 700 km from the coastline at 16 LT. At the same time, a new rainfall system had been generated over the Barisan Mountains. During DJF, MAM, and JJA in the central region, the westward migration reached only ~350, ~200, and ~500 km from the coastline, respectively. In the northern region, the westward migration reached ~250 and ~500 km during JJA and SON, respectively, and 200 km during both DJF and MAM. Meanwhile, the westward migration in the southern region reached ~350 and ~250 km during DJF and SON, respectively, and only ~150 km during both MAM and JJA.

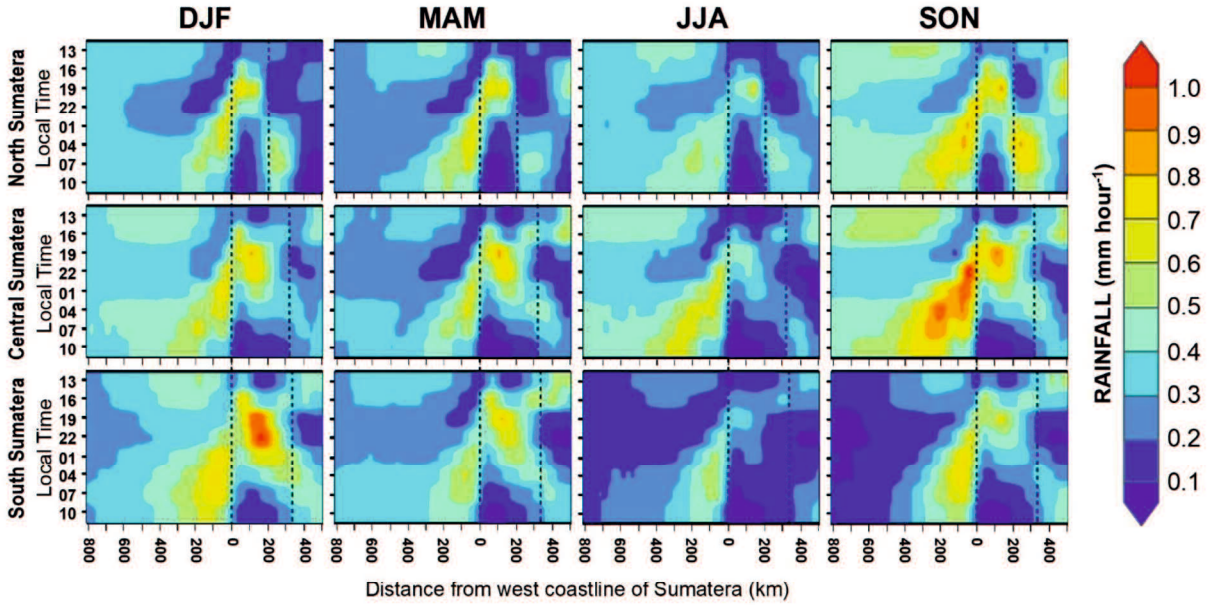

Figure 5.3. Hovmöller diagram for averaged diurnal variation of rainfall. Vertical dotted lines represent locations of coasts of Sumatera.

5.4 Discussions and Conclusion

5.4.1 Initiation of convection in Barisan Mountains and eastern islands

Previous studies had indicated that the rainfall on land is initiated along the Barisan Mountains and then migrates to the east and west (e.g., Mori et al., 2004). However, the present study revealed that early-afternoon rainfall peaks also appeared on the ECSIs (Figure 5.2(b)), such as Bangka and Belitung Islands in the southern region (appearing most clearly) and Mendol Island in the central region. At 13 LT, these peaks were clearly separated from the Sumatera

main island, although the shortest distance is less than the horizontal resolution (0.25°). Rainfall peaks' initiation in the ECSIs were also confirmed by analyzing the MTSAT-1R data for the period July 2005 to June 2010, with a higher time resolution (hourly) compared to that of the TRMM 3B42 data (3-hourly): the tall cloud frequency was enhanced near the east coast of Sumatera (at 300–400-km distance from the coastline) in the early afternoon (at around 13 LT) as shown in Figure 5.4.

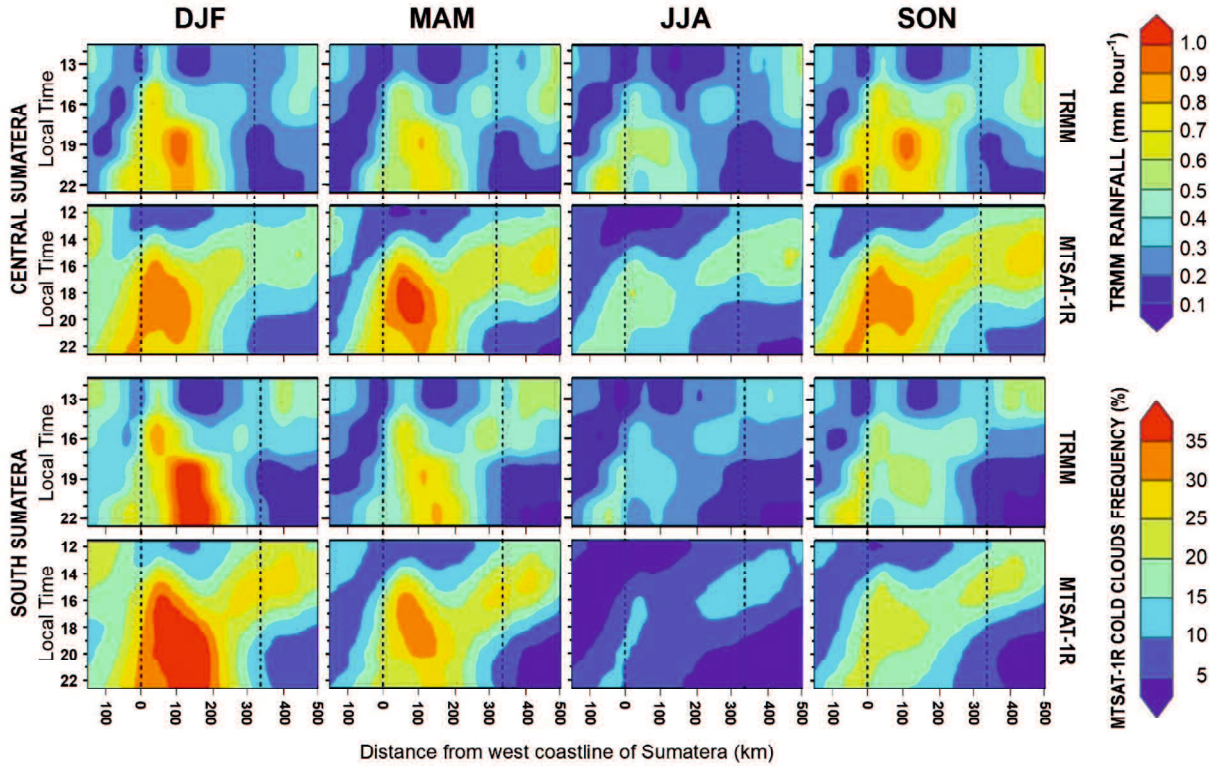

Figure 5.4. Hovmöller diagram for averaged diurnal variation of rainfall migration from 3-hourly TRMM 3B42 data and tall clouds migration from hourly MTSAT-1R data analysis in central and southern regions based on data from July 2005 through June 2010. Vertical dotted lines represent coasts of Sumatera.

As shown clearly by MTSAT-1R diagrams (Figure 5.4), rainfall peaks at 13 LT in the ECSIs were connected to the Sumatera main island at 16 LT, suggesting westward migration toward the inland plains of Sumatera until early evening (about 18 LT) in the central and southern regions (see also Figures. 5.2(b) and 5.3). The MTSAT-1R could confirm the cloud migration, although the temporal resolution of TRMM 3B42 was not enough to illustrate rainfall area migrations over distances longer than the sizes of the smaller islands. Therefore, there are in total two types of rainfall initiation/migration in central and southern Sumatera. Features similar to the two types of

rainfall/cloud initiation/migration were also seen in Figure 5 of Mori et al. (2004) via TRMM analysis and in Figure 4 of Sakurai et al. (2005) in a GMS study, although they mentioned only the westward migration from the Barisan Mountains (for comparison between TRMM and GMS, see, e.g., Imaoka and Nakamura, 2012).

Concerning the above-mentioned initiation of DRC, an important condition is considered to be the effect of size (width) of an island. Sobel et al. (2011, a correction in 2013) reported a statistically critical island size (315 km2) for DRC generation over the Indo-Pacific Oceans, including the IMC. Bangka and Belitung Islands have an east-to-west width of ~50–100 km. Mendol Island is smaller but is surrounded by other similar islands. Those small islands are collectively just larger than the critical value needed to generate convective clouds and heavy-rainfall events very quickly at ~13 LT, which are terminated rapidly and followed by similar events in the central region of the main island of Sumatera in subsequent hours. The northern region of the main island, which has an east-to-west width of ~200 km, slowly develops a rainfall peak in the early evening (19 LT). The southern region (~400 km wide) behaves the same way in late evening (22 LT), especially during DJF and MAM seasons.

There have been studies of DRC over small islands off the west coast of Sumatera (e.g., Wu et al., 2008; Kamimera et al., 2012) and also along a coastal region virtually free from the influence of any small islands (Yokoi et al., 2017). However, the small western islands are much more isolated (by a strait ~100 km wide) from the main island of Sumatera, and effects of only the latter on the former (such as two rainfall peaks, evening and early morning) have been observed, which is also similar to another case, for a small island off the north coast of Papua (Tabata et al., 2011). The effect of a neighboring large island (westward migration of DRC on the west coast of Kalimantan; e.g., Shibagaki et al., 2006) may contribute to the pattern of DRC in the ECSIs, but may be out of the scope of this paper focused on Sumatera.

5.4.2 Seasonal differences in eastward and westward diurnal rainfall migrations

As shown in Figure 5.3, the clearest migration pattern in the eastward direction occurs during DJF in the southern region, while in the westward direction such a pattern appears during SON in the central region. During JJA, the eastward migration in the northern region is clearer than in the central region, while eastward migration is virtually nonexistent in the southern region. These are consistent with results obtained by Sakurai et al. (2005) that illustrated the eastward rainfall

migration appears only when the dominant low-level tropospheric wind is westerly, which occurs with the ITCZ. Another seasonally hemispheric asymmetry of the Asia–Australia monsoon (Chang et al., 2005) may be responsible for the difference in the appearance, speed, and distance of the westward and eastward migrations of DRC systems. We analyzed these rainfall systems by using much longer-term TRMM 3B42 data and found that they are basically similar to those in the 3-year discontinuous TRMM PR data reported by Mori et al. (2004) and the cloud system features from the 1-year GMS blackbody-temperature data reported by Sakurai et al. (2005).

The westward-migration distances (e.g., ~700 km in SON and ~200 km in MAM for the central region, and ~350 km in DJF for the southern region) are consistent with the scale (i.e., hundreds of km) of rainfall concentration near the coastline described by Ogino et al. (2016) based on annual-mean analysis of TRMM PR data. Yamanaka et al. (2018) also show that regional rainfall is a function of the coastline length divided by the land area. However, they do not mention seasonal differences in coastal-rainfall concentration. Our study further revealed that the horizontal scale of coastal-rainfall concentration varies seasonally and meridionally.

Several mechanisms that may influence rainfall/cloud initiation/migration have been proposed and investigated in previous studies. Mori et al. (2004) proposed that in the early afternoon, along the west coast of Sumatera Island, initial convection is triggered when the sea breeze encounters the mountain range. Several studies (e.g., Yang and Slingo, 2001; Mori et al., 2004; Ichikawa and Yasunari, 2006; Yanase et al., 2017) suggested that the possible mechanisms of offshore migration are the advection process associated with background wind and/or the interaction between a gravity current and an ambient wind, which can trigger the self-replication of convective systems. Gravity waves due to strong diurnal signals over coastal land are also an important mechanism for the offshore migration of rainfall around midnight over Sumatera (Yokoi et al., 2017), and their propagation is highly dependent on and interacts with background wind that varies seasonally with monsoons (Yanase et al., 2017). The interaction between these mechanisms and the seasonal existence of the ITCZ can provide different favorable conditions for rainfall migration in each season. To study these mechanisms it is necessary to analyze also temperature, humidity and wind based on objective analysis data.

CHAPTER 6

Conclusions

In this chapter the main results are summarized and the possible extension of future works is discussed.

An extensive comparison between rain-gauge observations in Bali area and satellite-derived estimates of daily to monthly rainfall were performed over a five-year period on daily, monthly and seasonal timescales (wet and dry seasons). Over the Bali area, the rainfall from satellite data gave lower values than the gauge estimates. The daily data analysis for 3B42 with the gauge data indicated negative bias and large RMSE values. In contrast, monthly TMPA data products (3B42 and 3B43) show better agreement with the gauge data, yielding high correlation coefficients and similar performance during the wet and dry seasons, but still tend to underestimate with relatively large RMSE value. Furthermore, the comparison between wet (high rainfall values) and dry (low rainfall value) seasons presented that the larger errors were found during dry season, even though the correlation coefficient was higher than wet season. Similar results were also found in other places over Indonesia, especially the tendencies of the underestimation in the east part of Indonesia and the overestimation in the western part of Indonesia (see chapter 3). One of the potential reasons is that the succession of convective- and stratiform-type rainfall throughout the year differs for regions. According to Liao and Meneghini (2009), the attenuation in radar reflectivity of TRMM PR causes rainfall underestimation for convective-type rain, while does not affect much for stratiform-type rain. In addition, TMI gives overestimated rainfall values under heavy convective rain (Nakazawa and Rajendran 2004), which is a common feature over archipelago of Indonesia. However, in general, for most seasons and regions, the TMPA data products are reliable enough for monitoring climatic-scale rainfall over the IMC.

The analysis of rainfall from TRMM satellite data showed that monsoons, oceans, islands, and topographical diversity clearly affect the spatial patterns of rainfall in this region. Large-scale circulations, such as ITCZ and SPCZ, create heavy land-ocean rainfall, predominantly over oceans. Moreover, equatorial rainfall is more stable than that in northern and southern equatorial regions and occurs predominantly over land areas. Complex topography contributes to land-sea rainfall variability and causes much rainfall over land and offshore areas. Regionally, monsoons

and the ITCZ-SPCZ belt cause seasonal changes in rainfall variability over various locations in the MC, but not at other latitudes. Additionally, various characteristics related to wind direction, topography, and the existence of oceans cause different in local rainfall variability. A seasonal characteristic of rainfall is consistent with north-westward and south-eastward movements of the Asian–Australian monsoon system and the southward and northward movement of the ITCZ. Average rainfall of 1998 mm $year^{-1}$ was fallen over ocean, and 40% higher average value of 2780 mm $year^{-1}$ over islands. Though more rain falls on small islands with substantial elevation than on small flat islands, rainfall rate and elevation do not correlate for the large islands in this region. Moreover, rainfall values in archipelago of Indonesia are greatly affected by topography, which manifests more during wet seasons than dry or transition seasons. Linkage between island-topography and the large-scale circulation generates convective organization, and produces orogenic convective systems or nocturnal rainfall activity along the coastal area.

The seasonal to inter-annual variabilities of Indonesian rainfall are characterized mainly by the monsoon and atmosphere-ocean interactions near Indonesia such as the ENSO and El Niño Modoki. In general, the use of TRMM 3B43 can reveal spatial-temporal changes of rainfall with ENSO and El Niño Modoki for land and sea. The spatial-temporal clustering gives the exciting information on global climate which influences the difference in the ENSO and El Niño Modoki strength, such as the SST impact and possibility of ITCZ effect. ENSO and El Niño Modoki have similar spatial-temporal pattern in influencing the rainfall in this region and strongly influence the rainfall during all seasons, except in regions with heavy rainfall means. Spatial correlation between rainfall and the phenomena is high in the southeastern part of Sumatra Island and Java Island during JJA and SON. During the SON season, El Niño Modoki has higher correlation than ENSO in the area. In the spatial-temporal pattern, a dynamic change of the relationship between rainfall and the phenomena in Indonesia is observed. The influence of ENSO and El Niño Modoki starts during JJA in the southwest of Indonesia and ends in the DJF period in the northeast of Indonesia. The spatial and temporal pattern indicates the air-sea interaction in Indonesia and its surroundings. The interaction plays an important role against rainfall variability over Indonesia.

The diurnal rainfall cycle is the important elements of rainfall characteristics over Indonesia and closely associated with the land-sea distribution, the terrain, and local circulation. Based on 17 years (January 1998 to December 2014) of 3-hourly satellite data obtained from TRMM 3B42, seasonal and geographic characteristics of the diurnal rainfall cycle over Sumatera, Indonesia are

investigated. This study demonstrates that seasonal differences on diurnal variations in precipitation characteristics, where Sumatera is dividing into north, central, and south regions approximately perpendicular to the west coast. For the first time this study points out early-afternoon initiation of daily rainfall not only in the Barisan Mountains but also in the east-coastal small islands such as Bangka and Belitung. Westward and eastward migrations of rainfall areas from the Barisan Mountains vary with seasons and regions, with the most remarkable being westward during SON in the central region and the least remarkable occurring during JJA in the southern region. In the central region, the diurnal rainfall cycle reaches a distance of ~700 km off the west coast during SON and of only 200 km during MAM. The other afternoon initiation of daily rainfall and westward migrations from the east-coastal small islands in the central and southern regions (except for JJA) have been confirmed by 5-year hourly MTSAT-1R cloud-top data.

In summary, the present study indicates that rainfall data captured by satellite remote sensing (e.g., TMPA products) can be used to analyse the characteristics of Indonesian rainfall, because of the long-term accumulation of datasets, reliable spatial distribution, and better agreement with the gauge data, although they still have some errors (underestimation in the east and overestimation in the west of Indonesia). This study also demonstrates that TMPA data products can be applied for analysing climatological rainfall pattern over IMC, which has a complex land-sea-topography distribution, in different spatial scales (from local to regional) and different temporal scales (from diurnal to annual rainfall pattern), although in certain specific local conditions such as over small islands, the spatial and temporal resolutions are not enough to illustrate rainfall area migrations. Finally, this study shows that the state-of-the-art satellite meteorology can provide comprehensive information about Indonesian rainfall characteristics in land and sea, local to regional, and diurnal to annual.

However, the study leaves some unanswered questions and possible points to be further investigated, such as the comparison of satellite data with more rain gauge data over Indonesia. Bali region only represents a small part of Indonesia. Even though monthly satellite data has been verified using 5 rain gauges over Indonesia, it is still not enough to represent the entire Indonesia region. In addition, validation of 3-hourly rainfall is not covered by this study, although the satellite is quite capable in describing diurnal cycle as shown in chapter 5. The TRMM satellite were flying in non-Sun-synchronous orbit that can provide the information to figure out Indonesian diurnal rainfall pattern. Although the TRMM data itself do not play an

essential role, particularly in temporal frequency to illustrate rainfall migrations which have distances longer than the sizes of the smaller islands. However, the accuracy of the TRMM data in describing the diurnal rainfall cycle condition still need to be investigated, especially on large and important islands in Indonesia. Analyses of intra-seasonal (30–90 days) MJO phase of rainfall over Indonesia using satellite data also have not performed yet. Understanding the intra-seasonal phase of rainfall and the associated extreme high and low precipitation events over Indonesia is important, because these phenomena propagate eastward from the tropical Indian Ocean to the Pacific Ocean and create corresponding changes in the precipitation pattern over Indonesian region. Also, the effects on the diurnal rainfall cycle caused by the intra-seasonal changes need to be investigated. In addition, relationship between sea surface temperature and rainfall in quantitative form is still unclear for Indonesian region. An exciting opportunity to apply daily remote sensing data of rainfall and sea surface temperature over the region and local area of Indonesia to explain connectivity and time-lag relationship between both environmental variables.

New satellite observations by the GPM Core Observatory had started in early 2014 to explore global precipitation characteristics in a more detailed and advanced way, motivated by the splendid success of the TRMM satellite. TRMM had especially contributed to the measurement of precipitation over the regions where collecting data is particularly difficult, such as the Indonesian seas and jungles as well as mountain ranges such as the Bukitbarisan and Jayawijaya over Indonesian region. GPM takes advantage of and expands upon the technological and scientific advances from TRMM. Particular advances with GPM mission and their products are to have better ability to measure precipitation at lighter intensities, detect the presence of falling snow, and provide quantitative estimates of cloud/precipitation microphysics with higher spatial resolution (0.25^{o} for TRMM against 0.1^{o} for GPM) (Skofronick-Jackson et al., 2018). This study is the first step to understand the characteristics of Indonesian rainfall by utilizing meteorological satellites. Further studies of rainfall climatological patterns over Indonesia in comprehensive and quantitative manners will be needed, especially with the advantages of GPM compared to previous TRMM.

ACKNOWLEDGEMENTS

I would like to express my sincere and deepest gratitude to my supervisor Prof. Kakuji Ogawara and Assoc. Prof. Keiji Imaoka for his kindness, guidance, and support. Also, I would like to thank all of my graduate committee for supporting and commenting my work: Prof. Norikazu Shimizu, Prof. Takashi Saito, and Assoc. Prof. Kenji Suzuki.

I also wish to express my appreciation to Prof. Tasuku Tanaka and Assoc. Prof. Takahiro Osawa at Center for Remote Sensing and Ocean Science (CReSOS), Udayana University; Prof. I Wayan Arthana (also as Dean of Faculty of Marine Science and Fisheries), Prof. I Wayan Nuarsa, Prof. I Wayan Sandi Adnyana, and Prof. Made Sudiana Mahendra at Centre for Environmental Studies (PPLH), Udayana University; Prof. Fusanori Miura at Center for Research and Application of Satellite Remote Sensing (YUCARS), Yamaguchi University (also as Yamaguchi University Vice-President for International Cooperation); Prof. Manabu D. Yamanaka at Research Institute for Humanity and Nature (RIHN), Kyoto; Prof. Yuji Kashino at Department of Fishery Science and Technology, National Fisheries University; and Mr. Rakhmat Prasetia at Indonesian Meteorology, Climatology and Geophysics Agency (BMKG), Negara office for their invaluable comments throughout my Ph.D. work.

I gratefully acknowledge to the Japan Society for the Promotion of Science (JSPS) RONPAKU (Dissertation PhD) Program that has provided financial support to complete my doctoral degree at Graduate School of Sciences and Technology for Innovation, Yamaguchi University. My sincere acknowledgement is also extended to Faculty of Marine Science and Fisheries, Udayana University for their kind coordination and support since the scholarship application processes until graduation.

Special thanks to my colleagues and friends who are members of the Faculty of Marine Science and Fisheries, CReSOS, and PPLH at Udayana University. Friends at Yamaguchi University (Ube Campus) with whom I share wonderful memories. For technical support of the data analysis, I am grateful to Herlambang Aulia Rachman, I Nengah Jaya Nugraha, I Putu Ranu Fajar Maharta, I Wayan Matsya Deva Nagendra, and Mu'tasim Billah. Thank you for your help.

All research in this Dissertation, except chapter 5, was supported by CReSOS and JAXA mini-ocean projects in Indonesia. Meanwhile, the chapter 5 is funded by the Japan Society for the Promotion of Science (JSPS) RONPAKU (Dissertation PhD) Program. I gratefully acknowledge data received from the following organizations: TMPA V6 and V7 data from the National Aeronautics and Space Administration (NASA) and the Japan Aerospace Exploration Agency (JAXA); the MTSAT-1R data were used through the courtesy of Japan Meteorological Agency (JMA), Weathernews Inc., Earthquake Research Institute and Institute of Industrial Science (W. Takeuchi Lab.) of the University of Tokyo, and Center for Environmental Remote Sensing (CeRES) of Chiba University; the Shuttle Radar Topography Mission (SRTM) 30 Plus from Scripps Institution of Oceanography, University of California San Diego; rain gauge data from the Indonesian Meteorology, Climatology, and Geophysics Agency (BMKG); EMI data from the Japan Agency for Marine-Earth Science and Technology (JAMSTEC); Niño-3 data from the National Oceanic and Atmospheric Administration (NOAA) National Geophysical Data Center; and GPCP v2.2 data provided by the Laboratory for Atmospheres, NASA/Goddard Space Flight Center's.

I could never find proper words to show how thankful, grateful, and indebted I am to my dear parents, Taufikurrahman Yasin and Faizah. I love you with all my heart and soul, and wish this dissertation can serve as a very tiny gift to you in recognition of your worth in my life. I would also like to express my love and appreciation to my beautiful sister, Haifaturrahmah, as well as my dear extended family and in-laws, for their endless love, support, attention, and encouragement throughout my entire life.

Last, but not least, I would like to express my ultimate love and thanks to my wonderful wife, Ni Wayan Ekayanti, and my lovely son and daughter, Adla Gangga Dhiyaurrahman and Adilaturrahmany Visakha for their love, support, affection, and understanding. Without your support and understanding this dissertation would have not been completed.

REFERENCES

Adler, R. F., Huffman, G. J., Bolvin, D. T., Curtis, S., & Nelkin, E. J. (2000). Tropical rainfall distributions determined using TRMM combined with other satellite and rain gauge information. Journal of Applied Meteorology, 39(12), 2007-2023.

Aldrian, E. (2000). Pola hujan rata-rata bulanan wilayah Indonesia; tinjauan hasil kontur data penakar dengan resolusi ECHAM T-42. Jurnal Sains & Teknologi Modifikasi Cuaca, 1(2), 113-123.

Aldrian, E. (2003). Simulations of Indonesian rainfall with a hierarchy of climate models, (Doctoral dissertation). Examensarbeit Nr. 92, Max-Planck–Institut für Meteorologie, Bundesstrasse 55, D-20146, pp. 159 (Hamburg-Germany, University of Hamburg Hamburg).

Aldrian, E. (2011). Dominant factors of Jakarta's three largest floods. Jurnal Hidrosfir Indonesia, 3(3), 105 – 112.

Aldrian, E., & Djamil, Y. S. (2008). Spatio-temporal climatic change of rainfall in East Java Indonesia. International Journal of Climatology, 28(4), 435–448.

Aldrian, E., & Susanto, R. D. (2003). Identification of three dominant rainfall regions within Indonesia and their relationship to sea surface temperature. International Journal of Climatology, 23(12), 1435–1452.

Aldrian, E., Gates, L. D., & Widodo, F. H. (2007). Seasonal variability of Indonesian rainfall in ECHAM4 simulations and in the reanalyses: The role of ENSO. Theoretical and Applied Climatology, 87(1-4), 41-59.

Aldrian, E., Sein, D., Jacob, D., Gates, L. D., & Podzun, R. (2005). Modelling Indonesian rainfall with a coupled regional model. Climate Dynamics, 25(1), 1-17.

Alemohammad, S. H. (2014). Characterization of Uncertainty in Remotely-Sensed Precipitation Estimates (Doctoral dissertation, Massachusetts Institute of Technology)

Alhammoud, B., Claud, C., Funatsu, B., Béranger, K., & Chaboureau, J. P. (2014). Patterns of precipitation and convection occurrence over the mediterranean basin derived from a decade of microwave satellite observations. Atmosphere, 5(2), 370-398.

Anagnostou, E. N. (2007). Assessment of Satellite Rain Retrieval Error Propagation in the Prediction of Land Surface Hydrologi. In Measuring Precipitation from Space: EURAINSAT

and the Future, V. Levizzani, P. Bauer, and F.J. Turk (eds.), pp. 357–368 (Netherlands, Springer Verlag).

Artan, G., Gadain, H., Smith, J. L., Asante, K., Bandaragoda, C. J., & Verdin, J. P. (2007). Adequacy of satellite derived rainfall data for stream flow modeling. Natural Hazards, 43(2), 167–185.

As-Syakur, A. R. (2007). Identifikasi Hubungan Fluktuasi Nilai SOI Terhadap Curah Hujan Bulanan Di Kawasan Batukaru-Bedugul, Bali. Bumi Lestari, 7(2), 123–129.

As-Syakur, A. R. (2011). Status of the TRMM level 3 in Indonesia. In The 2nd CReSOS International Symposium on South East Asia Environmental Problems and Satellite Remote Sensing, pp. 21-22 (Denpasar-Indonesia, Udayana University).

As-Syakur, A. R., Tanaka, T., Osawa, T., & Mahendra, M. S. (2013). Indonesian rainfall variability observation using TRMM multi-satellite data. International journal of remote sensing, 34(21), 7723-7738.

As-Syakur, A. R., Tanaka, T., Prasetia, R., Swardika, I. K., & Kasa, I. W. (2011). Comparison of TRMM multisatellite precipitation analysis (TMPA) products and daily-monthly gauge data over Bali. International journal of remote sensing, 32(24), 8969–8982.

As-Syakur, A. R, Adnyana, I. W. S., Mahendra, M. S., Arthana, I. W., Merit, I. N., Kasa, I. W., Ekayanti, N. W., Nuarsa, I. W., & Sunarta, I. N. (2014). Observation of spatial patterns on the rainfall response to ENSO and IOD over Indonesia using TRMM Multisatellite Precipitation Analysis (TMPA). International Journal of Climatology, 34(15), 3825-3839.

As-Syakur, A. R., Osawa, T., Miura, F., Nuarsa, I. W., Ekayanti, N. W., Dharma, I. G. B. S., Adnyana, I.W. S., Arthana, I. W., Tanaka, T. (2016). Maritime Continent rainfall variability during the TRMM era: the role of monsoon, topography and El Ni˜no Modoki. Dynamics of Atmospheres and Oceans. doi: 10.1016/j.dynatmoce.2016.05.004

Ashok, K., & Saji, N. H. (2007). On the impacts of ENSO and Indian Ocean dipole events on sub-regional Indian summer monsoon rainfall. Natural Hazards, 42(2), 273–285.

Ashok, K., & Yamagata, T. (2009). Climate change: The El Niño with a difference. Nature, 461(7263), 481-484.

Ashok, K., Nakamura, H., & Yamagata, T. (2007). Impacts of ENSO and Indian Ocean dipole events on the Southern Hemisphere storm-track activity during austral winter. Journal of climate, 20(13), 3147–3163.

Ashok, K., Behera, S.K., Rao, S. A., Weng, H., & Yamagata, T. (2007). El Niño Modoki and its possible teleconnection. Journal of Geophysical Research: Oceans, 112(C11), C11007, 1–27.

Bannu, K. H., Takeuchi, N., & Suriamihardja, D. A. (2005). Impacts of the sea surface temperature anomaly in the Pacific and Indian Oceans on the Indonesian climate. In 11th CEReS International Symposium on Remote Sensing (pp. 13–14). Paper in the 11th CEReS International Symposium on Remote Sensing on 13 to 14 December 2005 at Chiba University. Chiba–Japan.

Barros, A. P., Joshi, M., Putkonen, J., & Burbank, D. W. (2000). A study of the 1999 monsoon rainfall in a mountainous region in central Nepal using TRMM products and rain gauge observations. Geophysical Research Letters, 27(22), 3683–3686.

Becker, J.J., Sandwell, D.T., Smith, W.H.F., Braud, J., Binder, B., Depner, J., Fabre, D., Factor, J., Ingalls, S., Kim, S.H., Ladner, R., Marks, K., Nelson, S., Pharaoh, A., Trimmer, R., Von Rosenberg, J., Wallace, G., & Weatherall, P. (2009). Global Bathymetry and Elevation Data at 30 Arc Seconds Resolution: SRTM30_PLUS. Marine Geodesy, 32(4), 355–371.

Behrangi, A., Andreadis, K., Fisher, J. B., Turk, F. J., Granger, S., Painter, T., & Das, N. (2014). Satellite-based precipitation estimation and its application for streamflow prediction over mountainous western US basins. Journal of Applied Meteorology and Climatology, 53(12), 2823-2842.

Bell, G. D., Halpert, M. S. (1998). Climate assessment for 1997. Bulletin of the American Meteorological Society, 79(5), S1–S50.

Bell, G. D., Halpert, M. S., Kousky, V. E., Gelman, M. E., Ropelewski, C. F., Douglas, A. V., & Schnell, R. C. (1999). Climate assessment for 1998. Bulletin of the American Meteorological Society, 80(5), S1–S48.

Bell, G. D., Halpert, M. S., Schnell, R. C., Higgins, R. W., Lawrimore, J., Kousky, V. E., Tinker, R., Thiaw, W., Chelliah, M., & Artusa, A. (2000). Climate assessment for 1999. Bulletin of the American Meteorological Society, 81(6), S1–S50.

Biasutti, M., Yuter, S.E., Burleyson, C.D., & Sobel, A.H. (2012). Very high resolution rainfall patterns measured by TRMM precipitation radar: seasonal and diurnal cycles. Climate dynamics, 39(1–2), 239–258.

Blair, T. A. (1918). Partial correlation applied to Dakota data on weather and wheat yield. Monthly Weather Review, 46, 71.

Cai, W., van Rensch, P., Cowan, T., & Hendon, H. H. (2011). Teleconnection pathways of ENSO and the IOD and the mechanisms for impacts on Australian rainfall. Journal of Climate, 24(15), 3910–3923.

Cai, Y., Jin, C., Wang, A., Guan, D., Wu, J., Yuan, F., & Xu, L. (2015). Spatio-Temporal Analysis of the Accuracy of Tropical Multisatellite Precipitation Analysis 3B42 Precipitation Data in Mid-High Latitudes of China. PloS one, 10(4). e0120026

Chang, C. P., Harr, P. A., McBride, J., & Hsu, H. H. (2004). Maritime continent monsoon: annual cycle and boreal winter variability (pp. 107-152). World Scientific.

Chang, C. P., Wang, Z., McBride, J., & Liu, C. H. (2005). Annual cycle of Southeast Asia-Maritime Continent rainfall and the asymmetric monsoon transition. Journal of climate, 18(2), 287–301.

Chang, C-W. J., Hsu, H. H., Wu, C. R., & Sheu, W. J. (2008). Interannual mode of sea level in the South China Sea and the roles of El Niño and El Niño Modoki. Geophysical Research Letters, 35(3). L03601-1–L03601-5.

Chen, G., Sha, W., Iwasaki, T., & Ueno, K. (2012). Diurnal variation of rainfall in the Yangtze River Valley during the spring-summer transition from TRMM measurements. Journal of Geophysical Research: Atmospheres, 117, D06106.

Chen, T.C., Tsay, J.D., Yen, M.C., & Matsumoto, J. (2012). Interannual variation of the late fall rainfall in Central Vietnam. Journal of Climate, 25(1), 392–413.

Chiu, L. S., Shin, D. B., & Kwiatkowski, J. (2006). Surface rain rates from tropical rainfall measuring mission satellite algorithms. In Earth Science Satellite Remote Sensing (pp. 317-336). Springer Berlin Heidelberg.

Chiu, L. S., Liu, Z., Vongsaard, J., Morain, S., Budge, A., Neville, P., & Bales, C. (2006). Comparison of TRMM and water district rain rates over New Mexico. Advances in Atmospheric Sciences, 23(1), 1–13.

Chokngamwong, R., & Chiu, L. S. (2004). Comparisons of daily Thailand rain gauge with GPCC and TRMM satellite precipitation measurements. In The 2nd TRMM International Science Conference. September 6–10, 2004, Nara, Japan.

Chokngamwong, R., & Chiu, L. (2006). TRMM and Thailand daily gauge rainfall comparison. In The American Meteorology Society, Conference Proceeding in 86th AMS Annual Meeting, January 29 – February 2, 2006, Atlanta, Georgia, USA.

Chokngamwong, R., & Chiu, L. S. (2008). Thailand daily rainfall and comparison with TRMM products. Journal of Hydrometeorology, 9(2), 256–266.

Chrastansky, A., & Rotstayn, L. D. (2012). The effect of ENSO-induced rainfall and circulation changes on the direct and indirect radiative forcing from Indonesian biomass-burning aerosols. Atmospheric Chemistry and Physics, 12(23), 11395-11416.

Clift, P. D., & Plumb, R. A. (2008). The Asian monsoon: causes, history and effects (Vol. 270). Cambridge: Cambridge University Press.

Collier, C. G. (2016). Hydrometeorology. John Wiley & Sons, UK.

Cramer, D. (2003). A cautionary tale of two statistics: partial correlation and standardized partial regression. The Journal of Psychology, 137(5), 507–511.

D'Arrigo, R., & Wilson, R. (2008). El Nino and Indian Ocean influences on Indonesian drought: implications for forecasting rainfall and crop productivity. International Journal of Climatology, 28(5), 611–616.

Dayem, K.E., Noone, D.C., & Molnar, P. (2007). Tropical western Pacific warm pool and maritime continent precipitation rates and their contrasting relationships with the Walker Circulation. Journal of Geophysical Research: Atmospheres, 112(D6).

de Angelis, C.F., McGregor, G.R., & Kidd, C. (2004). A 3 year climatology of rainfall characteristics over tropical and subtropical South America based on Tropical Rainfall Measuring Mission precipitation radar data. International Journal of Climatology, 24(3), 385–399.

Delbanco, S. F., Parker, M. L., McIntosh, M., Kannel, S., Hoff, T., & Stewart, F. H. (1998). Missed opportunities: teenagers and emergency contraception. Archives of pediatrics & adolescent medicine, 152(8), 727–733.

DiNezio, P.N., Vecchi, G.A., & Clement, A.C. (2013). Detectability of Changes in the Walker Circulation in Response to Global Warming. Journal of Climate, 26(12), 4038–4048.

Farr, T. G., Rosen, P. A., Caro, E., Crippen, R., Duren, R., Hensley, S., Kobrick, M., Paller, M., Rodriguez, E., Roth, L., Seal, D., Shaffer, S., Shimada, J., Umland, J., Werner, M., Oskin, M., Burbank, D., & Alsdorf, D. (2007). The shuttle radar topography mission. Reviews of geophysics, 45(2). RG2004

Farr, T. G., & Kobrick, M. (2000). Shuttle Radar Topography Mission produces a wealth of data. Eos, Transactions American Geophysical Union, 81(48), 583-585.

Feidas, H. (2010). Validation of satellite rainfall products over Greece. Theoretical and Applied climatology, 99(1-2), 193–216.

Feng, J., & Li, J. (2011). Influence of El Niño Modoki on spring rainfall over south China. Journal of Geophysical Research: Atmospheres, 116(D13), D13102, 1–10.

Feng, J., Wang, L., Chen, W., Fong, S.K., & Leong, K.C. (2010). Different impacts of two types of Pacific Ocean warming on Southeast Asian rainfall during boreal winter. Journal of Geophysical Research: Atmospheres, 115(D24). D24122, 1–9.

Firman, T. (2017). The urbanisation of Java, 2000–2010: towards 'the island of mega-urban regions'. Asian Population Studies, 13(1), 50-66.

Fleming, K., & Awange, J. (2013). Comparing the version 7 TRMM 3B43 monthly precipitation product with the TRMM 3B43 version 6/6A and Bureau of Meteorology datasets for Australia. Australian Meteorological and Oceanographic Journal. 63, 421–426

Fleming, K., Awange, J. L., Kuhn, M., & Featherstone, W. E. (2011). Evaluating the TRMM 3B43 monthly precipitation product using gridded raingauge data over Australia. Australian Meteorological and Oceanographic Journal, 61(3), 171.

Fujita, M., Kimura, F., & Yoshizaki, M. (2010). Morning precipitation peak over the Strait of Malacca under a calm condition. Monthly Weather Review, 138(4), 1474-1486.

Fujita, M., Takahashi, H. G., & Hara, M. (2013). Diurnal cycle of precipitation over the eastern Indian Ocean off Sumatra Island during different phases of Indian Ocean Dipole. Atmospheric Science Letters, 14(3), 153-159.

Geotis, S. G., & Houze Jr, R. A. (1985). Rain amounts near and over North Borneo during Winter MONEX. Monthly weather review, 113(10), 1824–1828.

Gianotti, R.L., & Eltahir, E.A. (2014a). Regional climate modeling over the Maritime Continent. Part I: New parameterization for convective cloud fraction. Journal of Climate, 27(4), 1488–1503.

Gianotti, R.L., & Eltahir, E.A. (2014b). Regional climate modeling over the Maritime Continent. Part II: New parameterization for autoconversion of convective rainfall. Journal of Climate, 27(4), 1504–1523.

Glantz, M. H. (2001). Currents of change: impacts of El Niño and La Niña on climate and society. Cambridge University Press.

Gunawan, D. (2006). Atmospheric variability in Sulawesi, Indonesia: regional atmospheric model results and observations, (Doctoral dissertation). Faculty of Forest Sciences and Forest Ecology, 148 pp. (Germany, University of Göttingen)

Gutman, G., Csiszar, I., & Romanov, P. (2000). Using NOAA/AVHRR products to monitor El Nino impacts: focus on Indonesia in 1997-98. Bulletin of the American Meteorological Society, 81(6), 1189–1205.

Hall, A. J. (1984). Hydrology in tropical Australia and Papua New Guinea. Hydrological sciences journal, 29(4), 399–423.

Hall, T. J., & Vonder Haar, T. H. (1999). The diurnal cycle of west Pacific deep convection and its relation to the spatial and temporal variation of tropical MCSs. Journal of the Atmospheric Sciences, 56(19), 3401-3415.

Han, W., Vialard, J., McPhaden, M. J., Lee, T., Masumoto, Y., Feng, M., & de Ruijter, W. P. (2014). Indian Ocean decadal variability: a review. Bulletin of the American Meteorological Society, 95(11), 1679–1703.

Hamada, J. I., Yamanaka, M. D., Matsumoto, J., Fukao, S., Winarso, P. A., & Sribimawati, T. (2002). Spatial and temporal variations of the rainy season over Indonesia and their link to ENSO. Journal of the Meteorological Society of Japan, 80(2), 285–310.

Hamada, J. I., Mori, S., Kubota, H., Yamanaka, M. D., Haryoko, U., Lestari, S., Sulistyowati, R. & Syamsudin, F. (2012). Interannual rainfall variability over northwestern Jawa and its relation to the Indian Ocean Dipole and El Niño-Southern Oscillation events. SOLA, 8(0), 69–72.

Harahap, F., Silveira, S., & Khatiwada, D. (2017). Land allocation to meet sectoral goals in Indonesia—An analysis of policy coherence. Land Use Policy, 61, 451-465.

Haylock, M., & McBride, J. (2001). Spatial coherence and predictability of Indonesian wet season rainfall. Journal of Climate, 14(18), 3882–3887.

Heil, A., Langmann, B., & Aldrian, E. (2007). Indonesian peat and vegetation fire emissions: Study on factors influencing large-scale smoke haze pollution using a regional atmospheric chemistry model. Mitigation and adaptation strategies for global change, 12(1), 113–133.

Hendon, H. H. (2003). Indonesian rainfall variability: Impacts of ENSO and local air-sea interaction. Journal of Climate, 16(11), 1775–1790.

Hendon, H. H., Wheeler, M. C., & Zhang, C. (2007). Seasonal dependence of the MJO-ENSO relationship. Journal of Climate, 20(3), 531–543.

Hidayat, R., & Kizu, S. (2010). Influence of the Madden–Julian Oscillation on Indonesian rainfall variability in austral summer. International Journal of Climatology, 30(12), 1816–1825.

Hirose, M., & Nakamura, K. (2005). Spatial and diurnal variation of precipitation systems over Asia observed by the TRMM Precipitation Radar. Journal of Geophysical Research: Atmospheres, 110(D5).

Hirose, M., Oki, R., Shimizu, S., Kachi, M., & Higashiuwatoko, T. (2008). Finescale diurnal rainfall statistics refined from eight years of TRMM PR data. Journal of Applied Meteorology and Climatology, 47(2), 544-561.

Hong, Y., Adler, R. F., Huffman, G. J., & Pierce, H. (2010). Applications of TRMM-based multi-satellite precipitation estimation for global runoff prediction: Prototyping a global flood modeling system. In Satellite Rainfall Applications for Surface Hydrology In Satellite Rainfall Applications for Surface Hydrology, M Gebremichael and F Hossain (eds.), pp. 245–265. Springer, Netherlands.

Hong, Y., Tang, G., Ma, Y., Huang, Q., Han, Z., Zeng, Z., Yang, Y., Wang, C., & Guo, X. (2019). Remote Sensing Precipitation: Sensors, Retrievals, Validations, and Applications. In Observation and Measurement of Ecohydrological Processes, X. Li, & H. Vereecken, (Eds.), pp. 107-128. Springer, Beijing-China.

Hou, A. Y., Skofronick-Jackson, G., Kummerow, C. D., & Shepherd, J. M. (2008). Global precipitation measurement. In Precipitation: Advances in Measurement, Estimation, and Prediction, S.C. Michaelides (ed.), pp. 131–170 (Berlin Heidelberg: Springer Verlag).

Houze Jr, R. A., Geotis, S. G., Marks Jr, F. D., & West, A. K. (1981). Winter monsoon convection in the vicinity of North Borneo. Part I: Structure and time variation of the clouds and precipitation. Monthly Weather Review, 109(8), 1595–1614.

Huffman, G. J. (1997). Estimates of root-mean-square random error for finite samples of estimated precipitation. Journal of Applied Meteorology, 36(9), 1191-1201.

Huffman, G. J., & Bolvin, D. T. (2013). TRMM and other data precipitation data set documentation. NASA, Greenbelt, USA, 1-40.

Huffman, G. J., Adler, R. F., Bolvin, D. T., & Nelkin, E. J. (2010). The TRMM multi-satellite precipitation analysis (TMPA). In Satellite rainfall applications for surface hydrology (pp. 3-22). Springer Netherlands.

Huffman, G. J., Adler, R. F., Rudolf, B., Schneider, U., & Keehn, P. R. (1995). Global precipitation estimates based on a technique for combining satellite-based estimates, rain gauge analysis, and NWP model precipitation information. Journal of Climate, 8(5), 1284-1295.

Huffman, G. J., Bolvin, D. T., Nelkin, E. J., Wolff, D. B., Adler, R. F., Gu, G., Hong, Y., Bowman, K.P., & Stocker, E. F. (2007). The TRMM multisatellite precipitation analysis (TMPA): Quasi-global, multiyear, combined-sensor precipitation estimates at fine scales. Journal of Hydrometeorology, 8(1), 38-55.

Huffman, G. J., Adler, R. F., Arkin, P., Chang, A., Ferraro, R., Gruber, A., Janowiak, J., McNab, A., Rudolf, B., & Schneider, U. (1997). The global precipitation climatology project (GPCP) combined precipitation dataset. Bulletin of the American Meteorological Society, 78(1), 5-20.

Hung, C.W., Liu, X., & Yanai, M. (2004). Symmetry and asymmetry of the Asian and Australian summer monsoons. Journal of Climate, 17(12), 2413–2426.

Ichikawa, H., & Yasunari, T. (2006). Time–space characteristics of diurnal rainfall over Borneo and surrounding oceans as observed by TRMM-PR. Journal of Climate, 19(7), 1238-1260.

Ichikawa, H., & Yasunari, T. (2008). Intraseasonal variability in diurnal rainfall over New Guinea and the surrounding oceans during austral summer. Journal of Climate, 21(12), 2852–2868.

Iguchi, T. (2007). Space-borne radar algorithms. In In Measuring Precipitation from Space: EURAINSAT and the Future, V. Levizzani, P. Bauer, F. J. Turk (eds.), pp. 199-212. Springer, Dordrecht-Netherlands.

Iguchi, T., Kozu, T., Meneghini, R., Awaka, J., & Okamoto, K. I. (2000). Rain-profiling algorithm for the TRMM precipitation radar. Journal of Applied Meteorology, 39(12), 2038-2052.

Ikai, J., & Nakamura, K. (2003). Comparison of rain rates over the ocean derived from TRMM microwave imager and precipitation radar. Journal of Atmospheric and Oceanic Technology, 20(12), 1709–1726.

Irawan, B. (2003). Multilevel impact assessment and coping strategies against El Nino: case of food crops in Indonesia CGPRT Centre Working Paper No. 75, Regional Co-ordination Centre for Research and Development of Coarse Grains, Pulses, Roots and Tuber Crops in the Humid Tropics of Asia and the Pacific: United Nations, 105 pp. (No. 32714).

Islam, M. N., & Uyeda, H. (2007). Use of TRMM in determining the climatic characteristics of rainfall over Bangladesh. Remote Sensing of Environment, 108(3), 264–276.

Ito, T., Kojima, A., Mckenzie, C., & Urata, S. (2011). ASEAN Economy: Diversity, Disparities, and Dynamics: Editors' Overview. Asian Economic Policy Review, 6(1), 1–21.

Imaoka, K., & Spencer, R. W. (2000). Diurnal variation of precipitation over the tropical oceans observed by TRMM/TMI combined with SSM/I. Journal of climate, 13(23), 4149-4158.

Izumo, T., Vialard, J., Lengaigne, M., de Boyer Montegut, C., Behera, S. K., Luo, J. J., Cravatte, S., Masson, S., & Yamagata, T. (2010). Influence of the state of the Indian Ocean Dipole on the following year's El Niño. Nature Geoscience, 3(3), 168-172.

Jamaluddin, A. F., Tangang, F., Chung, J. X., Juneng, L., Sasaki, H., & Takayabu, I. (2017). Investigating the mechanisms of diurnal rainfall variability over Peninsular Malaysia using the non-hydrostatic regional climate model. Meteorology and Atmospheric Physics, 1-23. https://doi.org/10.1007/s00703-017-0541-x

Janowiak, J. E., Kousky, V. E., & Joyce, R. J. (2005). Diurnal cycle of precipitation determined from the CMORPH high spatial and temporal resolution global precipitation analyses. Journal of Geophysical Research: Atmospheres, 110(D23).

Jourdain, N.C., Gupta, A.S., Taschetto, A.S., Ummenhofer, C.C., Moise, A.F., & Ashok, K. (2013). The Indo-Australian monsoon and its relationship to ENSO and IOD in reanalysis data and the CMIP3/CMIP5 simulations. Climate Dynamics, 41(11–12), 3073–3102.

Julian, P.R., & Chervin, R.M. (1978). A study of the Southern Oscillation and Walker Circulation phenomenon. Monthly Weather Review, 106(10), 1433–1451.

Juneng, L., & Tangang, F.T. (2005). Evolution of ENSO-related rainfall anomalies in Southeast Asia region and its relationship with atmosphere–ocean variations in Indo-Pacific sector. Climate Dynamics, 25(4), 337–350.

Juneng, L., & Tangang, F. T. (2010). Long-term trends of winter monsoon synoptic circulations over the maritime continent: 1962–2007. Atmospheric Science Letters, 11(3), 199-203.

Kamimera, H., Mori, S., Yamanaka, M. D., & Syamsudin, F. (2012). Modulation of diurnal rainfall cycle by the Madden-Julian oscillation based on one-year continuous observations with a meteorological radar in West Sumatera. SOLA, 8, 111-114.

Kanamori, H., Yasunari, T., & Kuraji, K. (2013). Modulation of the diurnal cycle of rainfall associated with the MJO observed by a dense hourly rain gauge network at Sarawak, Borneo. Journal of Climate, 26(13), 4858–4875.

Kao, H.Y., & Yu, J.Y. (2009). Contrasting eastern-Pacific and central-Pacific types of ENSO. Journal of Climate, 22(3), 615–632.

Kawanishi, T., Kuroiwa, H., Kojima, M., Oikawa, K., Kozu, T., Kumagai, H., Okamoto, K., Okumura, M, .Nakatsuka, H., & Nishikawa, K. (2000). TRMM precipitation radar. Advances in Space Research, 25(5), 969-972.

Kelkar, R. R. (2007). Satellite meteorology. BS Publications.

Khan, S. I., Hong, Y., Gourley, J. J., Huelsing, H. K., Khattak, M. U., & Vergara, H. J. (2015). Spatial and Diurnal Variability of Monsoon Systems Assessed by TRMM Rain Rate Over Indus Basin. IEEE Journal of Selected Topics in Applied Earth Observations and Remote Sensing, 8(9), 4325-4335.

Kidd, C. (2001). Satellite rainfall climatology: A review. International Journal of Climatology, 21(9), 1041-1066.

Kidd, C., & Huffman, G. (2011). Global precipitation measurement. Meteorological Applications, 18(3), 334-353.

Kidd, C., & Levizzani, V. (2011). Status of satellite precipitation retrievals. Hydrology and Earth System Sciences, 15(4), 1109-1116.

Kidd, C., & Levizzani, V. (2019). Quantitative precipitation estimation from satellite observations. Extreme Hydroclimatic In Events and Multivariate Hazards in a Changing Environment: A Remote Sensing Approach, V. Maggioni, and C. Massari (Eds.), pp. 3-40. Elsevier, Netherlands.

Kidd, C., Levizzani, V., & Bauer, P. (2009). A review of satellite meteorology and climatology at the start of the twenty-first century. Progress in Physical Geography, 33(4), 474-489.

Kidd, C., Matsui, T., Chern, J., Mohr, K., Kummerow, C., & Randel, D. (2016). Global precipitation estimates from cross-track passive microwave observations using a physically based retrieval scheme. Journal of Hydrometeorology, 17(1), 383-400.

Kidd, C., Becker, A., Huffman, G. J., Muller, C. L., Joe, P., Skofronick-Jackson, G., & Kirschbaum, D. B. (2017). So, how much of the Earth's surface is covered by rain gauges?. Bulletin of the American Meteorological Society, 98(1), 69-78.

Kirstetter, P. E., Karbalaee, N., Hsu, K., & Hong, Y. (2018). Probabilistic precipitation rate estimates with space - based infrared sensors. Quarterly Journal of the Royal Meteorological Society, 144, 191-205.

Kishore, K., & Subbiah, A.R. (2002). 1998-99 La Niña in Indonesia: Forecasts and institutional responses. In La Niña and Its Impacts: Facts and Speculation, MH Glantz (ed.), pp. 179–185 (Tokyo: United Nations University Press).

Kishtawal, C. M. (2016). Use of satellite observations in tropical cyclone studies. In Advanced numerical modeling and data assimilation techniques for tropical cyclone prediction, U. C. Mohanty, & S. G. Gopalakrishnan (Eds.), pp. 35-47. Springer, Dordrecht-Netherlands.

Können, G. P., Jones, P. D., Kaltofen, M. H., & Allan, R. J. (1998). Pre-1866 extensions of the Southern Oscillation Index using early Indonesian and Tahitian meteorological readings. Journal of Climate, 11(9), 2325–2339.

Koo, M. S., Hong, S. Y., & Kim, J. (2009). An evaluation of the tropical rainfall measuring mission (TRMM) multi-satellite precipitation analysis (TMPA) data over South Korea. Asia-Pacific Journal of Atmospheric Sciences, 45(3), 265-282.

Kubota, H., Numaguti, A., & Emori, S. (2004). Numerical experiments examining the mechanism of diurnal variation of tropical convection. Journal of the Meteorological Society of Japan, 82(5), 1245–1260.

Kubota, H., Shirooka, R., Hamada, J. I., & Syamsudin, F. (2011). Interannual rainfall variability over the eastern maritime continent. Journal of the Meteorological Society of Japan, 89, 111–122.

Kubota, T., M. Kachi, R. Oki, S. Shimizu, N. Yoshida, M. Kojima, K. Nakamura (2010), Rainfall Observation from Space - Applications of Tropical Rainfall Measuring Mission (TRMM) and Global Precipitation Measurement (GPM) Mission, paper presented at ISPRS Technical Commission VIII Symposium, International Society for Photogrammetry and Remote Sensing, Kyoto, Japan.

Kummerow, C., Barnes, W., Kozu, T., Shiue, J., & Simpson, J. (1998). The tropical rainfall measuring mission (TRMM) sensor package. Journal of atmospheric and oceanic technology, 15(3), 809-817.

Kummerow, C., Simpson, J., Thiele, O., Barnes, W., Chang, A. T. C., Stocker, E., Adler, R. F., Hou, A., Kakar, R., Wentz, F., Ashcroft, P., Kozu, T., Hong, Y., Okamoto, K., Iguchi, T., Kuroiwa, H., Im, E., Haddad, Z., Huffman, G. J., Ferrier, B., Olson, W. S., Zipser, E., Smith, E. A., Wilheit, T. T., North, G., Krishnamurti, T., & Nakamura, K. (2000). The status of the Tropical Rainfall Measuring Mission (TRMM) after two years in orbit. Journal of Applied Meteorology, 39(12), 1965–1982.

L'Heureux, M. L., Collins, D. C., & Hu, Z. Z. (2013). Linear trends in sea surface temperature of the tropical Pacific Ocean and implications for the El Niño-Southern Oscillation. Climate Dynamics, 40(5-6), 1223-1236.

Lensky, I. M., & Levizzani, V. (2008). Estimation of precipitation from space-based platforms. In Precipitation: Advances in measurement, estimation and prediction. Michaelides, S. (Ed.), pp. 195-217. Springer, Berlin, Heidelberg.

Levizzani, V., & Cattani, E. (2019). Satellite remote sensing of precipitation and the terrestrial water cycle in a changing climate. Remote Sensing, 11(19), 2301.

Levizzani, V., Amorati, R., & Meneguzzo, F. (2002). A review of satellite-based rainfall estimation methods. European Commission Project MUSIC Report (EVK1-CT-2000-00058), 66 pp.

Levizzani, V., Schmetz, J., Lutz, H. J., Kerkmann, J., Alberoni, P. P., & Cervino, M. (2001). Precipitation estimations from geostationary orbit and prospects for METEOSAT Second Generation. Meteorological Applications, 8(1), 23-41.

Li, G., Ren, B., Yang, C., & Zheng, J. (2010). Indices of El Niño and El Niño Modoki: An improved El Niño Modoki index. Advances in Atmospheric Sciences, 27, 1210–1220.

Liao, X., Ma, J., & Zhan, H. (2012). Effect of different types of El Niño on primary productivity in the South China Sea. Aquatic Ecosystem Health and Management, 15(2), 135–143.

Liao, L., & Meneghini, R. (2009). Validation of TRMM precipitation radar through comparison of its multiyear measurements with ground-based radar. Journal of Applied Meteorology and Climatology, 48(4), 804–817.

Liao, Z., Hong, Y., Wang, J., Fukuoka, H., Sassa, K., Karnawati, D., & Fathani, F. (2010). Prototyping an experimental early warning system for rainfall-induced landslides in Indonesia using satellite remote sensing and geospatial datasets. Landslides, 7(3), 317-324.

Liu, C., & Zipser, E. J. (2015). The global distribution of largest, deepest, and most intense precipitation systems. Geophysical Research Letters, 42(9), 3591-3595.

Liu, Q. Y., Wang, D., Wang, X., Shu, Y., Xie, Q., & Chen, J. (2014). Thermal variations in the South China Sea associated with the eastern and central Pacific El Niño events and their mechanisms. Journal of Geophysical Research: Oceans, 119(12), 8955-8972.

Love, B.S., Matthews, A.J., & Lister, G. (2011). The diurnal cycle of precipitation over the Maritime Continent in a high-resolution atmospheric model. Quarterly Journal of the Royal Meteorological Society, 137(657), 934–947.

Luo, J. J., Sasaki, W., & Masumoto, Y. (2012). Indian Ocean warming modulates Pacific climate change. Proceedings of the National Academy of Sciences, 109(46), 18701–18706.

Lyon, B., & Camargo, S. J. (2009). The seasonally-varying influence of ENSO on rainfall and tropical cyclone activity in the Philippines. Climate dynamics, 32(1), 125–141.

Lyon, B., Cristi, H., Verceles, E. R., Hilario, F. D., & Abastillas, R. (2006). Seasonal reversal of the ENSO rainfall signal in the Philippines. Geophysical research letters, 33(24), L24710

Madden, R. A., & Julian, P. R. (1971). Detection of a 40-50 day oscillation in the zonal wind in the tropical Pacific. Journal of the Atmospheric Sciences, 28(5), 702–708.

Maggioni, V., Meyers, P. C., & Robinson, M. D. (2016). A review of merged high-resolution satellite precipitation product accuracy during the Tropical Rainfall Measuring Mission (TRMM) era. Journal of Hydrometeorology, 17(4), 1101-1117.

Mandapaka, P. V., & Qin, X. (2013). Analysis and Characterization of Probability Distribution and Small-Scale Spatial Variability of Rainfall in Singapore Using a Dense Gauge Network. Journal of Applied Meteorology and Climatology, 52(12), 2781–2796.

Manton, M. J., Della-Marta, P. M., Haylock, M. R., Hennessy, K. J., Nicholls, N., Chambers, L. E., Collins, D. A., Daw, G., Finet, A., Gunawan, D., Inape, K., Isobe, H., Kestin, T. S., Lefale, P., Leyu, C. H., Lwin, T., Maitrepierre, L., Ouprasitwong, N., Page, C. M., Pahalad, J., Plummer, N., Salinger, M. J., Suppiah R., Tran, V. L., Trewin, B., Tibig, L., & Yee, D. (2001). Trends in extreme daily rainfall and temperature in Southeast Asia and the South Pacific: 1961–1998. International Journal of Climatology, 21(3), 269-284.

Matsumoto, J., Wang, B., Wu, G., Li, J., Wu, P., Hattori, M., Mori, S., Yamanaka, M., Ogino, S., Hamada, J-I., H., Syamsudin, F., Koike, T., Tamagawa, K., Ikoma, E., Kinutani, H., Kamahori, H., Kamiguchi, K., & Harada, Y. (2017). An overview of the Asian monsoon years 2007–2012 (AMY) and multi-scale interactions in the extreme rainfall events over the Indonesian Maritime Continent. In The Global Monsoon System: Research and Forecast, 3rd, eds. Chang,

McBride, J. L., Haylock, M. R., & Nicholls, N. (2003). Relationships between the Maritime Continent heat source and the El Niño-Southern Oscillation phenomenon. Journal of climate, 16(17), 2905–2914.

Mehta, A. V., & Yang, S. (2008). Precipitation climatology over Mediterranean Basin from ten years of TRMM measurements. Advances in Geosciences, 17, 87–91.

Meyers, G., McIntosh, P., Pigot, L., & Pook, M. (2007). The years of El Niño, La Niña, and interactions with the tropical Indian Ocean. Journal of Climate, 20(13), 2872–2880.

Misra, V., & DiNapoli, S. (2014). The variability of the Southeast Asian summer monsoon. International Journal of Climatology, 34(3), 893–901

Mori, S., Hamada, J-I., Tauhid, Y. I., Yamanaka, M. D., Okamoto, N., Murata, F., Sakurai, N., Hashiguchi, H., & Sribimawati, T. (2004). Diurnal land-sea rainfall peak migration over Sumatera Island, Indonesian maritime continent, observed by TRMM satellite and intensive rawinsonde soundings. Monthly weather review, 132(8), 2021–2039.

Mori, S., Hamada, J. I., Sakurai, N., Fudeyasu, H., Kawashima, M., Hashiguchi, H., Syamsudin, F., Arbain, A. A., Sulistyowati, R., Matsumoto, J., & Yamanaka, M. D. (2011). Convective systems developed along the coastline of Sumatera Island, Indonesia, observed with an X-band Doppler radar during the HARIMAU2006 campaign. Journal of the Meteorological Society of Japan. Ser. II, 89, 61-81.

Moron, V., Robertson, A. W., & Qian, J. H. (2010). Local versus regional-scale characteristics of monsoon onset and post-onset rainfall over Indonesia. Climate dynamics, 34(2-3), 281-299.

Murakami, T., & Matsumoto, J. (1994). Summer monsoon over the Asian continent and western North Pacific. Journal of the Meteorological Society of Japan. Ser. II, 72(5), 719-745.

Nakazawa, T., & Rajendran, K. (2004). Asian monsoon rainfall characteristics over land by TRMM satellite and surface station data. In The 2nd Tropical Rainfall Measuring Mission (TRMM) Science Conference. 5–10 September 2004 (Nara, Japan)

National Research Council. (2006). Assessment of the benefits of extending the Tropical Rainfall Measuring Mission: A perspective from the research and operations communities: Interim Report. Washington, DC, pp. 103.

Naylor, R. L., Battisti, D. S., Vimont, D. J., Falcon, W. P., & Burke, M. B. (2007). Assessing risks of climate variability and climate change for Indonesian rice agriculture. Proceedings of the National Academy of Sciences (PNAS), 104(19), 7752-7757.

Neale, R., & Slingo, J. (2003). The maritime continent and its role in the global climate: A GCM study. Journal of Climate, 16(5), 834-848.

Nesbitt, S. W., & Zipser, E. J. (2003). The diurnal cycle of rainfall and convective intensity according to three years of TRMM measurements. Journal of Climate, 16(10), 1456-1475.

Nicholls, N. (1988). El Niño-Southern Oscillation and rainfall variability. Journal of Climate, 1(4), 418–421.

Nicholson, S. E., Some, B., McCollum, J., Nelkin, E., Klotter, D., Berte, Y., Diallo, B. M., Gaye, I., Kpabeba, G., Ndiaye, O., Noukpozounkou, J. N., Tanu, M. M., Thiam, A., Toure, A., & Traore, A. K. (2003). Validation of TRMM and other rainfall estimates with a high-density gauge dataset for West Africa. Part I: Validation of GPCC rainfall product and pre-TRMM satellite and blended products. Journal of Applied Meteorology, 42(10), 1337–1354.

Nickl, E., Willmott, C.J., Matsuura, K., & Robeson, S.M. (2010). Changes in annual land-surface precipitation over the twentieth and early twenty-first century. Annals of the Association of American Geographers, 100(4), 729-739.

NOAA. (2007). NOAA's Role in Space-Based Global Precipitation Estimation and Application. Committee on the Future of Rainfall Measuring Missions National Research Council, pp. 131 (Washington, DC-USA, National Academy Press).

Nuarsa, I.W., Adnyana, I.W.S., Merit, I.N., As-Syakur, A.R. (2014). Comparison of TRMM 3B43 version 6 and 7 with monthly gauge standardized precipitation index over semi-arid region of Indonesia. The 12th Biennial Conference Pan Ocean Remote Sensing Conference 2014 (PORSEC 2014), Denpasar – Bali, Indonesia.

Ogino, S. Y., Yamanaka, M. D., Mori, S., & Matsumoto, J. (2016). How much is the precipitation amount over the tropical coastal region?. Journal of Climate, 29(3), 1231-1236.

Oh, J. H., Kim, K. Y., & Lim, G. H. (2012). Impact of MJO on the diurnal cycle of rainfall over the western Maritime Continent in the austral summer. Climate dynamics, 38(5–6), 1167–1180.

Oktaviani, R., Amaliah, S., Ringler, C., Rosegrant, M. W., & Sulser, T. B. (2011). The impact of global climate change on the Indonesian economy (No. 1148). International Food Policy Research Institute (IFPRI).

Oldeman, L. R. (1977). Climate of Indonesia. Central Research Institute for Agriculture.

Page, S. E., Siegert, F., Rieley, J. O., Boehm, H. D. V., Jaya, A., & Limin, S. (2002). The amount of carbon released from peat and forest fires in Indonesia during 1997. Nature, 420(6911), 61-65.

Peatman, S. C., Matthews, A. J., & Stevens, D. P. (2014). Propagation of the Madden–Julian Oscillation through the Maritime Continent and scale interaction with the diurnal cycle of precipitation. Quarterly Journal of the Royal Meteorological Society, 140(680), 814–825.

Petty, G. W. (1995). The status of satellite-based rainfall estimation over land. Remote Sensing of Environment, 51(1), 125–137.

Petty, G. W., & Krajewski, W. F. (1996). Satellite estimation of precipitation over land. Hydrological sciences journal, 41(4), 433–451.

Pfeifroth, U., Trentmann, J., Fink, A. H., & Ahrens, B. (2016). Evaluating satellite-based diurnal cycles of precipitation in the African tropics. Journal of Applied Meteorology and Climatology, 55(1), 23-39.

Philander, S. G. H. (1983). El Niño southern oscillation phenomena. Nature, 302, 295-301.

Philander, S. G. H. (1989). El Niño, La Niña, and the southern oscillation (Vol. 46). Academic press.

Pohl, B., & Matthews, A. J. (2007). Observed changes in the lifetime and amplitude of the Madden-Julian oscillation associated with interannual ENSO sea surface temperature anomalies. Journal of climate, 20(11), 2659–2674.

Prakash, S., Mahesh, C., & Gairola, R.M. (2013). Comparison of TRMM Multi-satellite Precipitation Analysis (TMPA)-3B43 version 6 and 7 products with rain gauge data from ocean buoys. Remote Sensing Letters, 4(7), 677–685.

Prasetia, R., As-Syakur, A. R., & Osawa, T. (2013). Validation of TRMM Precipitation Radar satellite data over Indonesian region. Theoretical and applied climatology, 112(3-4), 575–587.

Qian, J. H. (2008). Why precipitation is mostly concentrated over islands in the Maritime Continent. Journal of the Atmospheric Sciences, 65(4), 1428–1441.

Qian, J. H., Robertson, A. W., & Moron, V. (2010). Interactions among ENSO, the monsoon, and diurnal cycle in rainfall variability over Java, Indonesia. Journal of the Atmospheric Sciences, 67(11), 3509–3524.

Qian, J.H., Robertson, A.W., & Moron, V. (2013). Diurnal cycle in different weather regimes and rainfall variability over Borneo associated with ENSO. Journal of Climate, 26(5), 1772–1790.

Ramage, C. S. (1968). Role of a tropical “maritime continent” in the atmospheric circulation. Monthly Weather Review, 96(6), 365–370.

Ramage, C.S. (1971). Monsoon Meteorology. Volume. 15. Academic Press, New York and London.

Rao, S. A., Masson, S., Luo, J. J., Behera, S. K., & Yamagata, T. (2007). Termination of Indian Ocean dipole events in a coupled general circulation model. Journal of climate, 20(13), 3018–3035.

Rauniyar, S. P., & Walsh, K. J. (2011). Scale interaction of the diurnal cycle of rainfall over the Maritime Continent and Australia: Influence of the MJO. Journal of Climate, 24(2), 325–348.

Rauniyar, S.P., & Walsh, K.J. (2013). Influence of ENSO on the Diurnal Cycle of Rainfall over the Maritime Continent and Australia. Journal of Climate, 26(4), 1304–1321.

Robertson, A. W., Moron, V., Qian, J.-H., Chang, C.-P., Tangang, F., Aldrian, E., Koh, T.Y., Juneng, L. (2011). The maritime continent monsoon. In Chang, C.-P., Ding, Y., Lau, N,-C., Johnson, R.H., Wang, B., Yasunari, T. (Eds). The Global Monsoon System: Research and Forecast (World Scientific Series on Asia-Pacific Weather and Climate), pp. 85–98. World Scientific Publishing: Singapore.

Roca, R., Chambon, P., Jobard, I., Kirstetter, P. E., Gosset, M., & Bergès, J. C. (2010). Comparing satellite and surface rainfall products over West Africa at meteorologically relevant scales during the AMMA campaign using error estimates. Journal of Applied Meteorology and Climatology, 49(4), 715-731.

Ropelewski, C. F., & Halpert, M. S. (1987). Global and regional scale precipitation patterns associated with the El Niño/Southern Oscillation. Monthly weather review, 115(8), 1606–1626.

Ropelewski, C. F., & Halpert, M. S. (1989). Precipitation patterns associated with the high index phase of the Southern Oscillation. Journal of climate, 2(3), 268–284.

Ropelewski, C. F., & Halpert, M. S. (1996). Quantifying southern oscillation-precipitation relationships. Journal of climate, 9(5), 1043–1059.

Ropelewski, C. F., & Jones, P. D. (1987). An extension of the Tahiti-Darwin southern oscillation index. Monthly Weather Review, 115(9), 2161–2165.

Rosenfeld, D. (2007). Cloud top microphysics as a tool for precipitation measurements. In Measuring Precipitation from Space: EURAINSAT and the Future, V. Levizzani, P. Bauer, F. J. Turk (eds.), pp. 61-77. Springer, Dordrecht-Netherlands.

Saha, K. (2010), Tropical Circulation Systems and Monsoons, Springer-Verlag, Berlin Heidelberg, Germany.

Sahu, N., Behera, S. K., Yamashiki, Y., Takara, K., & Yamagata, T. (2012). IOD and ENSO impacts on the extreme stream-flows of Citarum river in Indonesia. Climate dynamics, 39(7-8), 1673–1680.

Saji, N. H., & Yamagata, T. (2003a). Structure of SST and Surface Wind Variability during Indian Ocean Dipole Mode Events: COADS Observations. Journal of Climate, 16(16), 2735–2751.

Saji, N. H., & Yamagata, T. (2003b). Possible impacts of Indian Ocean dipole mode events on global climate. Climate Research, 25(2), 151–169.

Saji, N. H., Goswami, B. N., Vinayachandran, P. N., & Yamagata, T. (1999). A dipole mode in the tropical Indian Ocean. Nature, 401(6751), 360–363.

Sakurai, N., Murata, F., Yamanaka, M.D., Mori, S., Hamada, J. I., Hashiguchi, H., Tauhid, Y. I., Sribimawati, T., & Suhardi, B. (2005). Diurnal cycle of cloud system migration over Sumatera Island. Journal of the Meteorological Society of Japan. Ser. II, 83(5), 835-850.

Salimun, E., Tangang, F., Juneng, L., Behera, S. K., & Yu, W. (2014). Differential impacts of conventional El Niño versus El Niño Modoki on Malaysian rainfall anomaly during winter monsoon. International Journal of Climatology, 34(8), 2763–2774.

Schumacher, C., & Houze Jr, R. A. (2003). The TRMM precipitation radar's view of shallow, isolated rain. Journal of Applied Meteorology, 42(10), 1519–1524.

Semire, F. A., Mohd-Mokhtar, R., Ismail, W., Mohamad, N., & Mandeep, J. S. (2012). Ground validation of space-borne satellite rainfall products in Malaysia. Advances in Space Research, 50(9), 1241–1249.

Serrat-Capdevila, A., Valdes, J. B., & Stakhiv, E. Z. (2014). Water management applications for satellite precipitation products: Synthesis and recommendations. JAWRA Journal of the American Water Resources Association, 50(2), 509-525.

Shibagaki, Y., Shimomai, T., Kozu, T., Mori, S., Fujiyoshi, Y., Hashiguchi, H., Yamamoto, M. K., Fukao, S., & Yamanaka, M. D. (2006). Multiscale aspects of convective systems associated with an intraseasonal oscillation over the Indonesian Maritime Continent. Monthly weather review, 134(6), 1682-1696.

Shimizu, S. (2009). Rainfall observation by radar satellite, Lecture Note. Japan Aerospace Exploration Agency (JAXA) and Earth Observation Research Center (EORC).

Shuanglin, L., and Qin, W. (2012) A new approach for classifying two types of El Niño events. Atmospheric and Oceanic Science Letters, 5(5), 414–419.

Simpson, J., Kummerow, C., Tao, W. K., & Adler, R. F. (1996). On the tropical rainfall measuring mission (TRMM). Meteorology and Atmospheric physics, 60(1–3), 19–36.

Siuki, S. K., Saghafian, B., & Moazami, S. (2017). Comprehensive evaluation of 3-hourly TRMM and half-hourly GPM-IMERG satellite precipitation products. International Journal of Remote Sensing, 38(2), 558-571.

Slezak, M. (2014). World is unprepared for major El Nino later this year. New Scientist, 222, 8–9.

Skofronick-Jackson, G., Kirschbaum, D., Petersen, W., Huffman, G., Kidd, C., Stocker, E., & Kakar, R. (2018). The Global Precipitation Measurement (GPM) mission's scientific achievements and societal contributions: reviewing four years of advanced rain and snow observations. Quarterly Journal of the Royal Meteorological Society, 144, 27-48.

So, D., & Shin, D. B. (2018). Classification of precipitating clouds using satellite infrared observations and its implications for rainfall estimation. Quarterly Journal of the Royal Meteorological Society, 144, 133-144.

Sobel, A. H., Burleyson, C. D., & Yuter, S. E. (2011). Rain on small tropical islands. Journal of Geophysical Research: Atmospheres, 116(D8).

Sobel, A. H., Burleyson, C. D., Yuter, S. E., & Biasutti, M. (2013). Correction to “Rain on small tropical islands”. Journal of Geophysical Research: Atmospheres, 118, 2301-2302.

Sorooshian, S., Gao, X., Hsu, K., Maddox, R. A., Hong, Y., Gupta, H. V., & Imam, B. (2002). Diurnal variability of tropical rainfall retrieved from combined GOES and TRMM satellite information. Journal of Climate, 15(9), 983-1001.

Su, F., Hong, Y., & Lettenmaier, D. P. (2008). Evaluation of TRMM Multisatellite Precipitation Analysis (TMPA) and its utility in hydrologic prediction in the La Plata Basin. Journal of Hydrometeorology, 9(4), 622–640.

Sulistyowati, R., Hapsari, R. I., Syamsudin, F., Mori, S., Oishi, S. T., & Yamanaka, M. D. (2014). Rainfall-driven diurnal variations of water level in the Ciliwung River, West Jawa, Indonesia. SOLA, 10, 141-144.

Sun, D., Xue, F., & Zhou, T. (2013). Impacts of two types of El Niño on atmospheric circulation in the Southern Hemisphere. Advances in Atmospheric Sciences, 30, 1732–1742.

Susanto, R. D., Gordon, A. L., & Zheng, Q. (2001). Upwelling along the coasts of Java and Sumatra and its relation to ENSO. Geophysical Research Letters, 28(8), 1599–1602.

Susanto, R. D., Moore, T. S., & Marra, J. (2006). Ocean color variability in the Indonesian Seas during the SeaWiFS era. Geochemistry, Geophysics, Geosystems, 7(5).

Susilo, G. E., Yamamoto, K., Imai, T., Ishii, Y., Fukami, H., & Sekine, M. (2013). The effect of ENSO on rainfall characteristics in the tropical peatland areas of Central Kalimantan, Indonesia. Hydrological Sciences Journal, 58(3), 539–548.

Stephens, G. L., & Kummerow, C. D. (2007). The remote sensing of clouds and precipitation from space: A review. Journal of the Atmospheric Sciences, 64(11), 3742-3765.

Swardika, I.K., Tanaka, T., & Ishida, H. (2012). Study on the characteristics of the Indonesian seas using satellite remote-sensing data for 1998–2007. International Journal of Remote Sensing, 33(8), 2378–2394.

Tabata, Y., Hashiguchi, H., Yamamoto, M. K., Yamamoto, M., Yamanaka, M. D., Mori, S., Syamsudin, S., & Manik, T. (2011). Observational study on diurnal precipitation cycle in equatorial Indonesia using 1.3-GHz wind profiling radar network and TRMM precipitation radar. Journal of Atmospheric and Solar-Terrestrial Physics, 73(9), 1031–1042.

Takahashi, H. G. (2016). Seasonal and diurnal variations in rainfall characteristics over the tropical Asian monsoon region using TRMM-PR data. SOLA, 12A, 22-27.

Takahashi, H. G., Fujinami, H., Yasunari, T., & Matsumoto, J. (2010). Diurnal rainfall pattern observed by Tropical Rainfall Measuring Mission Precipitation Radar (TRMM PR) around the Indochina peninsula. Journal of Geophysical Research: Atmospheres, 115(D7), D07109, 1–10.

Takahashi, H., Su, H., Jiang, J. H., Luo, Z. J., Xie, S. P., & Hafner, J. (2013). Tropical water vapor variations during the 2006–2007 and 2009–2010 El Niños: Satellite observation and GFDL AM2. 1 simulation. Journal of Geophysical Research: Atmospheres, 118(16), 8910–8920.

Tan, W., Wang, X., Wang, W., Wang, C., & Zuo, J. (2016). Different Responses of Sea Surface Temperature in the South China Sea to Various El Niño Events during Boreal Autumn. Journal of Climate, 29(3), 1127–1142.

Tang, Y., & Yu, B. (2008). MJO and its relationship to ENSO. Journal of Geophysical Research: Atmospheres (1984–2012), 113(D14).

Tangang, F. T., & Juneng, L. (2004). Mechanisms of Malaysian rainfall anomalies. Journal of Climate, 17(18), 3616–3622.

Tapiador, F. J., Navarro, A., Levizzani, V., García-Ortega, E., Huffman, G. J., Kidd, C., Kucera, P. A., Kummerow, C. D., Masunaga, H., Petersen, W. A., Roca, R.,Sánchezc, J. -L., Taod, W. -K., & Turk, F. J. (2017). Global precipitation measurements for validating climate models. Atmospheric Research, 197, 1-20.

Taschetto, A.S., & England, M.H. (2009). El Niño Modoki impacts on Australian rainfall. Journal of Climate, 22(11), 3167–3174.

Thies, B., & Bendix, J. (2011). Satellite based remote sensing of weather and climate: recent achievements and future perspectives. Meteorological Applications, 18(3), 262-295.

Tokinaga, H., Xie, S. P., Deser, C., Kosaka, Y., & Okumura, Y.M. (2012). Slowdown of the Walker circulation driven by tropical Indo-Pacific warming. Nature, 491(7424), 439–443.

Trenberth, K. E. (1989) Toga and Atmospheric Processes. In Berger, B. Dickinson, R. E., and Kidson, J. W. (eds.). Understanding Climate Change, pp. 117-125, American Geophysical Union, Washington, D. C.

Trenberth, K. E. (1997). The definition of El Niño. Bulletin of the American Meteorological Society, 78(12), 2771–2777.

Trenberth, K. E., Hurrell, J. W., & Stepaniak, D. P. (2006). The Asian monsoon: global perspectives. In Wang, B. "The Asian Monsoon", (pp. 67-87). Springer Berlin Heidelberg.

Varikoden, H., Samah, A. A., & Babu, C. A. (2010). Spatial and temporal characteristics of rain intensity in the peninsular Malaysia using TRMM rain rate. Journal of hydrology, 387(3), 312-319.

Vernimmen, R. R. E., Hooijer, A., Aldrian, E., & van Dijk, A. I. J. M. (2012). Evaluation and bias correction of satellite rainfall data for drought monitoring in Indonesia. Hydrology and Earth System Sciences, 16(1), 133–146.

Villafuerte II, M.Q., Matsumoto, J., Akasaka, I., Takahashi, H.G., Kubota, H., & Cinco, T.A. (2014). Long-term trends and variability of rainfall extremes in the Philippines. Atmospheric Research, 137, 1–13.

Villarini, G., Mandapaka, P. V., Krajewski, W. F., & Moore, R. J. (2008). Rainfall and sampling uncertainties: A rain gauge perspective. Journal of Geophysical Research: Atmospheres (1984–2012), 113(D11).

Vimont, D. J., Battisti, D. S., & Naylor, R. L. (2010). Downscaling Indonesian precipitation using large-scale meteorological fields. International Journal of Climatology, 30(11), 1706–1722.

von Storch, H., & Zwiers, F. W. (2001). Statistical analysis in climate research. Cambridge university press. , UK. 484 pp.

Waliser, D. E., Moncrieff, M. W., Burridge, D., Fink, A. H., Gochis, D., Goswami, B. N., Guan B, Harr P, Heming J, Hsu H-H, Jakob C, Janiga M, Johnson R, Jones S, Knippertz P, Marengo J, Nguyen H, Pope M, Serra Y, Thorncroft C, Wheeler M, Wood R, & Yuter, S. (2012). The "year" of tropical convection (May 2008-April 2010): Climate variability and weather highlights. Bulletin of the American Meteorological Society, 93(8), 1189–1218.

Wang, B., Wu, R., & Li, T. (2003). Atmosphere-Warm Ocean Interaction and Its Impacts on Asian-Australian Monsoon Variation. Journal of Climate, 16(8), 1195–1211.

Wang, B. I. N., Wu, R., & Li, T. I. M. (2003). Atmosphere–warm ocean interaction and its impacts on Asian–Australian monsoon variation. Journal of Climate, 16(8), 1195-1211.

Wang, G., & Hendon, H.H. (2007). Sensitivity of Australian rainfall to inter-El Niño variations. Journal of Climate, 20(16), 4211–4226.

Waple, A. M., & Lawrimore, J. H. (2003). State of the climate in 2002. Bulletin of the American Meteorological Society, 84(6), S1–S68.

Weng, H., Wu, G., Liu, Y., Behera, S. K., & Yamagata, T. (2011). Anomalous summer climate in China influenced by the tropical Indo-Pacific Oceans. Climate dynamics, 36(3-4), 769-782.

Weng, H., Ashok, K., Behera, S.K., Rao, S.A., & Yamagata, T. (2007). Impacts of recent El Niño Modoki on dry/wet conditions in the Pacific rim during boreal summer. Climate Dynamics, 29(2–3), 113–129.

Wentz, F. J., Gentemann, C., Smith, D., & Chelton, D. (2000). Satellite measurements of sea surface temperature through clouds. Science, 288(5467), 847–850.

Wheeler, M. C., & Hendon, H. H. (2004). An all-season real-time multivariate MJO index: Development of an index for monitoring and prediction. Monthly Weather Review, 132(8), 1917–1932.

Willmott, C. J. (1982). Some comments on the evaluation of model performance. Bulletin of the American Meteorological Society, 63(11), 1309–1313.

Wilson, E. A., Gordon, A. L., & Kim, D. (2013). Observations of the Madden Julian Oscillation during Indian Ocean Dipole events. Journal of Geophysical Research: Atmospheres, 118(6), 2588–2599.

Wolff, D. B., Marks, D. A., Amitai, E., Silberstein, D. S., Fisher, B. L., Tokay, A., Wang, J., & Pippitt, J. L. (2005). Ground validation for the tropical rainfall measuring mission (TRMM). Journal of Atmospheric and Oceanic Technology, 22(4), 365–380.

Wu, C. H., & Hsu, H. H. (2009). Topographic influence on the MJO in the Maritime Continent. Journal of Climate, 22(20), 5433–5448.

Wu, P., Mori, S., Hamada, J. I., Yamanaka, M. D., Matsumoto, J., & Kimura, F. (2008). Diurnal variation of rainfall and precipitable water over Siberut Island off the western coast of Sumatra Island. SOLA, 4, 125-128.

Wu, P., Arbain, A.A., Mori, S., Hamada, J.-I., Hattori, M., Syamsudin, F., & Yamanaka, M.D. (2013). The Effects of an Active Phase of the Madden-Julian Oscillation on the Extreme Precipitation Event over Western Java Island in January 2013. SOLA, 9, 79–83.

Wu, P., Hara, M., Hamada, J. I., Yamanaka, M. D., & Kimura, F. (2009). Why a large amount of rain falls over the sea in the vicinity of western Sumatra Island during nighttime. Journal of Applied Meteorology and Climatology, 48(7), 1345-1361.

Wu, P., Hara, M., Fudeyasu, H., Yamanaka, M. D., Matsumoto, J., Syamsudin, F., Sulistyowati, R., & Djajadihardja, Y. S. (2007). The impact of trans-equatorial monsoon flow on the formation of repeated torrential rains over Java Island. SOLA, 3, 93-96.

Wyrtki, K. (1961). Physical oceanography of the southeast Asian waters. NAGA Report, Vol. 2, Scripps Institution of Oceanography, pp. 195 (San Diego–USA, University of California).

Xie, F., Li, J., Tian, W., Zhang, J., & Shu, J. (2014). The impacts of two types of El Niño on global ozone variations in the last three decades. Advances in Atmospheric Sciences, 31(5), 1113–1126.

Xie, P., & Arkin, P. A. (1996). Analyses of global monthly precipitation using gauge observations, satellite estimates, and numerical model predictions. Journal of climate, 9(4), 840–858.

Xie, P., Chen, M., Yang, S., Yatagai, A., Hayasaka, T., Fukushima, Y., & Liu, C. (2007). A gauge-based analysis of daily precipitation over East Asia. Journal of Hydrometeorology, 8(3), 607–626.

Xin-Xin, Z., Xun-Qiang, B. I., & Xiang-Hui, K. (2015). Observed diurnal cycle of summer precipitation over South Asia and East Asia based on CMORPH and TRMM satellite data. Atmospheric and Oceanic Science Letters, 8(4), 201-207.

Xu, K., Zhu, C., & He, J. (2013). Two types of El Niño-related Southern Oscillation and their different impacts on global land precipitation. Advances in Atmospheric Sciences, 30, 1743–1757.

Xu, Z.X., Takeuchi, K., & Ishidaira, H. (2004). Correlation between El Niño–Southern Oscillation (ENSO) and precipitation in South-east Asia and the Pacific region. Hydrological processes, 18(1), 107–123.

Xue, X., Hong, Y., Limaye, A. S., Gourley, J. J., Huffman, G. J., Khan, S. I., Xue, X., Hong, Y., Limaye, A.S., Gourley, J.J., Huffman, G.J., Khan, S.I., Dorji, C., & Chen, S. (2013). Statistical and hydrological evaluation of TRMM-based Multi-satellite Precipitation Analysis over the Wangchu Basin of Bhutan: Are the latest satellite precipitation products 3B42V7 ready for use in ungauged basins?. Journal of Hydrology, 499, 91-99.

Yamanaka, M. D. (2016). Physical climatology of Indonesian maritime continent: An outline to comprehend observational studies. Atmospheric Research, 178, 231-259.

Yamanaka, M. D., Ogino, S. Y., Wu, P. M., Jun-Ichi, H., Mori, S., Matsumoto, J., & Syamsudin, F. (2018). Maritime continent coastlines controlling Earth's climate. Progress in Earth and Planetary Science, 5(1), 21.

Yamanaka, M. D., Hashiguchi, H., Mori, S., Wu, P. M., Syamsudin, F., Manik, T., Hamada, J-I., Yamamoto, M.K., Kawashima, M., Fujiyoshi, Y., Sakurai, N., Ohi, M., Shirooka, R., Katsumata, M., Shibagaki, Y., Shimomai, T., Erlansyah, Setiawan, W., Tejasukmana, B., Djajadihardja, Y.S., & Anggadiredja, J. T. (2008). HARIMAU radar-profiler network over the Indonesian maritime continent: A GEOSS early achievement for hydrological cycle and disaster prevention. J. Disaster Res, 3, 78-88.

Yanase, A., Yasunaga, K., & Masunaga, H. (2017). Relationship between the direction of diurnal rainfall migration and the ambient wind over the Southern Sumatra Island. Earth and Space Science, 4(3), 117-127.

Yang, G. Y., & Slingo, J. (2001). The diurnal cycle in the tropics. Monthly Weather Review, 129(4), 784-801.

Yang, S., & Smith, E. A. (2006). Mechanisms for diurnal variability of global tropical rainfall observed from TRMM. Journal of limate, 19(20), 5190-5226.

Yokoi, S., Mori, S., Katsumata, M., Geng, B., Yasunaga, K., Syamsudin, F., Nurhayati, N., & Yoneyama, K. (2017). Diurnal Cycle of Precipitation Observed in the Western Coastal Area

of Sumatra Island: Offshore Preconditioning by Gravity Waves. Monthly Weather Review, 145(9), 3745-3761.

Yulihastin, E., & Kodama, Y. M. (2010). Seasonal Variability of Rainfall over Indonesia Maritime Continent Based on TRMM PR Observations. In The 38th Committee on Space Research (COSPAR) Scientific Assembly. 18-15 July 2010 (Vol. 38, p. 182). 18-15 July 2010, (Bremen, Germany).

Zhang, T., Yang, S., Jiang, X., & Zhao, P. (2016). Seasonal–interannual variation and prediction of wet and dry season rainfall over the Maritime Continent: Roles of ENSO and monsoon circulation. Journal of Climate, 29(10), 3675-3695.

Zheng, X. T., Xie, S. P., Vecchi, G. A., Liu, Q., & Hafner, J. (2010). Indian Ocean Dipole Response to Global Warming: Analysis of Ocean-Atmospheric Feedbacks in a Coupled Model. Journal of Climate, 23(5), 1240–1253.

Zhou, L., & Wang, Y. (2006). Tropical Rainfall Measuring Mission observation and regional model study of precipitation diurnal cycle in the New Guinean region. Journal of Geophysical Research: Atmospheres (1984–2012), 111(D17), D17104, 1–18.